Top Quark Physics at the Tevatron

Frédéric Déliot*

Institut de Recherche sur les lois Fondamentale de l'Univers,
Service de Physique des Particules,
CEA Saclay - Bat 141,
F-91191 Gif-sur-Yvette Cedex,
France

Douglas A. Glenzinski[†]

Fermilab, Particle Physics Division,
P.O. Box 500, Batavia, IL 60510,
USA

(Dated: October 5, 2010)

We review the field of top-quark physics with an emphasis on experimental techniques. The role of the top quark in the Standard Model of particle physics is summarized and the basic phenomenology of top-quark production and decay is introduced. We discuss how contributions from physics beyond the Standard Model could affect the top-quark properties or event samples. The many measurements made at the Fermilab Tevatron, which test the Standard Model predictions or probe for direct evidence of new physics using the top-quark event samples, are reviewed here.

* frederic.deliot@cea.fr
† douglasg@fnal.gov

CONTENTS

I. INTRODUCTION

The Standard Model of particle physics (SM) contains six quarks arranged in three generations of two quarks each. The six leptons of the SM are similarly arranged. The top quark is the weak-isospin partner to the bottom quark, which together constitute the third generation of quarks. The existence of three quark generations was postulated as early as 1973 by Kobayashi and Maskawa since mixing among three generations (and no fewer) could provide a mechanism for CP violation (Kobayashi and Maskawa, 1973). Experimentally the multi-generation quark model found firm footing in 1974 with the discovery of the charm quark (Aubert *et al.*, 1974; Augustin *et al.*, 1974), the weak-isospin partner to the strange quark in the second generation of quarks. The discovery of the third generation tau lepton in 1975 (Perl *et al.*, 1975) implied the existence of a third generation of quarks. The bottom quark was discovered in 1977 (Herb *et al.*, 1997) and the search for its weak-isospin partner began in earnest. It was nearly two decades before the top quark was directly observed by experiment (Abachi *et al.*, 1995; Abe *et al.*, 1994, 1995) owing to its surprisingly large mass. Of course the immediate consequence of this discovery was to further solidify the SM. Indeed, by the time the direct observation was made there was mounting indirect evidence that the top quark existed and that it had to be heavy (Schaile and Zerwas, 1992). But it could be argued that this indirect evidence was model dependent and that an important consequence of the top-quark discovery was the definitive elimination of "top-less" theories that might otherwise still be viable. In fact, the principal interest in the top quark arises because of the possibility it will offer a window into new physics, into physics Beyond the Standard Model (BSM). Thanks to its very large mass (it weighs about as much as a gold atom) BSM contributions to physics involving top quarks can occur in a wide variety of ways - the production mechanisms can be affected, the decay widths can be altered, its intrinsic properties changed, or the experimental signature mimicked by a new particle of similar mass. A thorough exploration of all these possibilities is what constitutes the field of "Top Quark Physics", pioneered over the last 15 years by the experiments at the Fermilab Tevatron.

In this article we will concentrate on what has been experimentally established by the Tevatron experiments and the analysis techniques required to do so focused on already published results. The emphasis of this article will be on the $p\overline{p} \to t\overline{t}$ process responsible for most of the progress to date. The study of top quarks is expected to evolve over the next decade using data from CERN's Large Hadron Collider (LHC). Where appropriate we comment on differences between the Tevatron studies and the LHC possibilities.

II. STANDARD MODEL PRODUCTION AND DECAY

We begin by introducing some concepts and phenomenology to which we will refer throughout this article. We will not endeavor to summarize the Standard Model theory in any detail. This has already been done many times and interested readers should consult the references (Kronfeld and Quigg, 2010; Quigg, 2009) for in-depth discussions.

Simply put, high energy physics endeavors to enumerate the elementary particles which constitute all known matter and to characterize the interactions which govern their behavior. Their best guess to date is called the Standard Model of particle physics. The SM is a quantum gauge theory based on the $SU(3)$ gauge symmetry of quantum chromodynamics (QCD) and the $SU(2) \times U(1)$ gauge symmetry of quantum electrodynamics (QED).

In the SM there are twelve elementary particles - six quarks and six leptons, each arranged into three generations as shown here

$$
\begin{pmatrix} u \\ d \end{pmatrix} \quad \begin{pmatrix} c \\ s \end{pmatrix} \quad \begin{pmatrix} t \\ b \end{pmatrix}
$$
$$
\begin{pmatrix} \nu_e \\ e \end{pmatrix} \quad \begin{pmatrix} \nu_\mu \\ \mu \end{pmatrix} \quad \begin{pmatrix} \nu_\tau \\ \tau \end{pmatrix}. \tag{1}
$$

The up-type quarks, up (u), charm (c), and top (t), have electric charge $+\frac{2}{3}$ while the down-type quarks, down (d), strange (s), and bottom (b), have electric charge $-\frac{1}{3}$. The neutrinos, ν_e, ν_μ, and ν_τ are the electric-charge-neutral lepton partners to the electron (e), muon (μ) and tau (τ) leptons, respectively. The e, μ, and τ all carry electric charge -1. The measured masses of these particles are given in Tab. I. All these particles have anti-particles with the same mass and quantum numbers except they have the opposite electric charge, the opposite parity, and are singlets rather than doublets of the $SU(2)$ group. Often anti-particles are represented with the same symbol as the particle but with a bar; for example a quark is represented as q and an anti-quark as $\overline{q}$. An important subtlety worth noting is that the weak eigenstates of the down-type quarks are mixtures of the mass eigenstates. This mixing is represented

by the CKM matrix,

$$
\begin{pmatrix} d \\ s \\ b \end{pmatrix} = \begin{pmatrix} V_{ud} & V_{us} & V_{ub} \\ V_{cd} & V_{cs} & V_{cb} \\ V_{td} & V_{ts} & V_{tb} \end{pmatrix} \begin{pmatrix} d' \\ s' \\ b' \end{pmatrix}. \tag{2}
$$

The interactions of the elementary particles are governed by three forces, the strong force of QCD, and the electromagnetic and weak forces of QED. These forces are mediated by the exchange of bosons. The strong force is mediated by the exchange of gluons (g), the electromagnetic force by the exchange of photons (γ), and the weak force by the exchange of the charged W-bosons ($W^{\pm}$) or the neutral Z-bosons (Z^0). The strengths of these interactions are characterized by coupling constants with these approximate relative strengths $\alpha_{\mathrm{strong}} : \alpha_{\mathrm{em}} : \alpha_{\mathrm{weak}} \approx \frac{1}{10} : \frac{1}{100} : \frac{1}{10000}$. While the gluon and photon are massless, the W- and Z-bosons are massive and have been measured to be $m_W = 80.398\,\mathrm{GeV}/c^2$ and $m_Z = 91.188\,\mathrm{GeV}/c^2$ (Nakamura $et\ al.$, 2010). Figure 1 shows Feynman diagrams for an example of strong, electromagnetic, and weak interactions.

Not all of the elementary particles participate in all three interaction forces. The photons couple to the electric charge, so neutrinos do not participate in the electromagnetic interaction because they carry no electric charge. The gluons couple to the color charge. Only quarks carry color charge and participate in the strong interaction. All the quarks and leptons can participate in the weak interaction. The gauge bosons can interact subject to these same constraints. Gluons carry color and can self-interact. Similarly W- and Z-bosons can interact with each other. The electrically charged W-boson can couple to the photon.

In its simplest form the $SU(3) \times SU(2) \times U(1)$ symmetries of the SM predict that all the elementary particles and the gauge bosons are massless, which is clearly discrepant with experimental observations. The simplest way to remedy this is to introduce a scalar field that breaks the $SU(2) \times U(1)$ electroweak symmetry and introduces mass terms into the SM Lagrangian by acquiring a non-zero vacuum expectation value, $v = 246\,\mathrm{GeV}$. The physical manifestation of this scalar field is known as the Higgs boson, H^0, which imparts mass to the W- and Z-bosons via gauge interactions, and to the quarks and leptons via Yukawa interactions. The electroweak gauge interactions establish a well defined relationship between the Higgs vacuum expectation value and the masses of the W- and Z-bosons. The quark and lepton masses are linearly proportional to a Yukawa coupling, $Y_{q,\ell}$, and the Higgs vacuum expectation value. From their measured masses we can infer that the top-quark Yukawa coupling is of order $Y_t \sim 1$, while the others are significantly smaller ranging from $Y_e \sim 10^{-6}$ for the electron to $Y_b \sim 10^{-2}$ for the b-quark. The Higgs boson is the only SM particle that has not been experimentally observed. While the mass of the Higgs is not predicted by the SM, it can be inferred since quantum loops including the Higgs induce corrections to several experimental observables at a level comparable to the precision with which these observables are measured. A global fit to these so called "precision electroweak observables" predicts that the mass of the Higgs lies in the range of about $40 < m_H < 160\,\mathrm{GeV}/c^2$ at the 95% confidence level (Flächer $et\ al.$, 2009; Nakamura $et\ al.$, 2010). Direct searches for the Higgs at LEP and the Tevatron have ruled-out the masses $m_H < 115\,\mathrm{GeV}/c^2$ and $158 < m_H < 175\,\mathrm{GeV}/c^2$ at the 95% confidence level. It should be noted that all these constraints are valid only in the context of the SM. The electroweak symmetry may well be broken in some other way.

A peculiarity of QCD worth noting is that quarks can only be observed as bound state hadrons. There are two types of hadrons, mesons are quark-anti-quark bound states, and baryons are three-quark bound states. An important experimental consequence of this is that quarks produced in a high energy $p\bar{p}$ interaction manifest themselves as collimated streams of hadrons called "jets". The energy and direction of a jet are correlated to the energy and direction of its parent quark. The process by which the quark evolves into a jet is called "hadronization" and consists of a parton shower, which can be perturbatively calculated, and a fragmentation process, which is a non-perturbative process modeled using Monte Carlo techniques. As will be seen later in this article, the presence of jets in the final state gives rise to several experimental challenges.

Most hadrons are unstable and decay to lighter particles. The probability of decay occurring at a time t is described by an exponential, $P \sim e^{t/\lambda}$, where the lifetime, λ, is characteristic of the decaying particle. For example, hadrons containing a b-quark decay with a lifetime of about 1.5 ps. This is long enough that their flight distance in the lab frame is large (of order mm) compared to the experimental resolution - a fact exploited to identify b-hadrons in jets. The ability to identify b-jets is important in reducing background contributions for many of the $t\bar{t}$ measurements we will discuss.

From 1989-2009 top quarks could only be produced at one place in the world. The Tevatron is a proton (p) anti-proton ($\bar{p}$) collider with a center-of-mass energy of $\sqrt{s} = 1.96$ TeV located at Fermilab. For $p\bar{p}$ collisions at this energy top quarks are predominantly produced in pairs ($t\bar{t}$) via the strong interaction as shown in Fig. 2. The most recent production cross section calculations are accomplished at next-to-leading-order (NLO) and include logarithmic corrections that account for contributions from higher order soft gluon radiation (Ahrens $et\ al.$, 2010;

Cacciari *et al.*, 2008; Kidonakis and Vogt, 2008; Langenfeld *et al.*, 2009). For a top-quark mass of 172 GeV/c^2 the production cross section is calculated in (Langenfeld *et al.*, 2009) to be $\sigma(p\overline{p} \to t\overline{t}) = 7.57^{+0.50}_{-0.70}$ pb for $\sqrt{s} = 1.96$ TeV. The uncertainty includes contributions from varying the factorization and renormalization scales, and from varying the patron distribution functions (PDF). The PDFs describe the momentum distribution of the constituent quarks and gluons that make up the protons and anti-protons. They are empirically determined from fits to deep-inelastic-scattering (DIS) cross section measurements performed by a variety of experiments. The fits to the DIS data are performed by a number of different collaborations and are made available as software packages. Common choices are the MRST (Martin *et al.*, 2007) and CTEQ (Pumplin *et al.*, 2002) PDF fits. The cross section above uses the CTEQ6.6 PDF parameterization and changes by approximately ∓ 0.24 pb for a ± 1.0 GeV/c^2 change in the top-quark mass.

In the SM the top-quark decay is well specified and the branching fraction is completely dominated by $t \to W^+ b$ with the decays $t \to W^+ q$ ($q = s$, d) contributing at the $< 1\%$ level. Thus for $t\overline{t}$ events the experimental final state is determined by the decay of the W bosons. The leptonic decays ($l = e$, μ, τ) of the W boson have a branching fraction of $\mathcal{B}(W \to l\nu) = 10.8\%$ each while the hadronic decays have a total branching fraction of $\mathcal{B}(W \to q\overline{q}') = 67.7\%$ (Nakamura *et al.*, 2010). For $t\overline{t}$ events there are then three possible final states. The dilepton final state (*dil*) corresponds to both W bosons decaying leptonically, $t\overline{t} \to \ell^+ \nu b \ell^- \overline{\nu} \overline{b}$, and occurs 10% of the time. The lepton-plus-jets final state (*ljt*) corresponds to one W decaying leptonically and the other hadronically, $t\overline{t} \to \ell \nu q q' b \overline{b}$, and occurs 44% of the time. The all hadronic final state (*had*) corresponds to both W bosons decaying hadronically, $t\overline{t} \to q q' b q q' \overline{b}$, and occurs 46% of the time. Figure 3 shows the Feynman diagrams corresponding to these three final states, which, experimentally, are treated separately since the contributing sources of background and the dominant detector effects differ among them.

The decay width of the top quark is also well specified in the SM. Including radiative QCD and QED corrections the decay width for a top-quark mass of 172 GeV/c^2 is $\Gamma_t = 1.4$ GeV/c^2 (Jezabek and Kühn, 1993, 1994). The theoretical uncertainty is at the level of a few percent relative and is dominated by uncertainties in α_s and in missing higher order QCD corrections. The large decay width of the top quark has important experimental consequences. Since Γ_t is large relative to the hadronization scale of QCD, $\lambda_{QCD} = 250$ MeV, the top quark decays before quark/anti-quark bound states are formed. Essentially, the top quark is produced and decays as a free quark - it is unique among the quarks in this respect. As a result of this unique feature, many of the experimental techniques used to explore the properties of the lighter quarks are not useful in exploring the top quark so that new methodologies had to be developed.

III. NEW PHYSICS AFFECTING TOP-QUARK PROPERTIES

It is important to note that the SM has several short comings and is widely regarded to be a low energy approximation of a more complete description of particle physics (Quigg, 2009). There are numerous theories hypothesized that address these shortcomings and offer this more complete description. The theories differ primarily in the manner by which they impart mass to the elementary particles. The search to discover and describe the physics that breaks electroweak symmetry is among the most ardently pursued by high energy experimentalists and theorists alike. Is it the SM Higgs, or is it some new physics, something beyond the SM? The principal aim of top-quark physics is to help answer these questions. With a Yukawa coupling of order unity, the top quark strongly couples to the dynamics of electroweak symmetry breaking and is thus expected to be a good place to test this dynamics and probe for BSM effects. In addition, because of its large mass, quantum loop corrections to top-quark observables from possible new particle contributions can be large - significantly larger than for the lighter quarks and leptons. The strategy for probing for BSM effects using the top quark employs both direct searches for new particles and indirect searches by looking for deviations of experimental observables from the SM expectations.

New physics contributions can affect top-quark observables directly in two ways (Hill and Parke, 1994). First non-standard top-quark production can appear through intermediate heavy states such as new gauge bosons that decay into a $t\overline{t}$ pair or into a final state mimicking the SM $t\overline{t}$ signature. Secondly the top quark can decay into exotic particles such as a charged Higgs boson, $t \to H^+ b$, in models with multiple Higgs doublets. In the first case, BSM effects distort the SM top-quark production observables, while in the second case BSM effects produce discrepancies among the different decay observables. It is thus important to measure the top-quark properties using as many decay final states as possible and to compare them.

There are many examples of new physics models that affect the production or decay observables in $t\overline{t}$ samples. New heavy states that carry color charge can modify the $t\overline{t}$ production observables. Color singlet resonances can be either scalar or vector. Examples of models that predict color singlet scalar particles are the supersymmetric extension of the SM, SUSY (Chung *et al.*, 2005; Haber and Kane, 1985; Martin, 1997; Nilles, 1984), or more generally

models with multiple Higgs fields, MHDM (Grossman, 1994). Examples of models that predict color singlet vector particles include technicolor (Eichten *et al.*, 1986; Eichten and Lane, 1980), topcolor (Hill, 1991), or top assisted technicolor (Hill, 1995). Color non-singlet resonances can produce similar effects and are also predicted in several BSM theories (Chivukula *et al.*, 1996; Choudhury *et al.*, 2007; Simmons, 1997). Compactified extra dimension models can also affect $t\bar{t}$ production and decay. These models produce Kaluza-Klein (KK) modes that either decay preferentially into $t\bar{t}$ pairs or into final states that mimic the SM $t\bar{t}$ signature. The flat extra dimension TeV^{-1} models produce KK modes that can decay to $t\bar{t}$ pairs (Antoniadis *et al.*, 1994, 1999; Cheung and Landsberg, 2002; Dienes *et al.*, 1998, 1999; Rizzo and Wells, 2000). Universal extra dimension models pair produce a KK mode that each decay as KK $\to t\gamma$ so that they mimic the SM signature but also include additional photons in the final state (Appelquist *et al.*, 2001; Cheng *et al.*, 2002; Rizzo, 2001). Wraped Randall-Sundrum extra dimension models predict KK gravitons that can decay to $t\bar{t}$ (Davoudiasl *et al.*, 2001; Randall and Sundrum, 1999), while bulk Randall-Sundrum models with fermions and gauge bosons in the bulk predict in addition KK top quarks that would be produced in pairs and would decay to Wb as in the SM (Agashe *et al.*, 2003; Chang *et al.*, 2000; Csaki *et al.*, 2002; Davoudiasl *et al.*, 2000; Grossman and Neubert, 2000; Hewett *et al.*, 2002; Huber and Shafi, 2001; Pomarol, 2000; Randall and Schwartz, 2001, 2002). Some BSM theories predict a fourth family of (heavy) quarks and leptons. These additional generations naturally appear in grand-unified theories (Langacker, 1981) but some of the models cited above also predict new particles that look like heavier quarks. Similarly, Little Higgs models predict new heavy vector-like quarks (Dobrescu and Hill, 1998; Han *et al.*, 2003). All of these can produce decay final states that mimic the SM $t\bar{t}$ signatures.

New physics effects can also effect top-quark decays or other properties of the $t\bar{t}$ sample. For example, some SUSY and MHDM theories produce top-quark decays into new particles (Chung *et al.*, 2005; Grossman, 1994). Other models modify the SM top-quark branching fractions. For example flavor changing neutral current (FCNC) decays, $t \to cX^0$, or $t \to uX^0$ where X^0 is any neutral particle like a photon or a Z-boson, can be modified by BSM physics. Since these processes are extremely suppressed in the SM even small new physics effects can yield large changes in FCNC branching fractions (Aguilar-Saavedra, 2004). The $t\bar{t}$ sample can also be probed for the presence of more general anomalous couplings (Kane *et al.*, 1992) affecting the kinematic properties of top-quark decays and appearing as discrepancies with the SM predictions. These might affect the $t\bar{t}$ forward-backward charge asymmetry, the $t\bar{t}$ spin correlations, or the helicity fractions of W-bosons from top-quark decays (Cao *et al.*, 2010; Cheung *et al.*, 2009; Djouadi *et al.*, 2009; Shu *et al.*, 2010). The measured intrinsic properties of the top-quark might also be affected. For example some BSM theories predict particles with electric charge $-4/3$ or $+5/3$ that decay into top-quarks (Contino and Servant, 2008).

Over the last decade the Tevatron experiments have instituted a broad top physics program aimed at exploring these possibilities both by comparing measured top-quark properties to SM predictions, as discussed in Sec. IX, and by directly searching for new particles in the top-quark event samples, as discussed in Sec. X.

IV. EXPERIMENTAL APPARATUS

The $p\bar{p}$ collision data at the Tevatron are collected and analyzed by two collaborations, CDF and DØ. For both the CDF and DØ experiments the detector apparatus is designed to be a general purpose collider detector with the capability of reconstructing charged particle tracks and jets, identifying electrons, muons, photons, and b-quark jets, and measuring the energy and momentum of as many of the final state particles as possible. Functionally the two detectors behave very similarly, although they differ significantly in their technical details. They both have a cylindrical geometry centered on the $p\bar{p}$ beam line and employ a coordinate system with the z axis parallel to the beam line and pointing in the direction of the proton beam. The angle θ is the polar angle relative to the z axis and the angle ϕ is the azimuthal angle in the plane transverse to the z axis. The energy, E, and momenta, $\vec{p}$, of final state leptons, photons, and jets are estimated using information from calorimeters and a spectrometer. It is convenient to define the transverse energy, $E_T = E \sin\theta$, and the transverse momentum, $p_T = |\vec{p}| \sin\theta$. Since the $p\bar{p}$ beams are traveling along the z axis the initial state is known to satisfy $(E_T, p_T) = (0, 0)$ while the (E_z, p_z) components of the initial state are unknown event-by-event - and in general are non-zero - due to the ambiguities introduced by the parton distribution functions. Because the collision events are boosted along the z-axis hadron collider experiments often use pseudo-rapidity, $\eta = -\ln\tan\frac{\theta}{2}$, in place of $\cos\theta$ when defining angular regions since differences in pseudo-rapidity, $\Delta\eta$, are invariant under these boosts.

The CDF and DØ detectors are shown in Fig. 4 and are described in detail in references (Blaire *et al.*, 1996) and (Abazov *et al.*, 2006) and only a generic description is provided here. The detectors are divided into a central region covering (approximately) $|\eta| < 1.3$ and a forward region covering (approximately) $1.3 < |\eta| < 3.5$. In the central region at the inner most radii, immediately surrounding the $p\bar{p}$ beam line, are precision vertex systems comprised of

several concentric layers of silicon microstrip detectors with a per layer charged particle position resolution of around 10 μm. These detectors are important in reconstructing the primary $p\overline{p}$ interaction vertex as well as identifying displaced vertices from the decay of long lived particles (e.g. b-hadrons). The silicon systems are surrounded by large radii, multi-layered, low mass tracking chambers which achieve position resolutions of around 150 μm per hit. The silicon and tracking systems are inside superconducting solenoids, which provide magnetic fields parallel to the beam line and induce curvature in the tracks of charged particles from which their momentum can be deduced. The transverse momentum of charged particles is typically measured with a resolution of $\sigma_{p_T}/p_T < 0.01\ p_T$. Outside the solenoid are the calorimeters with an electromagnetic compartment in front of a hadronic compartment. The electromagnetic (EM) compartment consists of roughly 20 radiation lengths or more of material and fully contains $e^{\pm}$ and γ showers. The showers induced by pions, kaons, and other long lived hadrons are initiated in the EM calorimeter but continue through and are contained in the hadronic compartment. The energies of electrons and photons are typically measured with a resolution of approximately $\sigma_E/E = 14\%/\sqrt{E}$ while the energies of jets are typically measured with a resolution of approximately $\sigma_E/E = 10 - 15\%/\sqrt{E}$. The calorimeters are segmented into towers with a typical granularity of $\eta \times \phi = 0.1 \times 0.1$. Beyond the hadronic calorimeters are the muon chambers, small scintillator plus tracking systems which serve to identify muons, the only charged particles able to traverse the calorimeters without being absorbed. In the forward region there is some limited tracking capability from the silicon system, but with a much worse p_T resolution than that achieved in the central region. There are also EM and hadronic calorimeters together with muon chambers. In the far forward region, $|\eta| > 3.5$, is a luminosity monitor used to measure the $p\overline{p}$ collision rate in the detector during data taking. In total each experiment has about one million read-out channels.

The data acquisition system digitizes the read-out channels and records them to permanent storage (tape) for later analysis. The Tevatron delivers a collision to each experiment every 396 ns, which corresponds to about 2.5M collisions per second. This is far too many collisions to record them all and each experiment employs a three level trigger system to identify the most interesting events to keep for later analysis. The level one trigger is hardware based and employs simple thresholds and a coarse granularity to identify events with high energy depositions in the calorimeter or segments in the tracking system consistent with having originated from a high momentum particle. The level one system reduces the initial event rate by about two orders of magnitude. The level two trigger system employs some custom hardware and processing to match objects identified at level one and to achieve improved resolution with finer granularity. For example, at level two a high momentum track may be matched to a high energy deposition in the EM calorimeter or to a track segment in the muon chamber, consistent with what is expected from an electron or muon, respectively. The level two system reduces the event rate by another one order of magnitude. The level three system employs a computing farm and custom software to reconstruct the full event and confirm the level two decision with a resolution and granularity that nearly matches that achieved after final calibrations and offline event reconstruction. The level three system achieves an additional order of magnitude reduction in the event rate so that each experiment writes the most interesting events to tape at a rate of about 100 Hz.

V. EVENT RECONSTRUCTION

The events which are written to tape are later processed on large scale computing farms using custom software to perform event reconstruction. This offline processing uses final calibration constants and alignments and more sophisticated algorithms relative to what is used in the level three trigger in order to achieve improved efficiencies and resolutions. The reconstruction software combines information from the tracking, calorimeter, and muon chamber systems to provide particle identification. Charged particles reconstructed in the tracking systems are extrapolated to the calorimeters and muon chambers. Tracks matched to energy depositions in the EM calorimeter or to muon chamber hits are taken to be electron or muon candidates, respectively. An EM energy deposition without a track match is taken to be a photon candidate. A contiguous set of calorimeter towers with energy depositions above a predetermined noise threshold and matched to a collimated set of tracks in the tracking chamber is taken to be a jet originating from the hadronization of an initial quark or gluon state. A jet which contains tracks that form a secondary vertex significantly displaced from the primary interaction vertex is taken to be a candidate b-jet. The presence of a neutrino in the final state is inferred from a momentum imbalance in the transverse plane since neutrinos traverse the entire detector volume without interacting. In the events of interest the final state particles are all relativistic, so the momentum imbalance is calculated using the calorimeter energies and is called "missing E_T" or MET and is defined as $\not{E}_T = -\sum_i E_T^i \hat{i}$, where the index i runs over all calorimeter towers, E_T^i is the transverse energy measured in the ith tower and $\hat{i}$ is the unit vector pointing from the primary event vertex to the center of the ith tower in the transverse plane. The resolution of the $\not{E}_T$ calculation can be improved by correcting for muons and jets in the event.

Analyses using the $t\bar{t}$ all hadronic final state ($t\bar{t} \to qq'bqq'\bar{b}$) exploit the jet reconstruction and b-jet identification capabilities of the detector to identify events of interest. Analyses using the $t\bar{t}$ dilepton ($t\bar{t} \to \ell^+\nu b\ell^-\bar{\nu}\bar{b}$) or lepton-plus-jets ($t\bar{t} \to \ell\nu qq'b\bar{b}$) final state exploit the full range of detector capabilities using lepton and b-jet identification, jet reconstruction, and missing energy estimates to identify candidate $t\bar{t}$ events. Each analysis begins by choosing the subset of recorded data satisfying a particular set of trigger criteria. This eliminates the need to run the full analysis software over those events whose topologies and kinematics significantly differ from those expected of $t\bar{t}$ events. For each event satisfying the trigger criteria the primary interaction vertex is identified, leptons and jets are reconstructed, an estimate of $\slashed{E}_T$ is made, and b-jets are identified using a dedicated algorithm. The event sample at this stage is dominated by background events originating from non-$t\bar{t}$ processes. Additional, final state dependent, selection criteria are used to suppress these background contributions and improve the purity of the sample.

A. Trigger Criteria

The dil and ljt data sets are collected using several different sets of trigger criteria. The two most important sets of trigger criteria focus on identifying the electron or muon from the W-boson decays[1]. These leptons are typically high energy and isolated. The first set of trigger criteria is an inclusive high-E_T electron data set requiring a candidate electron with $E_T > 20$ GeV. The electron is identified at the trigger level as a high energy cluster in the EM calorimeter matched to a high momentum track in the tracking chamber. Additional requirements are made on the ratio of energy deposition in the EM calorimeter to the energy deposition in the hadronic calorimeter, and on the shape of the EM shower in the calorimeter. The electron candidate must be isolated, with few surrounding tracks and/or only small additional energy deposits in neighboring calorimeter towers. The second set of trigger criteria is an inclusive high-p_T muon data set requiring a candidate muon with $p_T > 20$ GeV/c. The muon is identified at the trigger level as a track segment reconstructed in the muon chambers matched to a high momentum track reconstructed in the tracking chamber. The muon candidate is additionally required to be isolated. Because these first two sets of trigger criteria make tracking requirements their acceptance is limited to the central detector region. The number of $t\bar{t}$ events collected can be significantly increased by including triggers which collect events in the forward detectors. In order to keep the purity of the trigger sample reasonable these forward triggers are less inclusive. They usually require some high energy jets (e.g. $E_T^j > 10$ GeV) in addition to a high energy EM calorimeter cluster in the forward region (e.g. $E_T^e > 20$ GeV) or large $\slashed{E}_T$ (e.g. $\slashed{E}_T > 35$ GeV). For each 1 pb^{-1} of collision data these triggers collect approximately 1-2 thousand $p\bar{p} \to W$ + jets and $p\bar{p} \to Z$ + jets events, depending on the details of the trigger selection.

The had data set is collected using trigger criteria requiring at least four jets each with an uncorrected energy of $E_T > 15$ GeV in events with large total transverse energy as determined by summing over all calorimeters towers (e.g. $\sum_i E_T^i > 175$ GeV). For each 1 pb^{-1} of collision data these triggers collect about 8-10 thousand events, depending on the details of the trigger selection, dominated by QCD production of multi-jet final states $p\bar{p} \to qqqq$ events.

B. Primary Interaction Vertex

The counter-rotating proton and anti-proton beams at the Tevatron are organized into 36 bunches each. The bunches are kept separated as they traverse the Tevatron ring and are only brought into collision near the centers of the CDF and DØ detectors. The exact location of the collision varies for each beam crossing. The shape of the luminous region is determined using tracks in di-jet events ($p\bar{p} \to q\bar{q}$), which are predominantly promptly produced and thus originate from the collision vertex. The tracks are constrained to a common origin and the distribution of the (x, y, z) position of the resulting vertex is determined using millions of events[2]. The distribution of the collision positions along the z axis can be approximated as a Gaussian with a mean near $z = 0$ and an RMS of approximately 30 cm. In the transverse plane the beam is well described by a two dimensional Gaussian whose mean varies as a function of z but is typically within $\mathcal{O}(1)$ mm on the z axis. The RMS width of the beam in the transverse plane also varies with z and increases from about 30 μm near $z = 0$ to about 40 μm for $|z| > 40$ cm. The mean x and y as a function of z are well described by linear functions whose parameters are determined run-by-run and stored in a beamline database. In order to achieve the best jet energy resolutions and highest b-jet identification efficiency it is

---

[1] Because of the additional experimental challenges they introduce, $t\bar{t}$ events with one of the W-bosons decaying to a tau lepton are not often used. Since the tau lepton quickly decays to a multi-particle final state the $W \to \tau\nu$ decay is difficult to trigger on in an inclusive manner. Those leptonic tau decays, $\tau \to e\nu\nu$ and $\tau \to \mu\nu\nu$, satisfying the inclusive muon and electron trigger criteria are included in the data set described here.

[2] For a vector of magnitude v we define $(v_x,\ v_y,\ v_z) = v(\sin\theta\cos\phi,\ \sin\theta\sin\phi,\ \cos\theta)$.

necessary to reconstruct the location of the interaction vertex for each event. For dil and ljt events the z coordinate of the highest energy lepton track can be used together with the known shape of the luminous region, as determined from the di-jet data as described above, to estimate the location of the interaction vertex with a resolution of a few hundred microns in z and about 35 μm in x and y. These resolutions can be improved by a factor of three to five by using the tracks in the event itself. In order to avoid bias from long lived b-hadron decays in b-jets, only tracks whose distance-of-closest-approach (also known as the impact parameter, d_0) to the beamline is comparable to the d_0 resolution are used. These tracks are then constrained to originate from a common point, whose coordinates are taken as the position of the $t\bar{t}$ interaction vertex. An iterative procedure is employed by eliminating tracks with large d_0 relative to the fitted vertex to form a new vertex. The process is repeated until no large impact parameter tracks are included in the vertex fit. For had events there is no lepton to seed the identification of the $t\bar{t}$ vertex. Again, tracks in the event are used and are constrained to originate from a common origin and an iterative procedure is used to remove the bias from tracks originating from b-hadron decay. Depending on event topology, resolutions of $5 - 20$ μm in the transverse plane and of 100 μm along z are achieved on an event-by-event basis.

Since the $p\overline{p}$ inelastic cross section is very large there is often more than one hard scatter interaction per beam-beam crossing. The mean number of expected hard scatters is linearly dependent on the instantaneous luminosity of the colliding beams and inversely proportional to the number of bunches. For the Tevatron parameters the mean number of expected hard scatters per beam-beam crossing is about 3.5 at an instantaneous luminosity of $\mathcal{L}_{\text{inst}} = 100 \times 10^{30}$ cm^{-2}/s. The actual number of hard scatters per event is Poisson distributed about the mean. These additional interactions are typically separated in z. Since the RMS of the luminous region along the z axis is large relative to the resolution with which a single interaction vertex is reconstructed, the experiments can efficiently reconstruct and readily resolve multiple interaction vertices in a single event. This is important since the typical Tevatron stores have an initial instantaneous luminosity that exceed 3×10^{32} cm^{-2}/s and an average instantaneous luminosity over the lifetime of a store of about 1.5×10^{32} cm^{-2}/s. For events with multiple reconstructed interaction vertices it is necessary to identify which of the vertices corresponds to the $t\bar{t}$ interaction vertex. For the leptonic final states the vertex closest to the high energy lepton is used. For the had final state, the scalar sum p_T of all tracks associated with each vertex is calculated and the vertex with the largest $\sum_i \left| p_T^i \right|$ is used. The $t\bar{t}$ interaction vertex is correctly identified nearly 100% of the time.

C. Electrons and Muons

The reconstruction of high energy electrons and muons from W-boson decays is important in identifying the signal $t\bar{t}$ events. The leptons from $Z^0 \rightarrow e^+e^-$ and $Z^0 \rightarrow \mu^+\mu^-$ decays are kinematically very similar to the W decay leptons and are thus used as data control samples to measure efficiencies and backgrounds for the lepton reconstruction and selection criteria employed in the $t\bar{t}$ analyses. The reconstruction of lower energy electrons and muons from semi-leptonic b-hadron decays is sometimes used to identify b-jets.

Electron reconstruction begins by identifying energy depositions in the EM calorimeter above a specified threshold, typically around 2 GeV. In the central detector region, tracks from the tracking chamber with momentum above a few GeV/c are extrapolated from the tracker outer radius to the front face of the EM calorimeter. If the extrapolated track position is consistent with the energy-weighted centroid of the calorimeter cluster within uncertainties, including contributions from multiple scattering in the material between the tracker and the calorimeter, the resulting EM calorimeter and track match are taken to be a candidate electron. To reduce contributions from hadrons mimicking electrons, the shape of the shower in the calorimeter, and the ratio of track p_T to calorimeter E_T are required to be consistent with that expected of electrons as determined from $Z^0 \rightarrow e^+e^-$ events and test beam data. The energy deposited in the hadronic calorimeter tower immediately behind the candidate electron is required to be small relative to the EM energy deposit. Electrons consistent with having originated from $\gamma \rightarrow e^+e^-$ conversions in the detector material are identified with dedicated algorithms and removed from further consideration. In the forward detector region where there is very limited coverage from the full tracking chamber, electrons are identified using stricter criteria on the EM cluster energy, shower shape, and hadronic to EM energy deposition ratios. The purity of the resulting forward electron sample can be significantly improved by searching for hits in the tracking system consistent with expectations derived from the E_T and position of the EM cluster and the location of the event primary interaction vertex.

Muon reconstruction begins by identifying track segments in the muon chambers. Tracks from the tracking chamber with momentum above several GeV/c are extrapolated from the tracker outer radius to the front face of the muon chamber. If the extrapolated track position is consistent with the position of the muon chamber track segment within uncertainties, including contributions from multiple scattering in the material between the tracker and the

muon chamber, the resulting segment and track match are taken to be a candidate muon. Through going cosmic ray muons are identified using dedicated algorithms and removed. Hadrons whose shower are not fully contained in the calorimeter and other intervening material are said to "punch-through" to the muon chambers and can mimic a muon signature. To reduce contributions from punch-through hadrons, stricter segment-track matching and track p_T criteria together with track quality criteria can be employed. The track quality criteria usually include requirements on the number hits used to form the track, the impact parameter, and the track fit chi-square. These track quality criteria also help reduce contributions from hadron decays-in-flight (e.g. $K^{\pm} \to \mu^{\pm}\nu$). The energy depositions in the calorimeter towers traversed by the muon can be required to be consistent with that expected from a muon as determined using $Z^0 \to \mu^+\mu^-$ and $J/\psi \to \mu^+\mu^-$ data control samples.

The leptons from W- and Z-boson decays are typically well separated from other objects in the event. To further suppress hadronic backgrounds isolation criteria are employed. Calorimeter isolation requires that the energy deposited in an annulus around the calorimeter towers associated with the lepton candidate be small. Tracking isolation requires that the scalar sum p_T of all tracks in a cone around the lepton candidate be small. The requirements are sometimes absolute (e.g. $E(\text{annulus}) < 3$ GeV) and sometimes relative (e.g. $E(\text{annulus})/E(\text{electron}) < 0.1$).

Samples of $Z^0 \to \ell^+\ell^-$ ($\ell = e$ or μ) events collected with the inclusive electron and muon triggers described above, are used to measure the trigger, reconstruction, and identification efficiencies for electrons and muons, respectively. The "tag-and-probe" method is employed where the lepton leg which fired the inclusive trigger is the "tag" leg, while the second leg is unbiased and used as a "probe" to measure the efficiency of interest. The efficiencies are measured with total uncertainties of $< 1\%$ relative and are characterized as a function of p_T, η, instantaneous luminosity, and number of reconstructed interaction vertices. A more detailed description of these measurements can be found in (Abulencia *et al.*, 2007).

The absolute momentum scale of the spectrometer is determined using J/ψ, Υ, Υ', and Z^0 decays to $\mu^+\mu^-$ by comparing the reconstructed invariant mass of the muon pairs to the known masses of each resonance. By using a variety of resonances any non-linearities in the momentum scale can be identified and corrected for. These studies result in a more precise understanding of the magnetic field uniformity, the distribution of material in the detector volume, and any small residual mis-alignments in the tracking systems. The absolute energy scale of the EM calorimeter is determined using $\pi^0 \to \gamma\gamma$, $J/\psi \to e^+e^-$ and $Z^0 \to e^+e^-$ decays and using the E/p distribution of electrons from $W \to e\nu$ decays. Again, by using a variety of decay processes non-linearities in the energy scale can be identified and corrected for. In both cases the absolute scales are determined to a relative precision well below 1% and are monitored continuously and kept constant at the $0.2-0.3\%$ level. The observed RMS widths of the reconstructed mass distributions are dominated by the detector resolutions. Studies of the di-muon and di-electron resonance widths help determine the momentum and energy resolutions, respectively. The absolute scales and resolutions are characterized as a function of energy/momentum, η, instantaneous luminosity, and number of reconstructed interaction vertices. These methodologies are described in more detail in (Aaltonen *et al.*, 2008; Abazov *et al.*, 2009).

D. Jets

Jets are reconstructed as a contiguous set of calorimeter towers each above a predetermined noise threshold. A variety of algorithms are available to determine which towers to group together. The algorithms differ in the criteria they use to combine towers to form jets and in the manner in which they identify and merge or separate jets which are near each other in $\eta - \phi$ space. The behavior of the algorithms, particularly with regard to their handling of nearby jets, affects the degree to which they are sensitive to soft QCD radiation. Algorithms which are insensitive to soft QCD radiation are said to be "infrared safe" and can be compared to theoretical predictions in a very clean manner. There are in general two classes of jet algorithms. The k_T algorithms combine calorimeter towers to form jets based on their relative transverse momentum as well as their $\eta - \phi$ separation. They are rigorously infrared safe. The cone algorithms combine calorimeter towers to form jets based only on their $\eta - \phi$ separation. The cone algorithms begin by identifying a set of seed towers with energy above some seed threshold, typically about 1 GeV. The Midpoint algorithm employed by CDF and DØ is such an algorithm with additional steps introduced in order to minimize the sensitivity to soft QCD radiation. While rigorously the Midpoint algorithm is not completely infrared safe, in practice the residual sensitivity is experimentally inconsequential. This is due to the fact that the energy of jets in $t\bar{t}$ events is large (approximately 50 GeV on average) compared to the seed threshold so that small fluctuations in tower-to-tower energy depositions from soft QCD radiation do not affect the results of the algorithm. The cone algorithms offer an experimental advantage because the physical extent of each jet is well defined to have a radius of $R = \sqrt{(\Delta\eta)^2 + (\Delta\phi)^2}$ while the physical extent of jets formed using a k_T algorithm vary from jet to jet. In practice the two algorithms yield very similar results (Aaltonen *et al.*, 2008). In the cone algorithms the cone radius employed

can be varied. For the $t\bar{t}$ analyses a relatively narrow cone size is employed, $R = 0.4$ for CDF and 0.5 for DØ.

The jet reconstruction algorithm uses raw calorimeter energies. The total energy of the jet is estimated as the sum of energies over all towers included in the jet. The direction of the jet is determined using an energy weighted average over all contributing calorimeter towers. The energy and direction of the jet are then used as an estimate of the four momenta of the parent parton (ie quark or gluon). The jet energy resolution is improved by employing a set of corrections which account for several effects. The effects fall into two broad categories, instrumental effects, and physics effects. The instrumental effects accounted for include corrections for non-uniform and non-linear response of each calorimeter tower as well as contributions from multiple interactions per event. The physics effects accounted for include corrections for contributions from the underlying event, from the hadronization process, and from out-of-cone showering. The calibration of the CDF and DØ jet energy corrections are described in detail in (Bhatti *et al.*, 2006) and (Abazov *et al.*, 200n) and are a function of jet transverse energy and pseudo-rapidity. The corrections vary from about 60% for jets with transverse energy around 20 GeV to about 20% for jets with transverse energy around $100\,\text{GeV}$. The corrections can be checked using $p\bar{p} \to \gamma+$jet and $p\bar{p} \to Z^0+$jet events. Given the initial constraint that $(E_T, p_T) = (0, 0)$, it is expected that the jet transverse energy after all corrections should be equal to the transverse energy of the well measured photon or Z-boson (when $Z^0/\gamma \to e^+e^-$ or $\mu^+\mu^-$) in the event. The uncertainties on the jet energy scale derive from many sources, some of which are experimental (e.g. the statistics of the control sample or an inadequate understanding of the detector response) and some of which are modeling (e.g. modeling of the underlying event, hadronization, and out-of-cone showering processes) related. Like the corrections, the uncertainties are jet E_T and η dependent and range from about 10% at low energies (< 40 GeV) to a few 1% at high energies (> 75 GeV). The dominant source of uncertainty is modeling related at the lower energies and experiment related at higher energies.

The full set of jet energy corrections are designed to give an accurate estimate of the energy and momentum of the parent parton that had initiated the jet. However, the full set of corrections are not always employed. Frequently jets are only corrected to the particle level, which effectively corrects for all the instrumental effects as well as contributions from the underlying event and multiple interactions. Jets corrected to this level are effectively independent of apparatus and environment and can be compared across experiments. For the selection criteria described below, the jets are corrected to the particle level. Later, when using the selected $t\bar{t}$ candidate events in analyses the jets are corrected to the parton level whenever a kinematic fit is employed.

E. Missing Transverse Energy

We exploit the fact that the initial state satisfies $(E_T, p_T) = (0, 0)$ and use an observed imbalance of momentum in the transverse plane to infer the presence of high energy neutrinos in an event. As mentioned above, because the final state particles are all relativistic at the relevant collider energies, we use the energy measured in the calorimeters as an estimate of the total momenta of particles produced (including neutral particles). For this reason the quantity examined is called missing transverse energy, $\not{E}_T$. The initial estimate of the missing transverse energy begins with using only calorimeter information: $\not{E}_T = -\sum_i E_T^i \hat{i}$, where the index i runs over all calorimeter towers, E_T^i is the transverse energy measured in the ith tower and $\hat{i}$ is the unit vector pointing from the primary event vertex to the center of the ith tower in the transverse plane. Corrections are made if there are identified muons in the event since they are minimum ionizing and the calorimeter energy deposition is a poor estimate of their momenta: $\not{E}_T = -\left(\sum_i E_T^i \hat{i} - E_T^\mu \hat{i}_\mu + p_T^\mu \hat{i}_\mu\right)$, where E_T^μ, $\hat{i}_\mu$, and p_T^μ are the calorimeter transverse energy, azimuthal angle unit vector, and tracker transverse momentum associated with the muon candidate. The $\not{E}_T$ resolution can be further improved when jets have been reconstructed by taking advantage of the jet energy corrections described above by removing from the initial sum any calorimeter tower included in a jet and substituting the jet transverse energy (corrected to the particle level) at the jet ϕ. For $t\bar{t}$ analyses the final expression is often rewritten: $\not{E}_T = -\left(\sum_\ell p_T^\ell \hat{i}_\ell + \sum_j E_T^{j,\text{crctd}} \hat{i}_j + \sum_{\text{uc}} E_T^{\text{uc}} \hat{i}_{\text{uc}}\right)$, where ℓ is the sum over identified leptons (electrons or muons) in the event, j is the sum over reconstructed jets, and uc is the sum over unclustered calorimeter towers (ie. those not included in a jet). For electrons (muons), p_T^ℓ is estimated from the EM calorimeter (spectrometer). For jets, $E_T^{j,\text{crctd}}$ is the jet transverse energy corrected to the particle level. For the unclustered calorimeter towers the raw calorimeter energy is used. This expression is equivalent to the original expression with corrections for the muons and jets as described.

At the trigger level only the "raw" $\not{E}_T$ estimate is available, without any of the corrections. At the event selection and later in the analyses employing kinematic fits, the fully correctly $\not{E}_T$ is used.

F. b-quark Jets

Most jets are initiated by a parent light quark (uds) or gluon (g). Thus the identification of at least one of the b-jets in $t\bar{t}$ events significantly reduces contributions from background processes. The b-jet identification algorithms employed by the Tevatron experiments generally exploit two main features of b-hadron decay - their long lifetime and their semi-leptonic decays. While c-hadrons also have some of these same features, on average their lifetimes are shorter and their semi-leptonic branching fractions smaller than those of b-hadrons so that the algorithms employed typically achieve b-identification efficiencies a factor of 2-4 larger than the corresponding c-identification efficiencies, which is sufficient to reduce charm quark related backgrounds to acceptable levels for the $t\bar{t}$ analyses described here.

The branching fraction for a b-hadron into e or μ plus anything is about 20% each (including sequential $b \to c \to eX$ or μX), which is about twice as large as that for c-hadrons, while $udsg$-jets have a negligible e/μ content. The energy of these leptons from b-decay is a few GeV on average, so much "softer" than those from W- or Z-boson decays. Consequently these algorithms are often called "Soft Lepton Tagging" algorithms. Additionally, since they are embedded in jets, these leptons are less isolated. The identification of these electrons and muons uses the same reconstruction algorithms as those discussed in Sec. V.C. To further suppress backgrounds from hadrons mimicking electron or muon signatures these algorithms demand the leptons to have a transverse momentum greater than about 3 GeV/c and make stricter matching requirements between the track and EM calorimeter cluster (electrons) or track segment in the muon chamber (muons). In addition the EM shower shape is exploited to suppress backgrounds for the electron case. The full set of identification criteria is usually combined in a single variable using a relative likelihood function, a global chi-squared, or other similar multivariate techniques. Data control samples of $J/\psi \to \mu^+\mu^-$, $\gamma \to e^+e^-$, and $Z^0 \to \mu^+\mu-$, e^+e^- are used to measure the identification efficiencies. Typical efficiencies achieved are 80-90% for muons in b-hadron jets above the p_T threshold and fiducial to the muon chambers. The efficiencies for electrons in b-hadron jets is about a factor of two lower because the EM tower often includes contributions from nearby hadrons in the jet thus degrading the shower shape criteria. The degree to which this is a problem will partly depend on the segmentation of the EM calorimeter. For both algorithms the rate at which hadrons are mis-identified is about 0.5% per track and varies by about $\pm 20\%$ (relative) as a function of track p_T, track η, or hadron species (ie. $\pi^\pm$ vs $K^\pm$ vs $p/\overline{p}$). These fake rates are determined using samples of $\Lambda \to p\pi^-$, $D^{+*} \to D^0\pi^+ \to K^-\pi^+\pi^+$, and $K_s^0 \to \pi^+\pi^-$ decays. Including the semi-leptonic branching fractions and the track multiplicities in $udsg$-jets these algorithms in combination achieve an efficiency of $\sim 25\%$ per fiducial b-jet in $t\bar{t}$ events and misidentify a $udsg$-jet at a rate of $\sim 0.02 - 0.03$ each. These algorithms and their performance are described in more detail in (Acosta et $al.$, 2005) and (Aaltonen et $al.$, 2010).

The most important b-jet identification algorithms exploit lifetime information by using tracks originating from the b-hadron decay and reconstructing a secondary vertex significantly displaced from the primary interaction vertex. These algorithms exploit all b-decay topologies and thus make use of the full branching fraction. They work on a per jet basis and begin by associating to each jet a set of tracks using the $\eta - \phi$ separation between the track and the jet axis. Only tracks within a given radius (e.g. $R < 0.4$), above a given p_T threshold (e.g. $p_T > 1$ GeV/c), and whose z coordinate at the distance of closest approach to the beam line is consistent with having come from the primary interaction vertex of the event are used to form the candidate secondary vertices. These tracks are vetoed if they form a good vertex and yield an invariant mass consistent with a K_s^0 or Λ when paired with any other track in the same jet. They are also vetoed if they are identified as originating from a photon conversion, $\gamma \to e^+e^-$, in the detector material using dedicated algorithms. At hadron colliders "build-up" algorithms are preferred to "tear-down" algorithms because non-b-decay tracks often out number tracks from b-decay owing to contributions from the under lying event and hadronization process. The build-up algorithms begin by taking the surviving tracks pair wise and making a seed vertex, often times beginning with those tracks having the largest impact parameters relative to the primary interaction vertex of the event. There can be multiple seed vertices per jet. Additional tracks are then added to these seed vertices. The p_T and impact parameter requirements for these additional tracks may be relaxed relative to the requirements made on the tracks forming the seed vertices. Only vertices with good fit-chi-squares are kept and tracks making large contributions to the chi-square are removed. Surviving vertices are then subject to additional selection criteria optimized to suppress the rate of fake tags from $udsg$-jets while maintaining high efficiency for b-jets. In particular the decay length, which is the magnitude of the vector connecting the primary interaction vertex of the event to the candidate secondary vertex is required to fall within the beam pipe (e.g. $\left|\vec{L}\right| < 1.5$ cm at CDF and $\left|\vec{L}\right| < 2.6$ cm at DØ) in order to eliminate interactions in the detector material, the angle between $\vec{L}$ and the jet momentum must be less than $\pi/2$, and the decay length significance must exceed some minimum (e.g. $\left|\vec{L}\right|/\sigma_L > 7$). The algorithms may exploit additional properties of the candidate secondary vertex, like the number

of tracks included in the vertex or the invariant mass of the tracks included in the vertex, to further discriminate b-decay vertices from backgrounds. The efficiency of these algorithms is determined from the data using control samples of b-jets collected with triggers which identify the soft electrons or muons from semi-leptonic b-decays. These samples thus yield the efficiency for semi-leptonic b-decays and tend to have a fairly soft E_T^{jet} spectrum. Monte Carlo simulation is used to extrapolate the efficiencies to generic b-decays and higher jet energies. The Monte Carlo and detector simulation are tuned to accurately reproduce the behavior of the algorithm as measured in the data control sample. Systematic uncertainties account for discrepancies between the data and the Monte Carlo modeling and for the uncertainties associated with the extrapolation to higher jet energies. The rate at which $udsg$-jets are mis-identified by these algorithms is measured in the data using a sample of generic QCD jets collected using only calorimetric trigger information. To get an estimate of the mis-identification rate the experiments exploit the fact that the observed decay length distribution for $udsg$-jets is nominally symmetric about zero with a width dominated by resolution effects. The negative decay lengths correspond to those jets for which the angle between $\vec{L}$ and the jet momentum is larger than $\pi/2$ and are dominated by contributions from $udsg$-jets. The rate of negative decay lengths is thus used to parameterize the mis-identification rate for $udsg$-jets reconstructed with positive decay lengths. The mis-identification rate is parameterized as a function of several variables, such as the number of tracks in the jet, the jet energy, the jet pseudo-rapidity, the number of additional interactions in the events, etc. Small corrections are made to account for the b-jet and c-jet contributions to the negative decay length sample and for contributions to the positive decay length rate from residual photon conversions in the material. These algorithms are tuned to several operating points. The most popular operating point is labeled "Tight" and achieves an efficiency of $\sim 50\%$ per fiducial b-jet in $t\bar{t}$ events and mis-identify $udsg$-jets at a rate of < 0.01 each. The efficiency has a total uncertainty of about 7% (relative) dominated by systematic contributions from uncertainties in the sample composition of the data control sample, the Monte Carlo modeling, and the extrapolation in E_T^{jet}. The mis-identification rates have a total uncertainty of $10 - 20\%$ (relative) dominated by systematic contributions from uncertainties in the sample composition, corrections accounting for trigger biases, and corrections for the b-jet and $\gamma \rightarrow e^+ e^-$ contributions. These algorithms and their performance are described in more detail in (Abazov et $al.$, 2010) and (Acosta et $al.$, 2005).

Other algorithms exploiting the long lifetime of b-decays are sometimes employed such at "jet probability" algorithms, or simple "counting" (displaced tracks) algorithms. In general these are less powerful than the vertex algorithm described above.

Often multiple algorithms are employed and then combined using various multivariate techniques to yield another 10-20% (relative) increase in the efficiency for identifying b-jets for the same $udsg$ misidentification rate. An example is described in detail in (Abazov et $al.$, 2010).

G. Kinematic Fits

In many analyses kinematic fits are employed to fully reconstruct the $t\bar{t}$ kinematics and improve the resolution on the reconstructed momenta of the final state partons from the top-quark decays. The fits constrain the kinematics of each event assuming the $t\bar{t}$ hypothesis and using the decay relevant for the final state in question. In the had channel the six highest E_T jets are assumed to correspond to the quarks from the top-quark and W-boson decays. In the ljt channel the four highest E_T jets are assumed to correspond to the quarks from the top-quark decays and the hadronically decaying W-boson, while the charged lepton is assumed to come from the leptonically decaying W-boson. In the dil channel the two highest E_T jets are assumed to correspond to the b-quarks jets from the top-quark decays and the two (oppositely) charged leptons are assumed to come from the two leptonically decaying W-bosons. In the ljt and dil channels the measured $\not{E}_T$ is used to constrain the x and y components of the neutrino momenta. The measured four-vectors for the jets are corrected using the jet energy corrections described in Sec. V.D and the four-vectors of the leptons incorporate the calibrations described in Sec. V.C. The calibration studies also yield estimates of the corresponding resolutions. The kinematic fit proceeds via a chi-squared minimization. As an example, the chi-squared function employed in the ljt channel, $t\bar{t} \rightarrow \ell\nu qq'b\bar{b}$, is

$$\chi^2 = \sum_{i=\ell,\,\text{jets}} \frac{(p_T^{i,\text{fit}} - p_T^{i,\text{meas}})^2}{\sigma_i^2} + \sum_{j=x,y} \frac{(p_j^{\text{uc, fit}} - p_j^{\text{uc, meas}})^2}{\sigma_{j,\text{uc}}^2} \tag{3}$$

$$+ \frac{(m_{\ell\nu} - m_W)^2}{\Gamma_W^2} + \frac{(m_{jj} - m_W)^2}{\Gamma_W^2} + \frac{(m_{b\ell\nu} - m_t)^2}{\Gamma_t^2} + \frac{(m_{bjj} - m_t)^2}{\Gamma_t^2}. \tag{4}$$

Similar expressions are used for the *had* and *dil* channels except that the $m_{\ell\nu}$ and $m_{b\ell\nu}$ terms are replaced by m_{jj} and m_{bjj} terms or vice versa, respectively. The first term constrains the p_T of the lepton and jets to their measured values within their assigned resolutions, σ_i. The second term makes the same constraints on the x and y components of the unclustered energy in the event. The $\not{E}_T$ is thus derived using these first two terms as discussed in Sec. V.E. The last four terms constrain the reconstructed invariant mass of some combination of final state partons to the pole mass of the object from which they are assumed to have originated. For example, m_{jj} is the invariant mass of the two jets assumed to have originated from the hadronically decaying W-boson and so it is constrained to equal m_W within some tolerance, taken to be the natural width of the W, Γ_W. Similarly for the decay products of the leptonically decaying W-boson and the decay products of each top quark. In the fit, the $p_T^{i,\mathrm{fit}}$ and $p_j^{\mathrm{uc,\,fit}}$ terms are varied to minimize the chi-squared. For most analyses the m_W and m_t values are fixed to the world average measured values. In analyses measuring the top-quark mass, discussed in Sec. IX.C.1, the m_t term is left a free parameter, m_t^{reco}, and corresponds to the reconstructed top-quark mass most consistent with the kinematics of that particular event.

In order to perform the minimization it is necessary to assign each jet as having originated from a particular final state quark. Since the flavors of the parent quarks are unknown, all possible combinations are tried and the combination yielding the lowest fit χ^2 is used. This procedure yields the correct jet-parton assignment 65-85% of the time depending on the details of the selection criteria and decay channel. This ambiguity in the jet-parton assignments gives rise to a combinatoric background from $t\bar{t}$ events for which the incorrect combination is used. The combinatoric background significantly dilutes the resolution with which the $t\bar{t}$ kinematics can be reconstructed. The number of possible jet-parton assignments for an event with N_j jets is $N_{\mathrm{comb}} = N_j!$. Since the χ^2 does not distinguish between a swap in the quark assignments for the jets assumed to have come from the hadronic W-boson decay, the effective number of jet-parton combinations is reduced by a factor of two for each $W \to jj$ decay in the final state. The number of combinations considered can be further reduced by rejecting combinations for which a jet identified as a b-jet is assigned as one of the light-quark jets from the hadronic W-boson decay. For example, in a ljt event reconstructed with 4 jets in the final state, there are $\frac{4!}{2} = 12$ jet-parton assignments considered; this is reduced to six different assignments if one of the jets is identified as a b-jet and only two possible assignments if two jets are identified as b-jets. The combinatoric background is less of a problem in the *dil* channel and is severe in the *had* channel.

The presence of neutrinos in the final state introduces a further ambiguity. In the ljt channel the x and y components are constrained using the estimated $\not{E}_T$, but the z component is unconstrained. In general, each jet-parton assignment yields two different solutions for p_z^ν and both are tried. This doubles the number of χ^2 minimizations performed for each ljt event. For the *dil* channel the kinematics is actually under-constrained due to the presence of two neutrinos from each of the leptonic W-boson decays. In this case it is necessary to make an additional kinematic assumption in order to obtain a reconstructed invariant mass for each event. An integration over the undetermined additional kinematic variable (e.g. the azimuthal angles of the escaping neutrinos) is made and a reconstructed mass is calculated for each assumed value utilizing the kinematic fit. A weight is assigned to each of these possibilities by comparing the observed kinematics with those expected for the assumptions being made (e.g. the direction of the measured $\not{E}_T$). The weighted distribution of reconstructed masses is then used to determined an m_t^{reco} estimate for each event. Specific examples of this methodology are discussed in Sec. IX.C.1.

H. Event Selection Criteria

After the full reconstruction software has been run, the following event selection criteria are employed to identify a sample of candidate $t\bar{t}$ *dil*, ljt, and *had* events. The three samples are statistically independent by construction.

The selection of *dil* events begins by requiring a pair of high energy leptons, e^+e^-, $\mu^+\mu^-$, or $e^\pm\mu^\mp$, with E_T^{lept} exceeding a value around 20 GeV. The events are collected using the inclusive lepton triggers described in Sec. V.A and reconstructed using the algorithms described above. Several lepton selection criteria categories are usually employed ranging from "tight", which yield a very pure sample of leptons, to "loose", which can significantly increase the acceptance but with hadron mis-identification rates that are significantly higher. The analyses usually treat the various lepton-lepton categories (e.g. tight-tight, tight-loose, etc) separately since their signal-to-background ratio are significantly different. The leptons are required to be isolated. Backgrounds from Z^0 events are removed by vetoing events for which either of the leptons, when combined with any other track in the event with $E_T > 10$ GeV, yields an invariant mass consistent with the mass of the Z-boson. The events are also required to have a large missing transverse energy, $\not{E}_T > 20 - 25$ GeV, and at least two jets with $E_T^{\mathrm{jet}} > 15 - 20$ GeV (after correcting to the particle level) and $|\eta| < 2.0 - 2.5$. To reduce contributions from backgrounds for which the $\not{E}_T$ arises from the mis-measurement of a jet or lepton energy, the angle between the $\not{E}_T$ vector and any jet or lepton in the event is required to be larger than some minimum (e.g. $\Delta\phi(\not{E}_T - \mathrm{jet}) > 20°$). To remove backgrounds from semi-leptonically decaying b-jets the lepton-lepton

invariant mass is required to be larger than 5 GeV/c^2. If an e^+e^- event is consistent with having originated from a photon conversion in material, or a $\mu^+\mu^-$ event is consistent with a through going cosmic ray event, they are vetoed. Events with 0 or 1 reconstructed jet are used as background dominated control regions to verify the accuracy of the background estimates. The total acceptance times branching fraction achieved is typically around 0.8% with a purity of around $70-75\%$. If a requirement that at least one of the jets is identified as a b-jet the acceptance times efficiency falls to about 0.5% and the purity rises to about $90-95\%$.

The selection of ljt events begins by requiring a single high energy lepton, typically with $E_T^{\mathrm{lept}} > 20$ GeV, collected using the inclusive $e^\pm$ and $\mu^\pm$ triggers described in Sec. V.A. After employing the reconstruction algorithms described above, "tight" lepton selection criteria are used to identify the primary lepton in each event, which is required to be isolated. Events in which another isolated lepton is identified with $E_T > 10$ GeV are vetoed in order to remove dilepton backgrounds. Dedicated algorithms are used to remove $e^\pm$ events consistent with having originated from photon conversion in the material. The events are also required to have large missing transverse energy, $\not{E}_T > 20-25$ GeV, and at least three jets with $E_T^{\mathrm{jet}} > 15-20$ GeV (after correcting to the particle level) and $|\eta| < 2.0-2.5$. Events with 1 or 2 reconstructed jets are used as background dominated control regions to verify the accuracy of background estimates. The total acceptance times branching fraction achieved is typically around $7-8\%$ with a purity of around $15-20\%$. To improve the purity, most $t\bar{t}$ analyses using the ljt final state require that at least one of the jets in the event be identified as a b-jet. Doing so yields an acceptance times branching fraction of around 4% with a purity of about 60%.

The selection of had events begins with a data sample collected using the multi-jet trigger described in Sec. V.A. After utilizing the reconstruction algorithms described above, events with an identified high energy lepton are removed. Since no missing transverse energy is expected in the all-hadronic final state, the observed $\not{E}_T$ is required to be small relative to the uncertainty with which it is measured, $\not{E}_T / \sqrt{\sigma_{\not{E}_T}} < 3$. Finally, the events are required to have 6-8 reconstructed jets, each with $E_T > 15$ GeV (after correcting to the particle level) and $|\eta| < 2$. Events with 4-5 jets are used as background dominated control regions in which to verify the accuracy of the background estimates. The total acceptance times branching fraction is about 13% with a purity of about 0.3%. To improve the purity, b-jet identification algorithms are employed, as well as multivariate discriminates that use kinematic and event shape information to suppress the background relative to $t\bar{t}$ events. After these additional selection requirements are made, the total acceptance times branching fraction falls to approximately 3% and the purity rises to about 9%.

All the analyses described below begin by using the samples obtained after employing these event selections. Often, depending on the analysis, additional criteria are used to further improve the $t\bar{t}$ purity of the sample. A variety of methodologies are employed to account for the remaining background contributions as described in the next section.

VI. BACKGROUND PROCESSES

After all selection criteria, background events still remain and must be accounted for in order to extract the $t\bar{t}$ physics parameters of interest. A variety of background processes contribute to each $t\bar{t}$ final state and fall into two basic categories: physics backgrounds and instrumental backgrounds. Physics backgrounds are those processes that share the same final state as the $t\bar{t}$ signal sample we are aiming to isolate. For example, the $p\bar{p} \to W + b\bar{b}q\bar{q}$ process, with the W decaying to $e\bar{\nu}$ or $\mu\bar{\nu}$, is a physics background to the $t\bar{t} \to \ell\nu qq'b\bar{b}$ sample. Instrumental backgrounds are those processes which mimic the $t\bar{t}$ final state of interest due to an instrumental effect resulting in a mis-identification of some of the final state objects. For example, the $p\bar{p} \to W + b\bar{b}q\bar{q}$ process, with the W decaying to $e\bar{\nu}$ or $\mu\bar{\nu}$, is an instrumental background to the $t\bar{t} \to \ell^+\nu b\ell^-\bar{\nu}\bar{b}$ sample when one of the jets is mis-identified as a high energy lepton. Although the mis-identification rates are typically very small, $< 1\%$, the instrumental backgrounds can still significantly contribute to the final selected samples due to the very large production cross sections for the relevant QCD and W+jets processes. In general, the acceptances for physics backgrounds are estimated using Monte Carlo simulations, while the instrumental backgrounds are estimated using data control samples. For background processes making small contributions to the final sample, or with well understood theoretical cross sections, the normalization is taken from theory calculations. For all other cases the normalization is taken from the data using background dominated control samples and then extrapolated to the final signal sample. A brief review of the background processes that contribute to the various $t\bar{t}$ final state event samples and how they are estimated is provided here.

The generic QCD process $p\bar{p} \to$ jets has a production cross section that is about 9 orders of magnitude larger than the $t\bar{t}$ production cross section. The jets produced pre-dominantly originate from uds-quarks or gluons, although b-quark jets are produced in a few percent of these events. These generic QCD processes are the dominant background for the $t\bar{t} \to qq'bqq'\bar{b}$ final state with the instrumental background originating from the mis-identification of a $udsg$-jet as a b-quark jet being the most important. For the $t\bar{t} \to \ell\nu qq'b\bar{b}$ final state, the QCD background is sometimes

referred to as the "non-W" background and accounts for roughly 1/5 of the total background. It is an instrumental background and is a consequence of the mis-identification of a jet as an isolated high energy lepton and the mis-measurement of the $\not{E}_T$ which makes it fall into the selected sample. If b-jet identification is required, a further mis-identification of one of the $udsg$-jets is also necessary in order for the event to survive all selection criteria. All these fake rates are taken from data control samples and applied successively in order to estimate the contribution of this background to the final selected sample. There are large uncertainties associated with this background which arise from the relatively low statistics of surviving events in the control samples once the identification criteria are applied (ie. because the mis-identification rates are quite small) and from systematic uncertainties accounting for kinematic differences between the control samples and the signal sample. For the $t\bar{t} \to \ell^+\nu b \ell^- \overline{\nu} b$ final state this background is negligible since two jets would need to be mis-identified as an isolated high energy lepton and the $\not{E}_T$ would have to be mis-measured.

The W-plus-jets processes have production cross sections about three orders of magnitude greater than the $t\bar{t}$ process and are an important background to the $t\bar{t} \to \ell\nu qq'b\bar{b}$ and $t\bar{t} \to \ell^+\nu b \ell^- \overline{\nu} b$ final states. When the W decays leptonically, there is a genuine high energy lepton and genuine $\not{E}_T$ in the event. For the ljt final state, prior to making a b-jet identification requirement, these processes appear as physics background. Accordingly their acceptance is estimated from Monte Carlo, however their normalization is taken from the data since there are large theoretical uncertainties associated with the predicted production cross-section. These uncertainties arise because complete calculations of the $W + 3$ jets and $W + 4$ jets cross sections, including heavy flavor contributions, are unavailable and current estimates rely on a mixture of partial calculations at lower orders and parton shower Monte Carlo models to extrapolate to larger jet multiplicities. When b-jet identification is required, this background is separated into two pieces: the $W+$ light flavor ($W + lf$) contributions, where the additional jets all originate from uds-quarks or gluons, and $W+$ heavy flavor ($W + hf$) contributions, where at least one of the additional jets originates from a c- or b-quark. The $W + lf$ contributions is then an instrumental background since one of the $udsg$-jets would need to be mis-identified as a b-quark jet. As mentioned above the mis-identification rate of the b-jet identification algorithm is taken from data control samples to estimate the contribution from this instrumental background, sometimes referred to as the "mis-tag" contribution. The $W + hf$ contribution to the background uses Monte Carlo samples to estimate the fraction of surviving events which contain c- or b-quark jets and the efficiency of the b-jet identification algorithm to determined the number of events surviving the full selection requirements. There are large uncertainties associated with the heavy flavor fractions determined from the Monte Carlo, which are cross checked in data control samples. The $W+$ jets processes are the dominant backgrounds to the $t\bar{t} \to \ell\nu qq'b\bar{b}$ final states. For the $t\bar{t} \to \ell^+\nu b \ell^- \overline{\nu} b$ final states these processes are an instrumental background since one of the jets must be mis-identified as a high energy isolated lepton in order to survive the full selection criteria. This background is estimated from the data starting with the single-lepton-plus-$\not{E}_T$ sample and then applying lepton mis-identification rates determined from data control samples to estimate the number of "lepton fakes" which populate the final dilepton sample.

A related background, $Z/\gamma+$ jets, has a production cross section roughly a factor of ten smaller than the $W+$-jets background. It contributes to the $t\bar{t} \to \ell\nu qq'b\bar{b}$ sample only if the Z^0/γ^* decays to e^+e^- or $\mu^+\mu^-$ and if one of the leptons escapes undetected to give rise to fake $\not{E}_T$. This latter effect is dominated by the limited geometric acceptance of the detector and is thus estimated from the Monte Carlo and found to be a negligible contribution to any of the samples. For the ljt sample the only significant contributions arises from Z^0/γ^* decays to $\tau^+\tau^-$ with the subsequent decay of one of the τ leptons to $\tau^\pm \to e^\pm \nu_\tau \overline{\nu_e}$ or $\tau^\pm \to \mu^\pm \nu_\tau \overline{\nu_\mu}$ in order to generate a lepton and $\not{E}_T$ to survive the selection criteria. Once the relevant branching fractions are included, this turns out to be a small background and is estimated from the Monte Carlo. If b-jet identification is required, the relevant efficiency and mis-identification rates are taken from data control samples and applied to the surviving Monte Carlo events. For the dil sample this is potentially an important background since Z^0/γ^* decays to e^+e^- or $\mu^+\mu^-$ yield two high energy isolated leptons. However to survive the full selection criteria the $\not{E}_T$ must be mis-measured. This is an instrumental background whose residual contribution to the final sample is estimated from the data using clean samples of identified $Z^0 \to e^+e^-$ or $\mu^+\mu^-$ parameterizing the fake $\not{E}_T$ distribution, and extrapolating to the $t\bar{t}$ signal region. There are relatively large uncertainties associated with this background associated with extrapolating this estimate from the low jet multiplicity region which dominates the data control sample, to the $>= 2$ jets region of the signal region.

The diboson processes $p\overline{p} \to VV$ ($V = W^\pm$, Z^0, or γ) have production cross sections within a factor of two of the $t\bar{t}$ cross section. When the $W^\pm$ and/or Z^0/γ bosons decay leptonically these processes make small contributions to the ljt samples and large contributions to the dilepton samples . These are physics backgrounds whose estimates are taken from Monte Carlo and normalized to theoretical predictions calculated to next-to-leading order. If b-jet identification is required, the relevant efficiency and mis-identification rates are taken from data control samples and applied to the Monte Carlo.

The production of a single top quark via the electroweak interaction, $p\overline{p} \to tq$, has a production cross section about

a factor of two smaller than the $t\bar{t}$ cross section and makes a small contribution to the $t\bar{t} \to \ell^+\nu b\ell^-\overline{\nu}\overline{b}$ final state. It is a physics background and is estimated using Monte Carlo samples normalized to the theory predicted cross section.

VII. SIMULATION SAMPLES

A variety of Monte Carlo generators are employed to estimate acceptances, efficiencies, and kinematics for $t\bar{t}$ and background events. A summary of which generators are used to model each physics process is given here. In several cases multiple generators are employed and their comparison is used to assess systematic uncertainties. For the analyses described in this review, the Monte Carlo generators are always combined with simulation software that models the detector response in detail. The resulting simulated samples are then treated just like the recorded $p\overline{p}$ collision data, using the same reconstruction software and particle identification algorithms described in Sec. V. For all samples the decay of tau leptons is handled using the TAUOLA package (Davidson *et al.*, 2010) and the decay of c- and b-quark hadrons is handled using the EVTGEN package (Lange and Ryd, 1998). The parton shower and fragmentation processes required to simulate the evolution of a parent quark or gluon into a final state jet are modeled using dedicated sub-routines in either the PYTHIA (Sjöstrand *et al.*, 2001) or HERWIG (Corcella *et al.*, 2001) Monte Carlo software packages. The parton shower is modeled using DGLAP evolution (Gribov and Lipatov, 1972) while the fragmentation process is simulated using a string model in PYTHIA and a cluster model in HERWIG. Initial and final state QED radiation effects are included for all initial and final state charged particles.

The CDF and DØ collaborations each employ several Monte Carlo generators to model $t\bar{t}$ events. The PYTHIA and HERWIG programs are general purpose event generators widely used throughout high energy physics. They model a wide variety of interactions and processes using leading order calculations. Although the programs include only leading order calculations (e.g. $p\overline{p} \to t\bar{t}$), the parton shower and QED radiation modeling can yield more complicated event topologies (e.g. $p\overline{p} \to t\bar{t} + \text{jets}$ or $t\bar{t} + \gamma$). However, the resulting cross sections and kinematics of these higher order final states usually carry large uncertainties since their modeling can be quite sensitive to arbitrary choices of control parameters offered by each generator. Reasonable choices of the various control parameters are made by making detailed comparisons between the data and Monte Carlo samples in dedicated studies using control samples of inclusive jet and minimum bias events. For most of all the $t\bar{t}$ analyses described in this review, the higher order contributions affect the physics parameters of interest at a level that is negligible compared to the sensitivity of the present measurements. Consequently the PYTHIA program is often used to model the $t\bar{t}$ events at the Tevatron. A more rigorous approach expected to yield improved cross section and kinematic modeling of more complicated final states is offered by the MADEVENT (Alwall *et al.*, 2007) and ALPGEN (Mangano *et al.*, 2003) programs. These programs explicitly calculate the lowest order contributions to a given process (e.g. $p\overline{p} \to t\bar{t} + 1$ parton) and then use PYTHIA or HERWIG to model the parton shower and fragmentation processes. To model an inclusive sample, as observed in the data, requires the summing of several samples. For example, to model a $t\bar{t} + \geq 0$ jets sample requires an ALPGEN simulation of $t\bar{t} + 0p$ plus $t\bar{t} + 1p$ plus $t\bar{t} + \geq 2p$ samples. Since the parton shower can generate additional final state jets in each sample, care must be taken to avoid double-counting. Common choices to remove this overlap include those described in (Alwall *et al.*, 2008). Several of the analyses described in this review employ a series of ALPGEN+ PYTHIA or MADEVENT+PYTHIA samples to simulate the inclusive $t\bar{t}$ signal samples. The MC@NLO (Frixione and Webber, 2002) program is a full next-to-leading order generator used to simulate $t\bar{t}$ samples employed for systematic studies.

The W+jets and Z+jets samples are generated using ALPGEN with the parton shower and fragmentation modeling provided by PYTHIA. Sometimes the PYTHIA generator is used by itself to model the fully inclusive sample. In all cases the normalization is taken from the data using selection criteria expected to yield a sample of events dominated by these processes.

The diboson processes, VV ($V = W^\pm$, Z^0, or γ), are modeled either using ALPGEN+ PYTHIA or PYTHIA by itself. The samples are normalized to the theory predicted cross sections calculated to next-to-leading order.

Electroweak processes which result in the production of a single top quark are generated using either SINGLETOP (Boos *et al.*, 2006) or MADEVENT with the parton shower and fragmentation modeling provided by PYTHIA. The samples are normalized using the next-to-leading order theory predicted cross section. The s-channel and t-channel processes are generated independently.

Generic QCD processes are modeled using PYTHIA or HERWIG or ALPGEN+ PYTHIA. In general the predictions for the QCD background contributions to the final selected sample are taken from data control samples. However, several parameters important for $t\bar{t}$ analyses are taken from dedicated studies performed using multi-jet samples dominated by genuine QCD production processes. These studies often require some inputs from these QCD Monte Carlo samples. For example, the efficiency of the b-jet identification algorithms is determined using a di-jet sample and the ratio of

the data determined efficiency to the Monte Carlo predicted efficiency is used to correct the Monte Carlo predicted efficiency in $t\bar{t}$ samples. Another example, di-jet samples are used to compare the heavy-flavor contribution between data and Monte Carlo in order to derive a correction for the Monte Carlo predicted ratio $W + hf/W + $ jets. The QCD samples used in these studies must be simulated in a manner consistent with that used to model the $t\bar{t}$ and other background Monte Carlo samples so that the corrections derived can be used in the final selected samples with confidence.

VIII. SOURCES OF SYSTEMATIC UNCERTAINTY

A variety of systematic uncertainties are evaluated for each of the analyses described in this review. They fall into three general categories: uncertainties associated with the background modeling, uncertainties associated with the signal modeling, and uncertainties associated with the methodology employed to extract the physics parameter(s) of interest. The sources of uncertainty affecting the signal and background modeling and the methods employed in evaluating them, are common across all the $t\bar{t}$ analyses and are summarized here.

A. Systematic Uncertainties Associated with Background Processes

The systematic uncertainties affecting the background modeling include instrumental effects related with the various mis-identification rates required to promote a background physics process into the signal region, theory related uncertainties such as variations of the factorization and renormalization scales, k-factors related to NLO corrections, and differences in parton shower and fragmentation modeling, as well as uncertainties in normalization arising from uncertainties in lepton, b-quark jet, etc. identification efficiencies. Several sources of uncertainty affect multiple background processes and their effects are accounted for in the analyses in a correlated manner.

The mis-identification rate for hadrons faking an electron or muon signature and for $udsg$-jets faking a b-jet are derived from data control samples. The mis-identification rates are parameterized by an empirically determined functional form, which includes the dependence of the rate on relevant kinematic variables (e.g. jet E_T or $|\eta|$). The validity of the parameterization is tested using statistically independent data control samples. Differences between the predicted rate, as determined using the parameterization, and the observed rate are used to assign systematic uncertainties on the mis-identification rates themselves. These uncertainties are then propagated to the number of predicted background events for those background processes for which the relevant mis-identification is required in order for that process to mimic a $t\bar{t}$ signal event. Since these mis-identification rates depend on the kinematics of the events, they also introduce a systematic uncertainty on the shape of the resulting kinematic distributions of background events surviving the full event selection criteria. These "shape" systematics are usually evaluated by re-weighting the relevant kinematic distributions using the mis-identification parameterizations varied by $\pm 1\sigma$.

When generating the $W + $ jets samples there is an ambiguity associated with the choice of factorization and renormalization scales, represented in the literature as μ_F, μ_R, and/or Q^2, at which to evaluate the relevant matrix element. Some typical choices for $W + $ jets processes are $Q^2 = p_{T,W}^2$, $(M_W^2 + p_{T,W}^2)$, or $(M_W^2 + \sum_i p_{T,i}^2)$, where the sum runs over all the outgoing partons at a given vertex. The nominal background estimates are estimated using the last choice. A full set of additional Monte Carlo samples are generated using other alternative choices of Q^2 and the background predictions and kinematic distributions are re-evaluated. Differences are assigned as a systematic uncertainty affecting the $W + $ jets background processes. It should be noted that this ambiguity affects all the generated samples. However in the other samples it produces negligibly small systematic uncertainties.

All the background processes are generated with at least two different Monte Carlo generators. For those Monte Carlo samples which reasonably model the observed data distributions, the background yields and kinematic distributions are evaluated in full. Differences between the nominal Monte Carlo sample and any viable alternative sample are assigned as systematic uncertainties. This systematic primarily accounts for differences in parton shower and fragmentation modeling.

Most all of the Monte Carlo samples employed in the analyses described here are based on leading order theory calculations. The inclusion of higher order corrections affect the predicted production cross section for the various background processes. These effects are accounted for in the analysis either by normalizing the Monte Carlo yields to next-to-leading order calculations, or by normalizing to the data itself. Some residual higher-order effects still remain. Most importantly is the $W + hf$ fraction of the $W +$ jets background. The fraction is taken from the ALPGEN generator, but scaled to the heavy flavor fraction measured in the $W + 1$ jet sample. There is a large uncertainty associated with extrapolating that measured fraction to the $W + \geq 2$ jets regions used in the $t\bar{t}$ analyses. The uncertainty is

evaluated by comparing the measured heavy flavor fraction derived using different methodologies as well as comparing the result derived using the $W + 1$ jet sample to that derived using the $W + 2$ jet for the ljt channel. The differences are assigned as systematic uncertainties and propagated to the predicted number of $W + hf$ events contributing to the final background.

The electron and muon identification efficiencies, the relevant trigger efficiencies, and the b-quark jet identification efficiencies all have associated statistical and systematic uncertainties. These uncertainties are propagated through each of the affected background processes by varying each in turn by $\pm 1\sigma$. These variations result in uncertainties on the number of contributing events for the affected background processes. For those efficiencies that have a kinematic dependence, their effect on resulting kinematic distributions is also evaluated by re-weighting the affected distributions using parameterizations that bracket the $\pm 1\sigma$ variations of the relevant kinematic dependencies.

The uncertainty on the jet energy scale is propagated by varying the parameterized jet energy corrections by $\pm 1\sigma$ and re-evaluating the predicted number of background events and the resulting kinematic distributions. This uncertainty affects all the background processes.

The total uncertainty on the predicted background events is the quadrature sum of these various sources. When a particular source of uncertainty affects multiple background sources, the resulting correlation is accounted for by adding the resulting uncertainties linearly and then adding the resultant sub-total quadratically with the rest of the systematic uncertainties.

B. Systematic Uncertainties Associated with $t\bar{t}$ Modeling

The systematic uncertainties affecting the modeling of $t\bar{t}$ production and decay include variations of initial and final state radiation, variations in the parton distribution functions, variations in the parton shower and fragmentation modeling, variations in the modeling of color reconnection effects in final state interactions between the t and $\bar{t}$ decay products, and uncertainties associated with the trigger, lepton identification, and b-jet identification efficiencies. Some of these sources of uncertainty also affect background processes and their effects are accounted for in the analyses in a correlated manner.

Uncertainties in the modeling of initial state radiation (ISR) and final state radiation (FSR) are evaluated by generating $t\bar{t}$ Monte Carlo samples with their ISR and/or FSR parameters varied by $\pm 1\sigma$ relative to the default sample. The range of variation which defines "1σ" is determined using $p\bar{p} \to Z^*/\gamma^* \to \mu^+\mu-$ samples. Like $t\bar{t}$ production at the Tevatron, this process is dominated by $q\bar{q}$ annihilation. The $p_T^{\mu^+\mu^-}$ and the N_{jet} distributions are used to constrain the parameters in the Monte Carlo affecting the ISR modeling. The constraints are derived in bins of $M_{\mu\mu}^2$ and extrapolated to $M_{\mu\mu}^2 = 4M_t^2$. Since the ISR and FSR processes in the Monte Carlos are both modeled using DGLAP evolution, the same variations are used to assign systematics for FSR. Samples are produced varying ISR only, FSR only, and ISR/FSR simultaneously. The sample resulting in the largest difference relative to the nominal sample is used to assign the associated systematic uncertainty.

The parton distribution functions result from multi-dimensional fits to dozens of measurements made by a variety of different experiments. The CTEQ and MRST collaborations provide eigenvectors representing $\pm 1\sigma$ variations of 20 uncorrelated parameters affecting the resulting PDFs. The difference associated with each variation is evaluated by reweighing the $t\bar{t}$ events in the nominal Monte Carlo sample using each eigenvector in turn. The $+1\sigma$ and -1σ variations are quadratically summed separately. In addition, samples generated with different α_s and PDF fits from different collaborations are also generated and differences included in the associated PDF systematic uncertainty.

The signal $t\bar{t}$ samples are generated with several different Monte Carlo generators. For those Monte Carlo samples which reasonably model the observed data distributions, the $t\bar{t}$ yields and kinematic distributions are evaluated in full. Differences between the nominal Monte Carlo sample and any viable alternative sample are assigned as systematic uncertainties. This systematic primarily accounts for differences in parton shower and fragmentation modeling but also includes possible effects from differences in the modeling of the $t\bar{t}$ p_T spectrum, $t\bar{t}$ spin correlations, and final state radiation.

Since top-quarks and W-bosons decay quickly relative to the timescale associated with the parton shower and fragmentation processes (i.e. $1/\Gamma_t, 1/\Gamma_W << 1/\lambda_{QCD}$) it is possible that the products from the *different* top-quark decays could interact with each other via color reconnections. By default, all Monte Carlo generators ignore such reconnections since they are non-existent or irrelevant for most processes. These color reconnection effects were first investigated at LEP2 (e.g. (Abbiendi *et al.*, 2006)). Since Tevatron's $p\bar{p}$ initial state carries the color charge, the situation and its modeling is significantly more complicated that at LEP, which used an e^+e^- initial state. Recently, Monte Carlo models providing an adequate description of Tevatron $p\bar{p}$ minimum bias and underlying events and including color reconnection effects have become available. The associated systematic uncertainty is evaluated by

generating $t\overline{t}$ samples with these various color reconnection models enabled and comparing to the nominal Monte Carlo sample. Difference are assigned as systematic uncertainties.

The uncertainties associated with the electron and muon identification efficiencies, the relevant trigger efficiencies, the b-quark jet identification efficiencies, and the jet energy scale uncertainties are all evaluated in the manner described in the sub-section above. These uncertainties also affect some or all of the background processes. The resulting correlations are correctly accounted for in the analyses.

The total uncertainty on the predicted $t\overline{t}$ yields and resulting kinematic shapes is the quadrature sum of these various sources. Correlations with the background processes are included.

IX. MEASUREMENTS OF TOP-QUARK PROPERTIES

A. Production Properties

1. $t\overline{t}$ Cross Section

At hadron colliders top quarks are predominantly produced in $t\overline{t}$ pairs via the strong interaction. Measuring the $t\overline{t}$ production cross section is interesting for several reasons. First it allows a precise test of the predictions from perturbative QCD. Computations of the $p\overline{p} \to t\overline{t}$ total rate are available at NLO (Nadolsky et $al.$, 2008). Several approximate NNLO computations, where the dominant (next to) next to leading logarithm terms are resummed to reduce sensitivity to the renormalization and factorization scales, are also available (Ahrens et $al.$, 2010; Cacciari et $al.$, 2008; Kidonakis and Vogt, 2008; Langenfeld et $al.$, 2009). For a top-quark mass of 172 GeV/c^2, the latest calculations predict a cross section of about $\sigma(p\overline{p} \to t\overline{t}) = 7.6$ pb with a relative precision of about ± 8 %. Comparing the measurements with these predictions is important since various BSM theories postulate new particles that couple preferentially to the top quark and thus predict a higher $t\overline{t}$ production rate. A typical example is the production of new resonant particles that decay into $t\overline{t}$ (Frederix and Maltoni, 2009).

It is also particularly important to measure the production cross section in different top-quark decay channels since new physics contributions can affect the various $t\overline{t}$ final states, differently. Examples of such models are Two Higgs Doublet Models among which are SUSY models (Chung et $al.$, 2005; Grossman, 1994) predicting the existence of charged Higgs bosons, $H^{\pm}$. If such a charged Higgs boson is light enough ($m_{H+} < m_t - m_b$), the decay $t \to H^+ b$ can compete with the SM decay $t \to W b$; the measured $t\overline{t}$ production rate will then differ among the various final states due to contributions from charged Higgs decays.

To make precise measurements of the $t\overline{t}$ production cross section requires a good understanding of the reconstruction and identification efficiencies as well as a careful evaluation of the background processes that mimic the $t\overline{t}$ signal. Because of this, the cross section analysis also then serves as a foundation on which most the rest of the $t\overline{t}$ analyses are built. The $t\overline{t}$ cross section measurement is performed by evaluating the following formula:

$$\sigma_{t\overline{t}} = \frac{N_o - N_b}{\epsilon_{t\overline{t}} \mathcal{B} \int \mathcal{L} dt} \tag{5}$$

where N_o is the observed number of events after selection, N_b is the estimated mean number of background events, $\epsilon_{t\overline{t}}$ is the signal efficiency evaluated using $t\overline{t}$ Monte Carlo, $\mathcal{B}$ is the relevant final-state-dependent $t\overline{t}$ branching fraction, and $\int \mathcal{L} dt$ is the integrated luminosity for the particular set of triggers used for the measurement. It is worth noting that since $\epsilon_{t\overline{t}}$ is increasing with the top-quark mass the measured cross section is quoted at a given m_t. The numerator in Eq. 5 can be evaluated either using event counting after applying the final selection criteria or by fitting a discriminant variable that separates signal and background to estimate the relative contributions of each to the surviving event sample. The use of b-tagging is helpful to discriminate $t\overline{t}$ signal from background. If b-tagging is employed, $N_o - N_b$ is usually evaluated by event counting as for events with many b-jets the signal purity is higher.

$t\overline{t}$ Cross Section in the Lepton-plus-jets Channel

In the ljt channel one of the W bosons decays into electron or muon plus a neutrino, while the other decays into two quarks. The final state thus contains at least four jets in the event, two of which are b-jets, plus a high energy electron or muon and large $\not{E}_T$. This final state has the advantage of a reasonable branching fraction while achieving a good signal-to-background ratio. The event selection begins as describes in Sec. V.H. For the cross section analyses additional selection criteria are often applied. For example, the total transverse energy of the event,

$H_T = \sum_l E_T^l + \sum_j E_T^j + \not{E}_T$, where the sums are over all high energy leptons and jet, respectively, is required to be above some minimum. At this point, further enrichment of the selected sample in $t\bar{t}$ events is achieved by applying either a multivariate discriminant using topological information or using b-jet identification. The topological information in the multivariate discriminate usually excludes any information explicitly related to b-jet identification. In this way the resulting cross section measurements make no assumption about the flavor of the quark in the $t \rightarrow Wq$ decay. Experimentally the final event samples are split according to lepton flavor (e or μ), jet multiplicity (3 or ≥ 4 jets) and (if used) number of identified b-jets (0, 1 or ≥ 2) and treated separately. Events with < 3 jets are used as background dominated control samples.

The main background processes that can mimic a $t\bar{t}$ event were discussed in Sec. VI. The most important contributions for the ljt final state are, in decreasing order of importance, W+jets production, QCD multi-jet processes, Z+jets, diboson processes and electroweak single top-quark production. The Z+jets, diboson, and single top backgrounds are evaluated using MC normalized to (N)NLO theoretical cross sections. As no reliable estimation of QCD multi-jet can be obtained by MC, this background is estimated using data. For the most important background: W+jets production, no reliable NLO calculation exists to estimate the W+jets cross section at the large jet multiplicities relevant for $t\bar{t}$ analyses. Therefore we derive the normalization from data and use the MC to estimate the W+jets kinematic distributions.

The QCD multi-jet background is estimated from data. For example, DØ uses a matrix method (Abazov *et al.*, 2006). It consists of solving a 2D system of linear equations based on the number of events selected in two datasets defined as:

$$N_{loose} = N_{QCD} + N_{sig}$$
$$N_{tight} = \epsilon_{QCD} N_{QCD} + \epsilon_{sig} N_{sig}$$

$$(6)$$

where N_{loose} is the number of events in a data sample surviving loose lepton selection criteria, while N_{tight} is the number of events in a subsample surviving tight lepton isolation requirements. N_{QCD} is the number of QCD multi-jet events in the sample we want to determine and N_{sig} is the number of events that do not come from multi-jet events (dominated by W+jets and $t\bar{t}$ events). The efficiency for the loose lepton from a W-boson decay to survive the tight lepton selection criteria is ϵ_{sig}, which is estimated using W+jets and $t\bar{t}$ MC corrected for any data-MC difference. Similarly, ϵ_{QCD} is the expected fraction of QCD events in the loose lepton sample that are expected to survive the tight lepton selection criteria. It is measured in a data sample with low $\not{E}_T$ which is dominated by wrongly isolated leptons after subtracting real isolated lepton contributions. Solving this linear system yields an estimate for the number of QCD multi-jet events in the sample of interest

$$N_{QCD} = \frac{\epsilon_{sig} N_{loose} - N_{tight}}{\epsilon_{sig} - \epsilon_{QCD}}.$$

$$(7)$$

CDF uses a slightly different method to obtain an estimate of the QCD background contributions. The $\not{E}_T$ distribution is fit to a combination of QCD multi-jet and W+jets shapes. The W+jets shape is taken from the ALPGEN MC. The QCD shape is formed from data events that fail at least two lepton identification criteria. The fraction of QCD multi-jet events in the high $\not{E}_T$ region is then extrapolated from a fit to the low $\not{E}_T$ region.

The total amount of W+jets contribution is normalized to the number of events in data minus the estimated number of $t\bar{t}$, QCD multi-jet and electroweak processes. Among the W+jets events the contribution from $W + hf$ is found to be underestimated in the MC simulation. An additional scaling determined from data is applied to the $W + hf$ MC samples. The $W + hf$ content is measured in data events with ≤ 2 jets using a neural network (NN) trained to separate $W + lf$ from $W + hf$. By counting the number of events in the part of the NN distribution dominated by $W + hf$ or performing a fit to the full NN distribution using templates for $udsg$-jets, c-jets, and b-jets, we determine the ratio $W + hf/W + lf$ after unfolding the relevant tagging efficiencies. This can be compared with the ratio predicted in MC and a correction applied to the MC if necessary. In practice the CDF and DØ experiments find that the data-to-MC ratio for this heavy flavor fraction varies between $1.0 - 1.6$ depending on the method employed and the event samples used. Their analyses typically use a value of around 1.3 with systematic uncertainties assigned that cover the full spread. This correction factor is then applied to all the jet multiplicity bins. DØ is using an additional scale factor for the $W + c$ samples based on next leading order computations.

The topological cross section measurements use the output of a multivariate discriminant, a neural network (NN) for CDF or a boosted decision tree (BDT) for DØ, to further discriminate $t\bar{t}$ signal from the background. These discriminants exploit differences in the kinematic properties of signal and background. Indeed because of the large top-quark mass, $t\bar{t}$ events are on average more energetic, more central, and more isotropic than W+jets and QCD

events. Hence several kinematic distributions that are well modeled by MC simulation and that have a good separation power between signal and background are used as input to the multivariate discriminant such as H_T, the planarity, the sphericity (defined below), the lepton-$\not{E}_T$-jets invariant mass, the minimum angle between two jets, the minimum invariant mass of any two jets, etc. Multivariate output templates for the $t\bar{t}$ signal and for the QCD, W+jets and diboson backgrounds are then formed and used in a likelihood fit of the observed NN or BDT data distribution to determine the fraction of $t\bar{t}$ events in the selected sample. This fraction can then be used to determine the $t\bar{t}$ cross section. DØ uses a nuisance parameter method (Sinervo, 2003) to simultaneously extract the result and constrain the corresponding systematic uncertainties. This method can lead to an improved total uncertainty.

Utilizing only topological information CDF uses a data set of 4.6 fb^{-1} to measure (Aaltonen *et al.*, 2010) $\sigma_{t\bar{t}} = 7.71 \pm 0.37$ (stat) ± 0.36 (syst) ± 0.45 (lumi) pb while DØ uses 4.3 fb^{-1} to measure (Abazov *et al.*, 2010) $\sigma_{t\bar{t}} = 7.70^{+0.79}_{-0.70}$ (stat + syst) pb, both for a 172.5 GeV/c^2 top-quark mass. These measurements are systematics limited. Apart from the uncertainty on the luminosity, the dominant sources of systematic uncertainty are the uncertainties on the jet energy scale, jet energy resolution, and signal modeling. The precision of these measurements is around 9 %. Figure 5 shows the distributions for the CDF NN and DØ BDT discriminants used in these topological analyses.

Aside from using pure topological information, the data sample can alternatively be enriched in $t\bar{t}$ events by identifying b-jets using one of the methods described in Sec. V.F. In that case, apart from the $W + hf$ background estimated as described above, the contribution from $W + lf$ events when a $udsg$-jet is mis-identified as a b-jet has to be determined. Since this mis-identification rate is difficult to model using MC, it is determined using a data sample dominated by generic QCD multi-jet events and parametrized as a function of the relevant kinematic variables (e.g. the jet p_T and η). This probability is then applied to MC $W + lf$ samples to estimate the number of mis-identified $W + lf$ events contributing to the final b-tagged sample. A maximum likelihood fit is performed on the data, using the predicted background as an input, to extract the $t\bar{t}$ production cross section. Often times the likelihood includes nuisance parameters that allow, for example, the background normalization and b-jet identification efficiency, to vary within their uncertainties. The likelihood is constructed to account for the correlations between the background and signal acceptances for each of the nuisance parameters.

Utilizing b-jet identification algorithms that exploit the long lifetime of b-hadrons CDF uses 4.3 fb^{-1} of data to measure (Aaltonen *et al.*, 2010) $\sigma_{t\bar{t}} = 7.22 \pm 0.35$ (stat) ± 0.56 (syst) ± 0.44 (lumi) pb while DØ uses 4.3 fb^{-1} to measure (Abazov *et al.*, 2010): $\sigma_{t\bar{t}} = 7.93^{+1.04}_{-0.91}$ (stat + syst) pb, both for a 172.5 GeV/c^2 top-quark mass. Apart from the uncertainty on the luminosity, the dominant sources of systematic uncertainty come from the estimation of the $W + hf$ background and from the uncertainty on the efficiency for identifying b-jets. Using b-jet identification algorithms that identify leptons from semi-leptonic b-hadron decays, CDF has measured cross sections consistent with those above but with larger uncertainties due to the lower efficiency and purity achieved by these soft-lepton algorithms (Aaltonen *et al.*, 2010; Acosta *et al.*, 2005). Figure 6 shows the jet multiplicity distribution in the CDF and DØ analyses that use lifetime information to identify b-quark jets.

The largest systematic uncertainty for both the topological and b-tag based measurements is the uncertainty on the luminosity. It originates from the uncertainty on the luminosity counter acceptance and from the uncertainty on the knowledge of the $p\bar{p}$ inelastic cross section and totals about ± 6 %. It can be effectively removed by measuring the $t\bar{t}$ cross section relative to a cross section whose theoretical predictions are known to much better than 6%. A good choice at the Tevatron is to normalize to the inclusive $Z/\gamma^* \to \ell\ell$ cross section. It can be collected on the same trigger as the $t\bar{t}$ sample, offers reasonably large statistics (1-2 orders of magnitude more than the $t\bar{t}$ sample), and can be reconstructed with high purity ($> 95\%$). The expression for determining the $t\bar{t}$ production cross section is then

$$\sigma_{t\bar{t}} = \left(\frac{\sigma_{t\bar{t}}}{\sigma_{Z/\gamma^* \to \ell\ell}} \right)_{measured} (\sigma_{Z/\gamma^* \to \ell\ell})_{theoretical}. \tag{8}$$

Hence the luminosity uncertainty is traded with the theoretical uncertainty on the Z/γ^* cross section. The inclusive $Z/\gamma^* \to \ell\ell$ cross section is measured using consistent trigger requirements and lepton identification with the $t\bar{t}$ cross section. The $Z/\gamma^* \to \ell\ell$ cross section times branching ratio measured by CDF (Aaltonen *et al.*, 2010) in the dilepton invariant mass range of 66-116 GeV/c^2 is $\sigma_{Z/\gamma^* \to \ell\ell} = 247.8 \pm 0.8$ (stat) ± 4.4 (syst) ± 14.6 (lumi) pb. Taking $(\sigma_{Z/\gamma^* \to \ell\ell})_{theoretical} = 251.3 \pm 5.0$ pb (Martin *et al.*, 2004) we can extract $\sigma_{t\bar{t}}$ using (8) taking all relevant systematic correlations between the $t\bar{t}$ and Z/γ^* cross sections into account (Aaltonen *et al.*, 2010) $\sigma_{t\bar{t}} = 7.82 \pm 0.38$ (stat) ± 0.37 (syst) ± 0.15 (theory) pb for the CDF topological selection and $\sigma_{t\bar{t}} = 7.32 \pm 0.36$ (stat) ± 0.59 (syst) ± 0.14 (theory) pb for the CDF b-tagging selection, both for a 172.5 GeV/c^2 top-quark mass. These two measurements are combined to give (Aaltonen *et al.*, 2010): $\sigma_{t\bar{t}} = 7.70 \pm 0.52$ pb for a 172.5 GeV/c^2 top-quark mass. The precision of the combined result is now 6.8%, which is more precise than the latest theory predictions.

In the dil channel both W bosons decay to leptons. The event then contains two high E_T isolated leptons, large $\not{E}_T$, and two b-jets. This channel is often sub-divided further according to the explicit lepton identification criteria employed. When both leptons are reconstructed as an electron or muon the sample is dominated by $t \to Wb \to e\nu b$ and $t \to Wb \to \mu\nu b$ decays ($\ell\ell$ channel). The acceptance can be significantly increased, particularly for $Wb \to \tau\nu \to h\nu\nu\nu$ decays, by applying very loose criteria for one of the lepton legs (ℓtrack). Measurements have also been performed in the final state with a τ lepton decaying into hadrons explicitly identified from the decay of one W boson and an accompanying electron or muon from the other W boson decay ($\ell\tau$ channel). In general the dil channel has the advantage of a good signal to background ratio even without using b-tagging but suffers from a smaller branching fraction than the ljt or had channels.

In the dil channel, the main source of background comes from the production of electroweak bosons that decay to charged leptons. For the $\ell\ell$ channel, it arises from Drell-Yan processes, $Z/\gamma^* \to \ell^+\ell^-$, and diboson processes when the bosons decays lead to at least two leptons in the final state. These backgrounds are reduced by requiring ≥ 2 jets and large $\not{E}_T$. In the $\ell\tau$ and ℓtrack channels, the main background comes from processes with jets mis-identified as an electron, τ, or isolated track, or from muons from semi-leptonic b-quark decay. This occurs mainly in W+jets or QCD events. The Z/γ^*+jets and diboson backgrounds are evaluated using MC normalized to (N)NLO theory cross sections. The W+jets normalization or QCD backgrounds are evaluated using data. The jet-to-lepton fake rates are computed in a background dominated sample orthogonal to the signal sample (QCD di-jets, $\gamma + jets$, same sign dilepton samples). By applying b-jet identification a very pure $t\bar{t}$ sample can be identified. For these analyses the background after b-tagging is estimated in the same manner employed for the ljt channel.

As it benefits from a favorable signal to background ratio, the $t\bar{t}$ dilepton selection, at least in the case of two well identified leptons, relies on a small number of simple requirements. Selecting $t\bar{t}$ events decaying to dilepton requires first an inclusive lepton trigger, two high p_T isolated electrons or muons (typically with $p_T > 20$ GeV) or one isolated electron or muon and one isolated high p_T track and generally at least two jets with $p_T > 20$ GeV. In the $\ell\tau$ channel, one τ lepton identified with a set of neural networks (Galea, 2007) developed to separate hadronically decaying τ leptons and jets is required. Large $\not{E}_T$ is further required (typically $\not{E}_T > 25$ to 35 GeV). The $\not{E}_T$ threshold is raised if the dilepton invariant mass is in the range of the Z resonance. Other topological cuts like a cut on H_T sometimes replace the $\not{E}_T$ requirement particularly for the $e\mu$ channel since it suffers from the Drell-Yan process only through double leptonic τ decays of $Z/\gamma^* \to \tau^+\tau^-$. In the $\ell\tau$ and ℓtrack channels, to reduce the contribution from events with fake $\not{E}_T$ due to misconstruction, requirements are made on the lepton-$\not{E}_T$ and jet-$\not{E}_T$ opening angle. In the $\ell\tau$ and ℓtrack channels, additional requirements are made to further suppress the QCD background and b-jet identification is often employed. In the $\ell\ell$ channel, the signal-to-background ratio after all selection criteria is about 3:1 prior to and $15 : 1$ after requiring at least one b-jet in the event. The cross section analyses typically use simple event counting and minimize a likelihood function that includes nuisance parameters constraining background contributions and other systematic uncertainties.

In the ℓtrack channel, using 1.1 fb^{-1} of data and for $m_t = 175$ GeV/c^2 CDF measures (Aaltonen $et~al.$, 2009) $\sigma_{t\bar{t}} = 8.3 \pm 1.3$ (stat) ± 0.8 (syst) ± 0.5 (lumi) pb without b-tagging and $\sigma_{t\bar{t}} = 10.5^{+1.4}_{-1.3}$ (stat)$^{+0.8}_{-0.7}$ (syst) ± 0.6 (lumi) pb using b-tagging. Combining these two measurements gives $\sigma_{t\bar{t}} = 9.6 \pm 1.2$ (stat)$^{+0.6}_{-0.5}$ (syst) ± 0.6 (lumi) pb. In this channel the main systematic uncertainties come from the uncertainty in the background determination for the result without b-tagging and from the uncertainty on the b-jet identification uncertainty in the second case.

Using 1 fb^{-1} of data, DØ measures in the $\ell\ell$ channel without b-tagging for a 170 GeV/c^2 top-quark mass (Abazov $et~al.$, 2009) $\sigma_{t\bar{t}} = 7.5^{+1.2}_{-1.1}$ (stat)$^{+0.7}_{-0.6}$ (syst)$^{+0.7}_{-0.5}$ (lumi) pb and in the $\ell\tau$ channel using b-tagging and treating $t\bar{t}$ events containing a τ lepton that is mimicked by a jet as background $\sigma_{t\bar{t}} = 7.6^{+4.9}_{-4.3}$ (stat)$^{+3.5}_{-3.4}$ (syst)$^{+1.4}_{-0.9}$ (lumi) pb. In the $\ell\ell$ channel, the main sources of systematic uncertainties come from the signal modeling and the jet energy scale while in the $\ell\tau$ channel, these come from the signal modeling and the background estimation.

Figure 7 shows the predicted and observed $\not{E}_T$ distribution in both CDF and DØ from these $t\bar{t}$ dilepton cross section measurements.

Both collaborations have provided preliminary updates of the $t\bar{t}$ cross section in the dil channel using more than 5 fb^{-1}. The latest measurement from CDF in the $\ell\ell$ channel for a 172.5 GeV/c^2 top-quark mass using 5.1 fb^{-1} of data is $\sigma_{t\bar{t}} = 7.40 \pm 0.58$ (stat) ± 0.63 (syst) ± 0.45 (lumi) pb without b-tagging and $\sigma_{t\bar{t}} = 7.25 \pm 0.66$ (stat) $\pm$ 0.47 (syst) ± 0.44 (lumi) pb using b-tagging. The latest measurement from DØ in the $\ell\ell$ channel without b-tagging for a 172.5 GeV/c^2 top-quark mass using 5.3 fb^{-1} of data is $\sigma_{t\bar{t}} = 8.4 \pm 0.5$ (stat)$^{+0.9}_{-0.8}$ (syst) $^{+0.7}_{-0.6}$ (lumi) pb. Both of these measurements are now limited by the systematic uncertainties.

$t\bar{t}$ Cross Section in the All Hadronic Channel

In the *had* channel, both W bosons decay hadronically into two quarks. The final state consists then of at least six jets among which two of them are b-quark jets. This channel has the advantage of a large branching fraction and no undetectable final state particles but is challenged by a QCD multi-jet background that dominates the signal by several orders of magnitude in cross section. The use of b-tagging in this channel is therefore essential. The purity of the sample can be further increased by using kinematical and topological characteristics of the $t\bar{t}$ events.

The trigger and event selection is described in Sec. V. After additionally requiring that two jets are identified as b-jets the signal-to-background ratio is around 1:2. To further separate the all hadronic $t\bar{t}$ signal from the QCD background multivariate approaches are used. CDF combines several kinematical jet or event variables into a neural network while DØ uses a relative likelihood. The choice of the input variables to these multivariate discriminants is based on the signal-to-background separation power and agreement between the data and the background MC model as evaluated in a background dominated control region. The input variables mainly measure the amount of energy in the event, and the topology of the event. For example, the event centrality, planarity, and sphericity are used. The centrality is defined as the scalar sum of the jet p_T divided by the sum of the jet energies. The event aplanarity and sphericity are defined through the normalized momentum tensor $\mathcal{M}$ (Brandt and Dahmen, 1979):

$$\mathcal{M}_{ij} = \frac{\sum_\alpha p_i^\alpha p_j^\alpha}{\sum_\alpha |\vec{p}^\alpha|^2}$$

where $\vec{p}^\alpha$ is the momentum vector of a reconstructed jet α and $i, j = 1, 2, 3$ denote the three spatial components of the jet momenta. The three eigenvalues of this tensor are noted in decreasing order λ_1, λ_2 and λ_3 with $\lambda_1 + \lambda_2 + \lambda_3 = 1$. The aplanarity is defined as $\mathcal{A} = \frac{3}{2}\lambda_3$ and reflects the isotropy of the event. The sphericity is defined as $\mathcal{S} = \frac{3}{2}(\lambda_2 + \lambda_3)$. Furthermore the di-jet or tri-jet invariant masses are also used. Additional variables like the η and ϕ moments of a jet (Aaltonen *et al.*, 2010) can be added as they show a good discrimination between quark-initiated and gluon-initiated jets, the former being the dominant case for $t\bar{t}$ events while the latter is the dominant case for QCD processes.

The QCD background estimate in the *had* channel is taken from the data using events from the lower jet multiplicity bins. To measure the amount of background remaining after b-tagging, CDF first evaluates the probability of tagging a $udsg$-jet in a sample with exactly four jets, which is QCD dominated. This rate is parametrized in terms of jet p_T, the number of tracks associated to the jet, and the number of primary vertices reconstructed in the event. This tag rate is then used to predict the number of tagged events in the signal region taking into account the possible correlation among the jets. The accuracy of this background model is validated by comparing the data with the estimated background in an intermediate NN region ($0.75 < NN < 0.85$) correcting for the small $t\bar{t}$ contamination that lies in this region. DØ creates a background sample from data by attaching low-p_T jets selected from events with six or more jets to events with four or five jets ensuring a compatible phase-space configuration between the two sources of jets. This is achieved by requiring some amount of $\not{E}_T$ in the four or five jets events with a low $\not{E}_T/H_T$ ratio to reduce effects from mis-reconstruction or from events containing hard neutrinos. This model of background is validated by comparing the five jets events in data with the constructed four+one jet background model. The background in the final sample used for the cross section measurement is constructed with four+two jet events mixed with five+one jet events. The difference between these two constructions is taken as systematic uncertainty.

Using 2.9 fb^{-1}, CDF measures (Aaltonen *et al.*, 2010) $\sigma_{t\bar{t}} = 7.2 \pm 0.5$ (stat) ± 1.0 (syst) ± 0.4 (lumi) pb while DØ uses 1 fb^{-1} to measure (Abazov *et al.*, 2010) $\sigma_{t\bar{t}} = 6.9 \pm 1.3$ (stat) ± 1.4 (syst) ± 0.4 (lumi) pb, both for $m_t = 175$ GeV/c^2. The uncertainty on the background modeling, on the jet energy scale, and on the b-jet identification efficiency dominate the systematic uncertainty on these measurements. Figure 8 shows the distributions of the multivariate discriminants employed by CDF and DØ in their $t\bar{t}$ cross section measurements in the *had* channel.

DØ also performed a $t\bar{t}$ cross section measurement in the τ+jets final state with the τ lepton decaying hadronically. The τ lepton identification criteria are similar to these used in the $\ell\tau$ channel described above. A neural network is built to separate $t\bar{t}$ signal from the main background coming from multi-jet events. The cross section is extracted from a fit to the entire output discriminant distribution. Using 1 fb^{-1} of data, DØ measures (Abazov *et al.*, 2010) $\sigma_{t\bar{t}} = 6.9 \pm 1.2$ (stat)$^{+0.8}_{-0.7}$ (syst) ± 0.4 (lumi) pb for a 170 GeV/c^2 top-quark mass.

$t\bar{t}$ Cross Section Combination and Ratio of Cross Sections

CDF and DØ have measured the $t\bar{t}$ cross section in almost all possible decay channels assuming the SM branching fractions. A comparison of the results is sensitive to potential BSM contributions that affect the various decay channel in ratios differing from the SM. A combination of all these results yields an improved precision on the $t\bar{t}$ cross section.

Within uncertainties all the measured $t\bar{t}$ cross sections in the different final states agree with each other. These measurements are further combined. To simplify the combination all channels are constructed to be statistically independent. To compute the combined cross section, DØ defines a joint likelihood function multiplying the Poisson probability for the different channels (Abazov *et al.*, 2009). Additional Poisson terms are added to constrain the QCD background in the relevant channels. Each systematic uncertainty is included in the likelihood function as a nuisance parameter. Correlations between channels are taken into account by using the same nuisance parameter. Combining the ljt, the $\ell\ell$ and the $\ell\tau$ channels measured using 1 fb^{-1}, DØ finds (Abazov *et al.*, 2009) $\sigma_{t\bar{t}} = 8.18^{+0.98}_{-0.87}$ pb for $m_t = 170$ GeV/c^2, in agreement with the theoretical prediction.

CDF performs a combination of its latest preliminary measurements, using up to 5.7 fb^{-1} of data in the *dil*, *had*, topological ljt, and b-tag ljt channels, by forming a best linear unbiased estimate (Lyons *et al.*, 1988; Valassi, 2003) and taking into account the statistical and systematic correlations. For $m_t = 172.5$ GeV/c^2 the preliminary combination yields $7.46^{+0.66}_{-0.80}$ pb in agreement with the theoretical computation. Figures 9 show a summary of the latest $t\bar{t}$ cross section measurements performed by CDF and DØ.

Calculating the ratio of $\sigma_{t\bar{t}}$ measured in different final states or with different numbers of b-tagged jets probes for the presence of non-SM decays of the top quark. Some BSM theories which might give rise to such effects were discussed in Sec. X.

An example of such an approach is the measurement of the ratio of top quark branching fractions, $R_b = \frac{\mathcal{B}(t\rightarrow Wb)}{\mathcal{B}(t\rightarrow Wq)}$, which can be expressed in terms of CKM matrix elements. By combining this with measurements of the single top-quark production cross section direct measurements of $|V_{tq}|$ can be obtained without invoking any assumptions about the number of quark families or the unitarity of the CKM matrix. DØ performed a simultaneous determination of R_b and $\sigma_{t\bar{t}}$ (Abazov *et al.*, 2008). In addition to applying b-tagging, a topological discriminant is used in the ≥ 4 jets and 0 b-tag subsamples to further constrain the number of $t\bar{t}$ events. Using 0.9 fb^{-1}, the result is: $R_b = 0.97^{+0.09}_{-0.08}$ (stat + syst) for a 175 GeV/c^2 top quark mass in agreement with the SM expectation. The main uncertainty comes from the limited statistics while the systematic uncertainty is dominated by the uncertainty on the b-jet identification efficiency.

Another example of BSM top-quark decays is $t \rightarrow H^+ b$. A large $H^+ \rightarrow \tau^+ \nu$ branching fraction would result in a larger fraction of $t\bar{t}$ events showing up in the $\ell\tau$ channel and fewer events in other channels than expected by the SM. On the other hand, a lepto-phobic charged Higgs would lead to fewer events in the $\ell\ell$ channel compared to ljt. The ratios of the $t\bar{t}$ cross sections as measured in the various decay channels was determined by DØ after taking correlations into account. The ratio of the $\ell\ell$ to ljt channel was measured as (Abazov *et al.*, 2009) $R_\sigma^{\ell\ell/lit} = 0.86^{+0.19}_{-0.17}$ while the ratio of the $\ell\tau$ determined cross section relative to all the others was measured as $R_\sigma^{\ell\tau/\ell\ell+\ell j} = 0.97^{+0.32}_{-0.29}$, both of which are compatible with the SM expectation. These were used to set limits on tau-onic and lepto-phobic charged Higgs decays as well as on the parameter space of the MSSM (Abazov *et al.*, 2009). CDF has also reinterpreted its cross section results to set limits on the charged Higgs production (Abulencia *et al.*, 2006) and assuming five possible Higgs decay modes: $t \rightarrow W^+ b$, $t \rightarrow H^+ b \rightarrow \bar{\tau}\nu b$, $t \rightarrow H^+ b \rightarrow c\bar{s}b$, $t \rightarrow H^+ b \rightarrow t^* \bar{b}b$ and $t \rightarrow H^+ b$ where $H^+ \rightarrow W^+ h$ and $h \rightarrow b\bar{b}$. Limits are set in the plane $(H^+, \tan\beta)$ for several MSSM scenarios. If no assumption is made on the charged Higgs decay, an upper limit on $\mathcal{B}(t \rightarrow H^+ b)$ of 0.91 is set at 95 % confidence level.

$t\bar{t}$ Differential Cross Section

The large statistics $t\bar{t}$ samples now available at the Tevatron enable a more thorough study of $t\bar{t}$ production. In addition to providing good statistics, the ljt channel also offers good resolution on reconstructed quantities, and good sample purity. Thus, the most constraining measurements of top-quark properties and searches for BSM physics in the top-quark sample predominantly come from the ljt channel. Both CDF and DØ have used full reconstructed ljt events to measure differential cross sections. Several BSM theories like technicolor, topcolor, or models with extra dimensions can distort the $t\bar{t}$ invariant mass spectrum or the transverse momentum distribution of the top quarks compared to the SM expectations (Frederix and Maltoni, 2009; Hill and Parke, 1994). Measurements of differential cross sections also test the perturbative QCD heavy-quark predictions.

CDF measures the $t\bar{t}$ differential cross section with respect to the $t\bar{t}$ invariant mass, $d\sigma/dm_{t\bar{t}}$ (Aaltonen *et al.*, 2009) using the ljt channel with b-jet identification. The event selection and background estimate is described above. To reduce the systematic uncertainty introduced by the jet energy corrections, which affects the measured $m_{t\bar{t}}$ spectrum, the jet energy scale is constrained *in situ* by comparing the measured invariant mass of the hadronically-decaying W boson to the world average W-boson mass. The reconstructed background subtracted $m_{t\bar{t}}$ distribution is corrected to the parton level using a regularized unfolding method (Hocker and Kartvelishvili, 1996). Apart from the statistical uncertainty, the largest systematic uncertainty arises from the PDF uncertainties since the tail of the $m_{t\bar{t}}$ distribution

is very sensitive to the large-x portions of the parton distribution functions. The resulting differential cross section shows no evidence of BSM physics.

DØ measures the inclusive differential cross section for $p\overline{p} \rightarrow t\overline{t} + X$ as a function of the top quark p_T, $d\sigma/dp_T^t$ (Abazov *et al.*, 2010) using the *ljt* channel selected as described above. A kinematic fit, which constrains the W-boson and top-quark masses to fixed values, is performed for all possible jet-parton assignments and the combination yielding the minimum fit chi-squared is used to associate the leptons and jets to the top quark. The reconstructed p_T^t spectrum is corrected to the parton level using a regularized unfolding method (Hocker and Kartvelishvili, 1996). The uncertainties on the shape of the p_T^t spectrum are dominated by statistics while the total systematic uncertainty integrated over p_T^t is around 10%. The NLO or NNLO perturbative QCD calculations agree with the measured cross section in normalization and shape while the results from the ALPGEN+PYTHIA and PYTHIA generators describe the shape of the data distribution but not its normalization.

Figure 10 shows the measured differential $t\overline{t}$ cross sections with respect to $m_{t\overline{t}}$ or the top quark p_T measured by CDF and DØ.

2. Forward-Backward Charge Asymmetry

At lowest order in QCD, the SM predicts that the top-quark pair production in $p\overline{p}$ interactions is charge symmetric. However radiative corrections involving either virtual or real gluon emissions lead to a small charge asymmetry (Kuhn and Rodrigo, 1998, 1999). This asymmetry has its origin in radiative corrections to $q\overline{q}$ fusion from interference of the box diagram with the Born diagram while the contribution to $t\overline{t}$ production from gluon fusion remains charge symmetric. The real emission corrections tend to push the top quark backward, opposite to the proton beam direction, while the virtual corrections push it forward, in the direction of the proton beam (Bowen *et al.*, 2006). This asymmetry is predicted to be around 5% (Almeida *et al.*, 2008; Bowen *et al.*, 2006; Dittmaier *et al.*, 2007) while the measured asymmetry depends strongly on the region of phase space being probed. Due to charge conjugation symmetry, the charge asymmetry can also be interpreted as a top-quark forward-backward asymmetry. Some extensions of the SM (Ferrario and Rodrigo, 2009), such as $Z' \rightarrow t\overline{t}$ decays (Malkawi *et al.*, 1996), t-channel W' exchange (Cheung *et al.*, 2009), a new color octet resonance (Antunano *et al.*, 2008; Ferrario and Rodrigo, 2008) or extra-dimension models (Djouadi *et al.*, 2009) predict different asymmetries. Both CDF (Aaltonen *et al.*, 2008) and DØ (Abazov *et al.*, 2008) have measured the forward-backward charge asymmetry using *ljt* events with b-jet identification.

The asymmetry A_{fb} is frame dependent and can be defined either in the $p\overline{p}$ or $t\overline{t}$ rest frame. The $t\overline{t}$ rest frame is more difficult to reconstruct but the asymmetry in the $p\overline{p}$ rest frame is predicted to be ≈ 30 % smaller (Antunano *et al.*, 2008). In the $p\overline{p}$ rest frame the asymmetry can be written as:

$$A_{fb}^{p\overline{p}} = \frac{N_t(\cos\theta > 0) - N_t(\cos\theta < 0)}{N_t(\cos\theta > 0) + N_t(\cos\theta < 0)} \tag{9}$$

where $\cos\theta = -Q_\ell \cdot \cos\alpha_p$, α_p is the polar angle between the top quark with the hadronic W-boson decay and the proton beam, and Q_ℓ is the lepton charge from the leptonic decaying W-boson. In the $t\overline{t}$ rest frame the asymmetry can be defined similarly except that θ^* is the production angle of the top quark in the $t\overline{t}$ rest frame. This angle is related to the rapidity, y, of the t and $\overline{t}$ in the $p\overline{p}$ frame by

$$\Delta y = y_t - y_{\overline{t}} = 2\tan^{-1}\left(\frac{\cos\theta^*}{\sqrt{1 + \frac{4m_t^2}{\hat{s} - 4m_t^2}}}\right) \tag{10}$$

where $\hat{s}$ is the square of the center-of-mass energy. So the $t\overline{t}$ rapidity difference in the $p\overline{p}$ rest frame can be used to measure the production angle θ^* in the $t\overline{t}$ rest frame. As both Δy and $\cos\theta^*$ have the same sign, the asymmetry can be written

$$A_{fb}^{t\overline{t}} = \frac{N_t(\Delta y > 0) - N_t(\Delta y < 0)}{N_t(\Delta y > 0) + N_t(\Delta y < 0)}. \tag{11}$$

CDF measures the asymmetry in both frames using fits to the $\cos\theta$ and to the Δy data distributions after background subtraction. The background fraction is constrained in these fits using the estimates from the cross section analysis described above. The $t\overline{t}$ kinematics are reconstructed using a kinematic fit that constrains the W-boson mass and the $m_t - m_{\overline{t}}$ difference. The combination of jet-parton assignments which minimizes the fit chi-squared is used in

the analysis. The results are corrected to the parton level using a matrix inversion technique. Using 1.9 fb^{-1} of data CDF measures (Aaltonen *et al.*, 2008)

$$A_{fb}^{p\overline{p}} = 0.17 \pm 0.07(\text{stat}) \pm 0.04(\text{syst}) \text{ and } A_{fb}^{t\overline{t}} = 0.24 \pm 0.13(\text{stat}) \pm 0.04(\text{syst}). \tag{12}$$

These results agree within 2 standard deviation with the SM expectation. Figure 11 shows the raw Δy distribution in the $t\overline{t}$ rest frame.

DØ measures the asymmetry in the $t\overline{t}$ frame and performs a simultaneous fit for the asymmetry and the background fraction using the Δy distribution and a likelihood discriminant designed to separate $t\overline{t}$ from W+jets processes. In an effort to remain independent of any potential BSM contributions, they do not correct for reconstruction effects but provide a parameterization of the resolution. The DØ measured asymmetry corrected for background contributions from 0.9 fb^{-1} of data is (Abazov *et al.*, 2008)

$$A_{fb}^{t\overline{t} \ obs} = 0.12 \pm 0.08(\text{stat}) \pm 0.01(\text{syst}). \tag{13}$$

This is consistent with the SM expectation estimated using a NLO QCD MC generator, applying the event selection criteria, and determining the resulting asymmetry. DØ derives from this limits on the mass of a leptophobic Z' decaying to $t\overline{t}$ as shown Fig. 11.

3. Fraction of gluon-gluon Fusion Produced $t\overline{t}$

At the Tevatron, a variety of production mechanisms can yield a pair of heavy quarks in the final state. Distinguishing between the various initial state mechanisms is difficult since information is lost as the heavy quarks hadronize and form bound states. However, as discussed in Sec. II, top quarks decay before they hadronize and the initial state spin information survives to the final state. This can be used together with other discriminating variables to determine the fraction of $t\overline{t}$ pairs produced via gluon-gluon fusion. At the Tevatron, the SM predicts that $gg \to t\overline{t}$ accounts for about 15% of $t\overline{t}$ production, with the remainder coming from $qq \to t\overline{t}$ processes. This fraction varies by about $\pm 5\%$ (absolute) due to uncertainties in the gluon PDFs. The measured $gg \to t\overline{t}$ contribution can be affected by BSM particles decaying to $t\overline{t}$.

CDF used the ljt channel with b-jet identification to measure the relative fraction of gluon-gluon produced $t\overline{t}$ pairs using two different methodologies. The first method exploits the fact that gluons are more likely to radiate additional gluons so that gluon initiated processes result in a higher track multiplicity on average than quark initiated processes. The observed low-p_T track multiplicity distribution is fit to a contribution from background, from $q\overline{q} \to t\overline{t}$, and from $gg \to t\overline{t}$ processes. The distributions used in the fit are taken from MC samples calibrated using data samples known to be gluon-rich or gluon-depleted (W+jets and QCD di-jet events). Corrections are made for the number of high energy jets in the event, for background contributions, and for acceptance effects. Using this first method CDF measures $\sigma(gg \to t\overline{t})/\sigma(p\overline{p} \to t\overline{t}) = 0.07 \pm 0.14$ (stat) ± 0.07 (syst) which corresponds to an upper limit of 0.33 at 95 % confidence level (Aaltonen *et al.*, 2008).

The second method uses kinematic information to discriminate between the two production mechanisms. A kinematic fit is used to determined the best jet-parton assignment to use. This allows a full reconstruction of the final state and of the top quarks and their kinematics. A variety of variables are combined using a NN, trained using $t\overline{t}$ MC samples. The variables include several top-quark production angles, and several that are sensitive to $t\overline{t}$ spin correlations as suggested in (Mahlon and Parke, 1997; Parke and Shadmi, 1996). A fit including background, $gg \to t\overline{t}$, and $q\overline{q} \to t\overline{t}$ contributions, is performed to the observed NN distribution. Using this second method CDF employs a Feldman-Cousins prescription (Feldman and Cousins, 1998) to set an upper limit of $\sigma(gg \to t\overline{t})/\sigma(p\overline{p} \to t\overline{t}) < 0.61$ at 95 % confidence level (Aaltonen *et al.*, 2009). The dominant systematic uncertainties on this measurement come from the background shape and composition and from the difference between LO and NLO predictions.

The two measurements are combined to yield $\sigma(gg \to t\overline{t})/\sigma(p\overline{p} \to t\overline{t}) = 0.07^{+0.15}_{-0.07}$ (Aaltonen *et al.*, 2009) consistent with the SM expectation.

B. Decay Properties

1. W-Boson Polarization Fractions

Since the top quark decays before forming a bound state, the $t \to W^+ b$ process provides an opportunity to directly probe the tWb interaction vertex. In particular, measurements of the polarization fractions of the resulting W

bosons can be used to test for BSM tWb interactions. In the SM the fraction of W^+ bosons from top-quark decay produced with longitudinal polarization is about $f_0 = 0.70$, about $f_- = 0.30$ with left-handed polarization, and about $f_+ = 0.0004$ with right-handed polarization. Contributions from BSM physics can give rise to anomalous couplings at the tWb vertex that change these polarization fractions (Aguilar-Saavedra *et al.*, 2007; Kane *et al.*, 1992). Some examples include the SM extensions discussed in (Bernreuther *et al.*, 2004; Nam, 2002). Measurements of the W-boson polarization fractions can be used to set constrains on the vector and tensor form factors, f_1^R, f_1^L, f_2^R, and f_2^L. These terms appear in the general form of the Lagrangian describing the tWb vertex. In the SM only f_2^L has a non-zero value.

The W-boson polarization affects several kinematic variables, which can be used to measure (f_0, f_+). The most commonly used is θ^*, the angle between the W-boson momentum in the rest frame of the top quark and the direction of the down-type fermion decay product of the W-boson (charged lepton or d, or s quark) in the rest frame of the W boson. The W-boson differential decay rate can be written in terms of $\cos\theta^*$ as:

$$\frac{1}{\Gamma}\frac{d\Gamma}{d\cos\theta^*} = \frac{3}{8}f_-(1-\cos\theta^*)^2 + \frac{3}{4}f_0(1-\cos^2\theta^*) + \frac{3}{8}f_+(1+\cos\theta^*)^2. \tag{14}$$

Estimating $\cos\theta^*$ requires each $t\bar{t}$ event be fully reconstructed using, for example, a kinematic fit. The charged lepton p_T is also sometimes used since it is correlated to the W-boson polarization. It produces a less precise measurement, but is insensitive to uncertainties in the jet energy scale. Both CDF and DØ have recently used $\cos\theta^*$ to measure the W-boson helicity fractions with 2.7 fb^{-1} and 1 fb^{-1} of data, respectively.

CDF uses the matrix element method described in Sec. IX.C.1 to determine the polarization fractions in the ljt channel with b-jet identification. In this analysis the LO $t\bar{t}$ differential cross section is expressed in terms of $\cos\theta^*$ and the fractions (f_0, f_+) while the top mass is fixed at 172.5 GeV/c^2. The fit to the data is performed under three different scenarios, a) a model independent fit to both f_0 and f_+ simultaneously, b) a fit to determine f_+ with f_0 fixed to its SM value, and c) a fit to determine f_0 with f_+ fixed to zero (its SM value given the current level of precision). Corrections for background contributions and corrections for the variation of the event selection acceptance as a function of (f_0, f_+) are included. The model independent fit yields (Aaltonen *et al.*, 2010) $f_0 = 0.88 \pm 0.11$ (stat) ± 0.06 (syst) and $f_+ = -0.15 \pm 0.07$ (stat) ± 0.06 (syst) with a correlation coefficient of -0.59. Fixing f_0 to its SM value yields $f_+ = -0.01 \pm 0.02$ (stat) ± 0.05 (syst). Fixing f_+ to zero yields $f_0 = 0.70 \pm 0.11$ (stat) ± 0.04 (syst). These measurements are statistics limited. The dominant systematic uncertainties arise from uncertainties in the background modeling and from uncertainties in ISR/FSR and parton shower modeling in $t\bar{t}$ events.

DØ uses a kinematic fit to fully reconstruct the event and calculate $\cos\theta^*$ in the ljt and dil channels. In the ljt channel events are reconstructed using a kinematic fit with fixed W-boson and top-quark masses. In the dil channel, given a top-quark mass, a four-fold ambiguity exists for each set of jet-parton assignments considered. In the analysis all real solutions are considered. The resulting reconstructed $\cos\theta^*$ distributions are compared with templates derived from $t\bar{t}$ MC with different W-boson polarization fractions and taking into account background and reconstruction effects. For a top-quark mass of 172.5 GeV/c^2 the measured W-boson polarization fractions determined from a model independent fit are (Abazov *et al.*, 2008) $f_0 = 0.425 \pm 0.166$ (stat) ± 0.102 (syst) and $f_+ = 0.119 \pm 0.090$ (stat) ± 0.053 (syst). This measurement is statistics limited. The main systematic uncertainties come from the background or $t\bar{t}$ modeling and from the MC template statistics.

DØ combines the measured W-boson polarization fractions with the measurement of the electroweak single top production cross section (Abazov *et al.*, 2007, 2008) to set limits on the f_1^L, f_1^R, and f_2^R BSM form factors (Abazov *et al.*, 2009).

2. Decays via Flavor Changing Neutral Currents

In the SM quarks can change flavor only via W-boson interactions, so that at tree level decays of the type, $t \to qZ^0$ or $t \to q\gamma$, where $q = u$, c, are forbidden. Thus the rates for these decays are suppressed because they can only occur through quantum loops involving the W-boson. Because the top-quark is so massive, the quantum loop corrections arising from new particle loops are much larger than is the case for the light-quarks. This makes the top-quark a potentially great place to look for evidence of BSM Flavor Changing Neutral Currents (FCNC) decays. For example, the SM predicts $\mathcal{B}(t \to qZ^0) \approx \mathcal{O}(10^{-14})$ (Aguilar-Saavedra, 2004), while new physics models like 2HDM, supersymmetry, and topcolor-assisted technicolor predict branching fractions as large as $\mathcal{O}(10^{-4})$ (Larios *et al.*, 2006). An observation of a branching fraction significantly larger than predicted by the SM would be unambiguous evidence of BSM physics.

CDF has searched for the FCNC decay $t \to qZ^0$ using $t\bar{t}$ events when the top quarks decay as $t\bar{t} \to qZ^0qZ^0$ or $t\bar{t} \to qZ^0bW^{\pm}$ and one of the Z-bosons decays into a e^+e^- or $\mu^+\mu^-$ pair (Aaltonen $et\ al.$, 2008), while the other boson in the event decays hadronically. The experimental signature is thus very similar to the ljt channel except that the final state neutrino is replaced by a charged lepton. The dominant background process is the production of Z+jets. Smaller background contributions come from the SM $t\bar{t}$, WZ and ZZ processes. The event sample is divided into sub-samples depending on whether or not any of the jets have been identified as b-quark jets. A kinematic fit is employed similar to the one described in Sec. V.G except that one or both of m_W constraints are replaced by m_Z constraints depending on which final state hypothesis is being tested. To separate the FCNC signal from the background, requirements are made on the transverse mass of the Z^0 and the four leading jets, the E_T of the four leading jets, and on the kinematic fit χ^2. A binned likelihood fit to the χ^2 distribution is simultaneously performed for the sub-samples with and without an identified b-jet and the fraction of FCNC decays in the data is extracted. In the fit the normalization for the dominant Z+jets background is allowed to float, while the $t\bar{t}$ cross section is fixed to the observed $t\bar{t} \to \ell\nu qq'b\bar{b}$ cross section. The systematic uncertainties affecting the signal and background shapes and normalizations are taken into account using the technique of (Read, 1999). The dominant systematic uncertainty arises from the jet energy corrections and in uncertainties related to the fraction of Z-jet events that have identified b-jets. A Feldman-Cousins procedure (Feldman and Cousins, 1998) is employed to set the limit. Using 1.9 fb^{-1}, CDF data is consistent with the SM expectation and an upper limit of $\mathcal{B}(t \to qZ^0) < 3.7\%$ is established at 95 % confidence level. Similar searches can also be performed using the electroweak production of single top quarks (Abazov $et\ al.$, 2010).

3. Decays to Charged Higgs Bosons

Many theories beyond the SM propose an extension of the Higgs sector to multiple Higgs doublets (Grossman, 1994). The simplest extension of the SM Higgs sector is the two Higgs-doublet model (2HDM) (Gunion $et\ al.$, 1989). In the 2HDMs, the Higgs sector consists of three neutral Higgs bosons (h, H, A) and two charged ones $(H^{\pm})$. Several types of 2HDMs exist and differ in their strategies to avoid large flavor changing neutral current effects. In type I 2HDM, only one of the Higgs doublets couple to fermions. In type II, one doublet couples to the up-type quarks and neutrinos and the other to down-type quarks and charged leptons. The minimal supersymmetric standard model (MSSM) is an example of type II 2HDM. In models of type III, both doublets couple to fermions and FCNCs are suppressed through other mechanisms. An observation of a charged Higgs boson would be unambiguous proof of a BSM Higgs sector.

At the Tevatron direct production of a single charged Higgs boson can occur by $q\bar{q}'$ annihilation. Searches for $q\bar{q}' \to H^+ \to tb$ have been performed by DØ assuming a charged Higgs boson mass larger than the top quark mass (Abazov $et\ al.$, 2009). This channel has the same signature as the electroweak production of single top quarks. Direct production of H^+H^- through the weak interaction has a rather small expected cross section, of the order of 0.1 pb (Carena and Haber, 2003) and so no such search was performed so far. For $m_{H+} < m_t$ in 2HDM, the top quark can decay to H^+b, hence competing with the SM decay to W^+b. As seen in section IX.A, the ratio of $t\bar{t}$ cross sections as measured in different decay channels is thus sensitive to BSM top-quark decays. The measured $t\bar{t}$ cross sections have been used to set limits in the plane $(m_{H+}, \tan\beta)$ where $\tan\beta$ is the ratio of vacuum expectation values of the two Higgs doublets (Abazov $et\ al.$, 2009). At small $\tan\beta$ ($\lesssim 1$), the top branching fraction into charged Higgs, $\mathcal{B}(t \to H^+b)$, can be large. In that regime, the charged Higgs boson predominately decays to $c\bar{s}$ for low charged Higgs mass ($\lesssim 130$ GeV) or to $t^*\bar{b} \to Wb\bar{b}$ for large mass. At larger $\tan\beta$ ($\gtrsim 15$), $\mathcal{B}(t \to H^+b)$ can also be large, but in that case the charged Higgs boson decays almost 100 % of the time to $\tau^+\nu$.

Using 2.2 fb^{-1}, CDF has performed a direct search for decays of top quarks into charged Higgs bosons assuming $H^+ \to c\bar{s}$ using the ljt final state including b-jet identification. The di-jet invariant mass distribution, which is otherwise assumed to come from the W-boson decay, is used to search for evidence of such decays (Aaltonen $et\ al.$, 2009). The $t\bar{t}$ kinematics are reconstructed using a kinematic fitter similar to the one described in Sec. V.G except that the m_W constraint for the hadronically decaying W-boson candidate is dropped and templates are built for signal and background processes. The signal is modeled using H^+ MC where the H^+ decay is forced to $c\bar{s}$ and $\Gamma_{H+} = 0$ is assumed for $60 < m_{H+} < 150$ GeV$/c^2$. A binned likelihood fit, including systematic effects, is used to exclude $\mathcal{B}(t \to H^+b)$ larger than 0.1 to 0.3 at the 95% confidence level assuming $\mathcal{B}(H^+ \to c\bar{s}) = 1$.

C. Intrinsic Properties

1. Mass

The top-quark mass is a free parameter in the SM and must be experimentally determined. A precision determination of m_t is important since quantum loops including top quarks contribute large corrections to theory predictions for many precision electroweak observables. For example, the SM predicts a precise relationship between the W- and Z^0-boson masses,

$$\left(\frac{m_W}{m_Z}\right)^2 = \left(1 - \sin^2\theta_W\right)\left(1 + \Delta\rho\right) \tag{15}$$

where $\sin\theta_W$ is the weak mixing angle and $\Delta\rho$ is 0 at tree level and non-zero once quantum loop corrections are included. The dominant quantum corrections are quadratically dependent on the top-quark mass and logarithmically dependent on the higgs-boson mass, $\Delta\rho = f(m_t^2, \ln m_H)$. As discussed in more detail in (Flächer et $al.$, 2009; Nakamura et $al.$, 2010), the experimental program then consists of measuring m_W, m_Z, and m_t as precisely as possible in order to constrain m_H. The experiments at LEP and SLAC precisely determined m_Z, the Tevatron and LEP2 experiments precisely determine m_W, and the Tevatron experiments alone precisely determine m_t. It is important to measure m_t in all the different top decay channels since BSM contributions can affect them differently (Kane and Mrenna, 1996).

For a free particle, the physical mass is usually defined as the pole of its renormalized propagator. However this definition is ambiguous when dealing with colored particles like quarks. Thus the definition of the top-quark pole mass is intrinsically ambiguous on the order of Λ_{QCD} due to non-perturbative QCD effects (Beneke and Braun, 1994; Bigi et $al.$, 1994; Smith and Willenbrock, 1997). For an unstable particle (like the top quark), the pole mass enters the description of the resonance through a Breit-Wigner function. Other mass definitions exist such as the $\overline{\text{MS}}$-mass using the $\overline{\text{MS}}$ renormalization scheme (Bardeen et $al.$, 1978) or those discussed in (Hoang and Stewart, 2008). The $\overline{\text{MS}}$-mass is only sensitive to short distance QCD effects and is often used to describe the mass of the light quarks when the typical energy of the process is much larger than the quark mass in question. At the Tevatron and LHC, the top-quark mass will be directly measured through the reconstruction of its decay products and the measured mass is taken to be the pole mass. However, aside from the theoretical ambiguity mentioned above, additional ambiguities are introduced since the measurements are calibrated using MC generators that include model dependent descriptions of the parton shower and hadronization processes. These affect the experimentally reconstructed top-quark mass in a model dependent way and introduce a set of modeling related systematic uncertainties that are of the order Λ_{QCD}.

Aside from having to isolate a relatively pure sample of $t\bar{t}$ events, there are a few experimental challenges to making a precise determination of m_t. The most sensitive analyses fully reconstruct the $t\bar{t}$ kinematics using a kinematic fit or a matrix element technique. In order to do so it is necessary to assign each final state jet as having originated from a particular final state quark. As discussed in Sec. V.G, this gives rise to a combinatoric ambiguity that dilutes the resolution of the reconstructed $t\bar{t}$ kinematics. The resolution with which the $t\bar{t}$ kinematics can be reconstructed is further diluted by the addition of ISR/FSR jets, the loss of quark jets due to limited geometric acceptance, and jet algorithm merging/splitting effects. Moreover, large systematic uncertainties can arise from uncertainties in the jet energy corrections. Roughly, each $\pm1\%$ of uncertainty in the jet energy corrections gives a ±1 GeV/c^2 uncertainty in the top-quark mass. This was a limiting systematic uncertainty for early m_t measurements. With larger statistics samples the jet energy corrections can be calibrated in $situ$ by constraining the corresponding jet-jet invariant mass to the world average m_W in events containing a $W \to qq'$ decay. Doing so significantly reduces the associated systematic uncertainty, which then scales with the statistics of the $t\bar{t}$ sample itself. Most measurements in the ljt and had channels now take advantage of this in $situ$ calibration by performing simultaneous fits to m_t and the jet energy scale. Other measurements seek to identify experimental observables that are only weakly dependent on the jet energy corrections.

For all analyses described below it is necessary to calibrate the measured m_t using MC pseudo-experiments (ie. ensemble testing) in order to quantify the influence of the simplifications made in the employed techniques. Each pseudo-experiment is built from a mix of $t\bar{t}$ signal and background events in the proportions estimated from the relevant cross section analysis. The number of events contributed by each physics process is allowed to fluctuate according to a Poisson distribution. Once a set of pseudo-events have been assembled, they are then treated just like the data and a determination of m_t is made. Then, from an ensemble of pseudo-experiments, the relationship between the true top-quark mass (ie. the m_t value used when generating the $t\bar{t}$ MC sample) and the mean measured m_t can be established and, if necessary, corrections can be derived - usually as a linear function of the measured value. This is done separately for each analysis technique. The ensemble of pseudo-experiments is also used to study the expected

statistical uncertainty and the statistical behavior of each analysis technique. Once a particular analysis has been calibrated, its performance is checked using blinded MC samples.

Three methods are used at the Tevatron to measure the top-quark mass. They are described below. For a recent detailed review on top-quark mass measurements, see (Fiedler, 2010).

Template Method

This traditional method begins by choosing an observable correlated with the top-quark mass. Distributions of this observable are then constructed using MC samples generated with varying m_t as input. The data distribution is then compared with these MC templates using a maximum likelihood fit. The observable most correlated with m_t is the reconstructed invariant mass of the $t\bar{t}$ decay products, m_t^{reco}, which is the most often used and is estimated using the kinematic fits discussed in Sec. V.G. If a given analysis uses the hadronic W-boson decay to calibrate the jet energy corrections, an observable correlated with m_W is used - usually the invariant mass of the associated jets, m_{jj} - and the maximum likelihood fit is extended to two dimensions. The template method is relatively simple and can be easily extended to several decay channels or sub-samples. The observable(s) used as estimators can be chosen to minimize sensitivity to specific systematic uncertainties. The statistical sensitivity of this method is sometimes worse than other methods discussed because it does not use the full event information, nor take advantage of event-by-event differences to weight more heavily those events with kinematics resulting in improved m_t^{reco} resolution.

A detailed description of using the template method to measure m_t in the ljt channel can be found in (Abulencia et al., 2006). The most recent published result uses 1.9 fb^{-1} of CDF data and simultaneously fits the ljt and dil channels using the in situ $W \to qq'$ decays to constrain the jet energy corrections and reduce the associated systematic uncertainties (Aaltonen et al., 2009). In the ljt channel a kinematic fit is used to determine $(m_t^{\mathrm{reco}}, m_{jj})$ for each event. Since the $t\bar{t}$ kinematics are under constrained in the dil channel, a neutrino weighting algorithm described below is used to determine m_t^{reco}. It is used together with H_T in this particular analysis. Two dimensional templates are constructed for each channel and a joint likelihood fit is performed to measure m_t. Templates are built from simulated samples of $t\bar{t}$ and background events using MC generated at discrete values of m_t. The shape of the templates at these discrete points is described using kernel density estimators (Scott, 1992; Silverman, 1998) and then smoothed and interpolated using the method of (Loader, 1999) to enable an estimate of the template shapes for any arbitrary value of m_t. The data in each channel is further divided into sub-samples of varying signal purity and m_t^{reco} resolution using the number of reconstructed jets and the number of identified b-jets in the events. A full set of templates are created for each sub-sample. The two dimensional data distributions are compared to the resulting templates using an unbinned maximum likelihood fit to determine m_t, the best-fit jet energy scale correction, and their associated uncertainties. The resulting top-quark mass is $m_t = 171.9 \pm 1.7$ (stat + JES) ± 1.1 (syst) GeV/c^2. The dominant systematic uncertainties arise from residual uncertainties in the jet energy corrections[3] and from variations of the MC generator used to model $t\bar{t}$ events. An example of one of the m_t^{reco} distributions is shown in Fig. 12. CDF has also used the template method to determine m_t from a sample of ljt events in which the b-jets are identified using one of the soft lepton tagging algorithms described in Sec. V.F (Aaltonen et al., 2009).

CDF has also performed template measurements of m_t using observables with minimal sensitivity to the jet energy corrections (Aaltonen et al., 2009, 2010). Since the transverse momenta of the top-quark decay products depend approximately linearly on m_t, the decay length of the b-hadron measured in the transverse plane, L_T, or the p_T of the lepton from the W decays can be used to build templates. These observables are almost completely independent of the jet energy corrections. Small dependencies remain due to uncertainties in $t\bar{t}$ and background acceptances that arise from changes in the event selection efficiencies when the jet energies are varied. The shape of the L_T distribution is calibrated using di-jet data samples enriched in $b\bar{b}$. The lepton p_T scales are calibrated as discussed in Sec. V.C. The two-dimensional L_T and lepton p_T distribution is used to determine m_t and the resulting likelihood curve is shown in Fig. 12. Using 1.9 fb^{-1} CDF measures with these observables $m_t = 170.7 \pm 6.3$ (stat) ± 2.6 (syst) GeV/c^2. The measurement will clearly benefit from more statistics and has a very low systematic uncertainty coming from jet energy calibration. However it suffers from large systematic uncertainties arising from the L_T and p_T calibration. The precision of these calibrations should improve as the statistics of the relevant control samples increases.

A detailed description of using the template method to measure m_t in the dil channel can be found in (Abulencia et al., 2006). Recent measurements use essentially the same methodologies on significantly larger data sets. As

---

[3] The measurement treats the jet energy scale as a constant. The residual jet energy scale systematic accounts for the known variations of these corrections as a function of jet E_T and η.

described in Sec. V.G, since the kinematics of the *dil* events is under constrained it is necessary to make an additional kinematic assumption in order to obtain a reconstructed invariant mass for each event. The CDF and DØ template analyses in the *dil* channel primarily differ in the additional kinematic assumption they choose to make.

CDF's most recent template analysis in the *dil* channel uses the neutrino ϕ weighting method (Aaltonen *et al.*, 2009), which integrates over the azimuthal angles for the two neutrinos in each event. A χ^2 function is minimized to estimate m_t^{reco} for each event. This χ^2 function includes a term that constrains the measured quantities within their uncertainties to the assumed $t\bar{t}$ kinematics. Templates of the m_t^{reco} distributions are obtained from simulated samples of $t\bar{t}$ signal and background events generated at discrete values of m_t. The shape of the templates is fit to a Landau plus two Gaussians function and the resulting parameterizations are smoothed and interpolated to enable an estimate of the template shape at any arbitrary m_t value. The top-quark mass is determined using an unbinned likelihood fit to the data. CDF also developed a template based measurement where the m_t dependent SM $t\bar{t}$ cross section is included as an additional constraint (Aaltonen *et al.*, 2008).

The most recent DØ template analyses in the *dil* channel use a neutrino weighting method and the so called matrix weighting method (Abazov *et al.*, 2009). The neutrino weighting algorithm employed integrates over the neutrino rapidities as the assumed input to the kinematic fit. Weights are assigned by comparing the resulting neutrino momenta solutions to the measured $\not{E}_T$. The first two moments of the weighted distributions are used from each event to build m_t^{reco} templates and extract from the data distribution the most probable top-quark mass. The templates are constructed in two different manners, using binned probability density histograms and using probability density fit functions, which are later combined. The matrix weighting technique integrates over assumed top-quark masses and solves for the t and $\bar{t}$ momenta. Each solution is then weighted by the probability to measure the observed lepton energy in the top-quark rest frame given the assumed top-quark mass using the matrix element based expressions in (Dalitz and Goldstein, 1992). For each event m_t^{reco} is taken from the maximum of the resulting weighted distribution and used to build templates.

Using 2.9 fb^{-1}, CDF measures in the *dil* channel (Aaltonen *et al.*, 2009): $m_t = 165.5^{+3.4}_{-3.3}$ (stat) ± 3.1 (syst) GeV/c^2. Using 1 fb^{-1}, DØ combines the results from the neutrino weighting and the matrix weighting techniques in the *dil* channel to measure (Abazov *et al.*, 2009) $m_t = 174.7 \pm 4.4$ (stat) ± 2.0 (syst) GeV/c^2. These measurements are still limited by statistics. The systematic uncertainty is completely dominated by the uncertainty in the jet energy corrections as no *in situ* jet energy scale calibration is possible in the *dil* channel.

A detailed description of using the template method to measure m_t in the *had* channel can be found in (Aaltonen *et al.*, 2010) in which CDF performs a simultaneous measurement of the $t\bar{t}$ cross section and the top-quark mass using a NN based event selection and requiring at least one identified *b*-jet. A kinematic fit is used and all possible jet-parton assignments consistent with the *b*-jet information are considered. The combination yielding the smallest fit chi-squared is used to determine m_t^{reco}, m_{jj}^{W+}, and m_{jj}^{W-} for each event. Templates are built from the m_t^{reco} distribution and from the m_{jj} distribution for a set of MC samples generated at discrete m_t and jet energy correction values. These templates are fit to a Gamma plus Gaussian function, and the resulting parameters are smoothed and interpolated to enable an estimate of the template shape at any arbitrary m_t value. The top-quark mass is determined from an unbinned likelihood fit to the data that includes an *in situ* constraint on the jet energy corrections using the m_{jj} distributions. Using 2.9 fb^{-1}, CDF measures $m_t = 174.8 \pm 2.4$ (stat + JES)$^{+1.2}_{-1.0}$syst GeV/c^2. The measurement is limited by statistics and the dominant source of systematic uncertainty arises from residual jet energy correction uncertainties and in method related systematics.

Matrix Element Method

The matrix element method is a more sophisticated method for measuring a particle property and constructs a likelihood curve for each event by comparing the observe kinematics to those expected as a function of the particle property of interest (e.g. m_t). The event probability density is estimated using a leading order matrix element and integrating over the unmeasured quantities. Detector effects are incorporated by integrating over resolution functions. The total likelihood for a given sample of events is obtained from the product of the individual event probability densities. Although it will not be discussed separately, it should be noted that the dynamic likelihood method is very similar to the matrix element method described here. The matrix element method offers superior statistical sensitivity since it uses the full kinematic information available in each event and since it effectively gives more weight to events whose kinematics afford a more precise estimate of m_t^{reco} by virtue of having a narrower event probability density. The principal downside is that it is enormously cpu intensive, typically requiring hours of cpu per event. This limitation renders these analyses less nimble than analyses using the template method.

The method is based on an approach suggested in (Dalitz and Goldstein, 1999; Kondo *et al.*, 1993) and close to the

method suggested for the measurement of the mass of the W boson at LEP (Abreu *et al.*, 1998; Berends *et al.*, 1998; Juste, 1999). The method was first employed by DØ (Abazov *et al.*, 2004) to measure the top-quark mass. Currently, all the most precise m_t determinations use the matrix element method. It has been applied in all the decay final states. In the ljt and *had* channels it is extended to include an integration over the jet energy corrections, which are then constrained *in situ* using hadronic W-boson decays. A detailed description of the matrix element technique applied to measure the top-quark mass can be found in (Fiedler *et al.*, 2010).

The event probability P_{evt} is built from a $t\bar{t}$ probability ($P_{t\bar{t}}$) and a background probability (P_{b}),

$$P_{\text{evt}}(x; m_t, f_{t\bar{t}}) = f_{t\bar{t}} \cdot P_{t\bar{t}}(x; m_t) + (1 - f_{t\bar{t}}) \cdot P_{\text{b}}(x) \tag{16}$$

where x denotes the set of observed variables (i.e. the jet and lepton momenta) and $f_{t\bar{t}}$ is the $t\bar{t}$ signal fraction in the event sample. The signal and background probability densities are constructed by integrating over the appropriate parton-level differential cross section, $d\sigma(y)/dy$, convoluted with parton distribution functions ($f(q)$) and resolution effects. The resolution effects are described by the transfer functions, $W(x; y)$, which give the probability of observing the set of variables x given the underlying partonic quantities, y. Typically the jet and lepton angles are taken to be exactly measured so that the relevant transfer functions are simply Dirac delta functions. The transfer functions for the jet energies are parameterized as a function of parton energy and rapidity using fully simulated MC events. Separate transfer functions are derived for uds, gluon, and b-jets. The transfer functions for the lepton energies are usually taken to be Dirac delta functions but are sometimes treated in a manner similar to the jets. It should be noted that the transfer functions are not assumed to be Gaussian, and more sophisticated functions can be used to obtain a more accurate description of the relevant resolutions. The $t\bar{t}$ probability density is expressed as

$$P(x) = \frac{1}{\sigma^{\text{obs}}} \sum_{\text{j}-\text{p comb}} \int \sum_{\text{flavors}} \frac{d\sigma(y)}{dy} f(q_1) f(q_2) dq_1 dq_2 W(x; y) dy \tag{17}$$

where the first sum is over all possible jet-parton combinations and the second sum is over all relevant PDF parton flavors. The probability density is normalized to the total observed cross section, σ^{obs}, after including event selection effects. For signal the differential cross section is taken from the leading order matrix element, $\mathcal{M}(q\bar{q} \rightarrow t\bar{t} \rightarrow y)$, found in (Mahlon and Parke, 1997), which depends on m_t, $\frac{d\sigma(y)}{dy} \rightarrow \frac{\sigma(m_t,y)}{dy}$. For background the differential cross section is taken from a sum of matrix elements, calculated by dedicated MC generators, and is independent of m_t. The background probability density usually includes contributions from just the dominant background processes. The effect of the resulting approximation on the measured m_t is included as part of the systematic uncertainties and is usually found to be quite small. For analyses that constrain the jet energy corrections using hadronic W-boson decays, the jet energy transfer functions, and thus the event probability densities, are additionally expressed in terms of an overall jet energy scale factor, JES, $W(x; y) \rightarrow W(x; y, \text{JES})$.

Both CDF and DØ have recently published measurements of the top-quark mass in the ljt channel using the matrix element technique. In their most recent analysis (Aaltonen *et al.*, 2009) CDF also takes into account the finite angular resolution of the jets by replacing the Breit-Wigner terms in the matrix element with "effective propagators" estimated from MC by replacing the parton direction with th direction of their corresponding reconstructed jet. In this analysis the gluon fusion diagrams are also included in the $t\bar{t}$ matrix element and the jet-parton combinations are weighted using information from a b-jet identification algorithm. A NN discriminant is used to separate $t\bar{t}$ from background events rather than the matrix elements for the background processes. Events with very small likelihoods are vetoed in order to remove poorly behaved $t\bar{t}$ events arising, for example, from the presence of ISR/FSR jets. The jet energy corrections are constrained using the $W \rightarrow qq'$ decays. The method is calibrated using MC samples generated at various values of m_t and assuming different JES factors. Using 1.9 fb^{-1} of data CDF measures $m_t = 172.7 \pm 1.8$ (stat + JES) ± 1.2 (syst) GeV/c^2 (see Fig. 13). The dominant systematic uncertainty arises from difference between MC generators.

The DØ analysis (Abazov *et al.*, 2008) includes only the $q\bar{q} \rightarrow t\bar{t}$ component in the signal matrix element and calculates the background probability density using only the matrix element for the $W + 4$ partons process. The jet-parton combinations are weighted using information from a b-jet identification algorithm and an *in-situ* JES calibration is performed. The method is calibrated using MC samples generated at various values of m_t and assuming different JES values. Using 1 fb^{-1} of data DØ measures $m_t = 171.5 \pm 1.8$ (stat + JES) ± 1.1 (syst) GeV/c^2 (see Figure 13). The dominant systematic uncertainty arises from uncertainties associated with calibrating the response of the calorimeter to b-quark jets.

CDF has also published a measurement using the matrix element technique in the *dil* channel (Aaltonen *et al.*, 2009). In this channel, no JES *in-situ* calibration is possible. In this analysis, the event selection has been optimized to get the best statistical precision on m_t using neuroevolution (Stanley and Miikkulainen, 2002) to train a NN

discriminant. The signal matrix element includes only the $q\bar{q} \to t\bar{t}$ component. Background probability densities are computed using the matrix elements for the $Z/\gamma^* \to ee, \mu\mu$+jets, $W+ \geq 3$ jets where a jet is misidentified as a lepton, and WW+jets processes. Events with or without identified b-jets are fit separately. Using 2 fb^{-1}, CDF measures $m_t = 171.2 \pm 2.7$ (stat) ± 2.9 (syst) GeV/c^2. The dominant systematic uncertainty is due to uncertainties in the jet energy corrections.

Ideogram Method

The ideogram method can be thought of as an approximation to the matrix element method. A kinematic fit is used to determine $m_t^{\rm reco}$ for each event. A per event probability density is calculated as a function of m_t by calculating the probability of observing $m_t^{\rm reco}$ assuming the true top-quark mass is m_t and knowing the resolution $\sigma_{m_t^{\rm reco}}$. All jet-parton combinations are considered for each event and each carries a weight derived from its corresponding fit chi-squared. Typically, additional weights are included that use information from b-jet identification algorithms. Like the matrix element method the event probability density is built from a signal and a background piece. The signal probability density is a convolution of a Gaussian with a Breit-Wigner while the background probability density is taken from MC simulation. The total likelihood for a given sample of events is obtained from the product of the individual event probability densities. A JES constraint can be incorporated by repeating the kinematic fits for different assumptions on the jet energy corrections scale factor. Like the matrix element method, the ideogram method offers improved statistical sensitivity since it will effectively give more weight to events whose kinematics afford a more precise estimate of $m_t^{\rm reco}$ by virtue of having a narrower event probability density. In terms of sophistication, CPU budget, and statistical sensitivity the ideogram method typically falls between the template and matrix element methods. It should be noted that since it requires a full reconstruction of the $t\bar{t}$ kinematics, this method can only be used in the ljt and had final states.

DØ has performed a measurement using this technique in the ljt channel (Abazov et al., 2007). The event probability density is factorized into the product of two separate probabilities for signal and background each. The first probability depends on m_t and JES and provides the necessary information to constrain the jet energy corrections and to measure the top-quark mass. The second probability depends on the output of a multivariate discriminant designed to separate $t\bar{t}$ from background processes. The variables used in the discriminant are chosen and the discriminant itself is constructed to be uncorrelated with m_t and JES. This second probability helps constrain the observed $t\bar{t}$ fraction in the event sample and to de-weight events that have kinematics more consistent with having originated from background processes. MC simulation is used to account for contributions from wrong jet-parton assignments and background events. The method is calibrated using MC samples generated at a various m_t values. Using 0.43 fb^{-1}, DØ measures $m_t = 173.7 \pm 4.4$ (stat + JES)$^{+2.1}_{-2.0}$ (syst) GeV/c^2. The dominant systematic uncertainty arises from uncertainties associated with calibrating the response of the calorimeter to b-quark jets and from uncertainties associated with modeling the $t\bar{t}$ signal.

The method was first used to measure m_t by CDF, which produced a result in the had channel using 310 pb^{-1} (Aaltonen et al., 2007). The result was limited by the uncertainties in the jet energy corrections. Subsequent m_t determinations in the had channel exploit $W \to qq'$ decays to reduce the jet energy correction systematic and also include significantly larger data sets as described above.

Using the $t\bar{t}$ Cross Section

As mentioned above, there is some ambiguity associated with the theoretical interpretation of the m_t parameter measured by the above techniques. Assuming SM production and decay, an estimate of the top-quark mass can also be made by comparing the measured production cross section to theory predictions. While less precise, this method has the advantage that the m_t parameter in the predictions is theoretically well defined.

DØ has performed this measurement (Abazov et al., 2009). The signal acceptance is estimated as a function of m_t using MC samples generated at various m_t values. The resulting acceptances are smoothed and the production cross section is then measured as a function of m_t as shown in Fig. 14. The m_t dependence of the acceptance arises from the event selection lepton p_T and jet E_T requirements. The measured cross section is compared to several NLO predictions (Beenakker et al., 1989; Cacciari et al., 2008; Moch and Uwer, 2008; Nadolsky et al., 2008) that define m_t as the pole mass. A normalized likelihood function is formed as a function of m_t by comparing the theory prediction with the measured cross section at each assumed top-quark mass. The uncertainty in the theory arising from variations in PDFs and in the renormalization and factorization scales and the uncertainty in the measured cross

section are accounted for in the comparison. Using (Moch and Uwer, 2008) and the combined $ljt + dil$ measured cross section from 1 fb^{-1} of data, DØ measures $m_t = 169.1^{+5.9}_{-5.2}$ GeV/c^2. This result is in agreement with the direct top-quark mass measurements.

Combination

The world average top-quark mass is obtained from a combination of CDF and DØmost precise m_t measurements using up to 5.6 pb^{-1} of data (Aaltonen et al., 2010). Five measurements using data taken in an earlier run (1990-1995) and six measurements using data from the ongoing run (2001-) are used. Work has been performed between the two collaborations to standardize the assessment of systematic uncertainties. For the combination a detailed breakdown of the various sources of uncertainty has been established in order to properly account for correlations among the various measurements. The combination uses the method described in (Lyons et al., 1988). The preliminary combined value for the top-quark mass is $m_t = 173.32 \pm 0.56$ (stat) ± 0.89 (syst) GeV/c^2 which corresponds to a total uncertainty of 1.06 GeV/c^2 and a relative precision of 0.61 %. The combination has a χ^2 of 6.1 for 10 degrees-of-freedom indicating good consistency among the measurements across different experiments and different decay channels. The most recent CDF and DØ measurements in the ljt channel using the matrix element method carry the largest weights in the combination followed by the CDF template measurement in the had channel.

In the future, the statistical and in-situ JES related uncertainties will continue to decrease with the statistics of the data samples employed. The systematic uncertainty has roughly equal contributions from residual jet energy correction uncertainties and uncertainties associated with modeling the $t\bar{t}$ signal from variations in MC generators and color reconnection effects. Work is in progress to better understand these sources of systematic uncertainty with the aim of reducing them. A total top-quark mass uncertainty below 1 GeV/c^2 is potentially achievable in the near future.

2. Mass Difference

The triple product of the discrete symmetries of charge conjugation (C), parity conjugation (P), and time reversal (T) is an exact symmetry of any local Lorentz-invariant quantum field theory and requires that the particle and anti-particle masses be identical. However, CPT can be violated in some non-local new physics models (Colladay and Kostelecky, 1997). Tests of CPT have been performed in many sectors with no evidence of CPT violation (Nakamura et al., 2010). Measuring a $q - \bar{q}$ mass difference is usually difficult since hadronization introduces QCD binding and non-perturbative showering effects. However, since it decays before hadronizing the top quark provides a unique opportunity to measure a $q - \bar{q}$ mass difference free from these QCD effects (Cembranos et al., 2008).

DØ performed the measurement of the $t - \bar{t}$ mass difference in the ljt final state using 1 fb^{-1} of data (Abazov et al., 2009). This analysis uses the matrix element technique as in (Abazov et al., 2008) to form probability densities for each event as a function of the mass of the t and the $\bar{t}$ and the $t\bar{t}$ signal fraction. SM $t\bar{t}$ production and decay is assumed and the lepton charge is used to determine whether the $\ell\nu b$ invariant mass should be assigned as m_t or $m_{\bar{t}}$. Many of the systematic uncertainties relevant for the top-quark mass measurements cancel here. The result is $m_t - m_{\bar{t}} = 3.8 \pm 3.4$ (stat) ± 1.2 (syst) GeV/c^2 (Abazov et al., 2009), consistent with CPT invariance. This measurement is statistically limited.

CDF has released a preliminary measurement using 5.6 fb^{-1} and finds $m_t - m_{\bar{t}} = -3.3 \pm 1.4$ (stat) ± 1.0 (syst) GeV/c^2, also consistent with CPT invariance.

3. Charge

The electric charge is a fundamental property of the top quark predicted in the SM to be $+2/3$ in units of the electric charge of the electron. An experimental determination of the top-quark electric charge serves as a check of SM consistency. In the all the $t\bar{t}$ analyses so far discussed the assumption is made that $t \to W^+ b$ and $\bar{t} \to W^- \bar{b}$. However, since none of these analyses have attempted to differentiate a b-jet from a $\bar{b} - jet$, it is possible that what is being observed is an exotic top-like particle that decays to $W^+ \bar{b}$ and $W^- b$. Just such a particle can be found in (Chang et al., 1999; Choudhury et al., 2002), a four generation model that postulates a $-4/3$ charged quark that decays to $W^- b$. In this model, the right-handed b-quark mixes with a $-1/3$ charged heavy quark Q_1. Its weak isospin partner Q_4 has charge -4/3, a mass around 172.5 GeV/c^2 and would be the particle observed at the Tevatron while

the left-handed real top quark has a mass around 270 GeV/c^2 and would thus far have escaped detection. It is worth noting that the precision electroweak data can be satisfactorily described by this model.

The electric charge of the top-quark can be determined from measurements of the electromagnetic coupling strength using $t\bar{t}\gamma$ events or by reconstructing the electric charges of the top-quark decay products. The production cross section for $p\bar{p} \to t\bar{t}\gamma$ is proportional to the square of the top-quark electric charge. However this measurement suffers from a large irreducible background coming from processes where the photon is radiated from the b-quark or the W-boson. Both CDF and DØ use the second approach to measure the top-quark electric charge in the ljt channel. A kinematic fit is used to fully reconstruct the $t\bar{t}$ kinematics and choose particular jet-parton and b-jet pairings (ie. is the b-quark jet paired with the leptonically decaying W, $\ell\nu b$, or the hadronic decaying W, $qq'b$). The flavor of the b-jets must then be specified by determining whether the jet originated from a b-quark or a $\bar{b}$-quark. The sum of the electric charges of the charged lepton and the appropriate electric charge of the b-jet for the $\ell\nu b - jet$ pairing is used as an estimate of the top-quark charge.

CDF requires that at least one jet is identified as a b-jet using an algorithm that exploits the long lifetime of b-hadrons. A kinematic fit is employed and the jet-parton and b-jet pairings are taken from the permutation yielding the lowest fit chi-squared. This corresponds to the correct assignment about 76% of the time. Soft lepton taggers identify the flavor of the b-jets with a 69% purity. The purity of the b-jet flavor determination is calibrated using $b\bar{b}$ data and MC events. Using 2.7 fb^{-1} the CDF data is consistent with the SM expectation (Aaltonen *et al.*, 2010) and excludes the exotic -4/3 charged quark interpretation at 95% confidence level.

DØ requires that at least two jets are identified as b-jets and also uses a kinematic fit to reconstruct the $t\bar{t}$ kinematics and choose the jet-parton and b-jet pairings. Using the permutation with the lowest fit chi-squared yields the correct assignments about 84% of the time. A jet-charge algorithm is used to identify the flavor of the b-jet. The optimized estimator of the jet charge is $q_{jet} = (\sum_i q_i p_{Ti}^{0.6})/(\sum_i p_{Ti}^{0.6})$ where i runs over all tracks associated with the jet in question. The expected q_{jet} distributions for b, $\bar{b}$, c and $\bar{c}$ jets are derived from di-jet data samples enhanced in heavy flavor. For the SM case, the leptonic decaying top-quark charge is reconstructed as the sum of lepton charge and the charge of the b-jet assigned to this top quark while the hadronic decaying top-quark charge is computed as the sum of the second b-jet minus the lepton charge. Using 0.4 fb^{-1} the DØ data is consistent with the SM expectation (Abazov *et al.*, 2007) and excludes the exotic -4/3 charged quark interpretation at the 92.2% confidence level.

4. Width

The total width of the top quark is precisely determined in the SM once m_t is specified. Because m_t is large, so is the top-quark width, Γ_t, and consequently its lifetime, $\sim 1/\Gamma_t$, is extremely short, which precludes measuring the width using reconstructed displaced vertices from $t \to Wb$ decays. A measurement of Γ_t can also be determined from the width of the $m_t^{\rm reco}$ distribution. In the SM at NLO, neglecting terms of order m_b^2/m_t^2 , α_s^2, and $\alpha_s^2/\pi m_W^2/m_t^2$, the top-quark total width is (Jezabek and Kuhn, 1989):

$$\Gamma_t = \Gamma_t^0 \left(1 - \frac{m_W^2}{m_t^2}\right)^2 \left(1 + 2\frac{m_W^2}{m_t^2}\right) \left[1 - \frac{2\alpha_s}{3\pi}\left(\frac{2\pi^2}{3} - \frac{5}{2}\right)\right] \tag{18}$$

which yields approximately $\Gamma_t = 1.5$ GeV/c^2 for a 175 GeV/c^2 top-quark mass. Deviations from the SM expectation could signal the precense of BSM physics contributions arising, for example, from $t \to H^+b$ decays, anomalous tWb form factors, enhanced rates of $t \to dW^+$ or $t \to sW^+$ decays, or the existence of a fourth-generation b' quark.

CDF uses 1 fb^{-1} of data in the ljt channel with at least one identified b-jets and employs a kinematic fit to obtain the $m_t^{\rm reco}$ distribution (Aaltonen *et al.*, 2009). The shape of the $m_t^{\rm reco}$ distribution is sensitive to the top-quark width and a template method is employed to measure Γ_t. The CDF data is shown in Fig. 15. A confidence interval based on the method of (Feldman and Cousins, 1998) is used to determine (Aaltonen *et al.*, 2009) $\Gamma_t < 13.1$ GeV/c^2 at 95% confidence level. The dominant systematic uncertainties arise from uncertainties in the jet energy corrections and in modeling the jet energy resolutions.

Since the SM top-quark width is far smaller than the experimental resolution on $m_t^{\rm reco}$ it is difficult to reach high precision using the direct measurement technique described above. However it is also possible to extract Γ_t by determining its partial width $\Gamma(t \to Wb)$ using the measured cross section for the electroweak production of single top quarks and the measured top-quark branching fraction $\mathcal{B}(t \to Wb)$, $\Gamma_t = \Gamma(t \to Wb)/\mathcal{B}(t \to Wb)$ (Carlson and Yuan, 1995; Yuan, 1993, 1995). This method assumes that the couplings at the tWb production and decay vertices are the same, that the production via flavor changing neutral currents is negligible, and that $|V_{td}|$, $|V_{ts}| << |V_{tb}|$. The $\mathcal{B}(t \to Wb)$ is determined from the R_b measurement discussed in Sec. IX.A assuming $\mathcal{B}(t \to Wq) = 1$. Electroweak

single top production can occur via an s-channel or a t-channel exchange of a W boson. If the $s + t$-channel cross section is used to extract Γ_t, then the SM ratio (s/t) is assumed. To minimize the model dependence of this method, the dominant t-channel cross section can instead be used.

DØ uses the 1 fb^{-1} R_b measurement (Abazov *et al.*, 2008) and a 2.3 fb^{-1} t-channel single top-quark production cross section measurement (Abazov *et al.*, 2010) to determine the top-quark width using this method. A NLO QCD calculation is used to determine $\mathcal{B}(t \to Wb)$ from the t-channel cross section and the correlated systematic uncertainties have been taken into account. Using these inputs the top quark-width (Abazov *et al.*, 2010) is measured to be: $\Gamma_t = 1.99^{+0.69}_{-0.55}$ GeV/c^2 which is equivalent to a lifetime of $\tau_t = (3.3^{+1.3}_{-0.9}) \times 10^{-25}$ s in agreement with the SM expectation (cf. Fig. 15). This top-quark width measurement can be used to extract a limit on $|V_{tb'}|$, an element of a four generation CKM matrix characterizing the coupling strength of the top quark with a hypothetical fourth-generation b' quark. Assuming $m_{b'} > m_t - m_W$ and the unitarity of the extended CKM matrix, this measurement yields $|V_{tb'}| < 0.63$ at 95% confidence level.

5. Spin Correlations

At the Tevatron the spins of the t and $\bar{t}$ at production are correlated (Barger *et al.*, 1989; Mahlon and Parke, 1996). The top quarks decay on a time scale that is short relative to the hadronization and spin-flip time scale and, hence, the spin correlations are preserved and affect the angular distributions of the top-quark decay products (Falk and Peskin, 1994). Calculations show that the angular correlations are strongest for the charged leptons (θ_ℓ) or the down-type quarks (θ_d) from the decay of the W-bosons (Mahlon and Parke, 2010). Experimentally, the two dimensional distribution ($\cos\theta_\ell$, $\cos\theta_d$) or ($\cos\theta_{\ell+}$, $\cos\theta_{\ell-}$) is used to determine the spin-correlation coefficient, C,

$$\frac{1}{\sigma}\frac{d\sigma}{d\cos\theta_1 d\cos\theta_2} = \frac{1}{4}(1 - C\cos\theta_1\cos\theta_2) \tag{19}$$

where σ denotes the total $t\bar{t}$ cross section in the relevant decay channel. This relationship has been calculated to order α_s^3 (Bernreuther *et al.*, 2004). The angles are measured relative to a given axis. Three common choices are a) the beam basis, which uses the direction of one of the colliding hadrons as the reference axis, b) the helicity basis, which uses the t flight direction as the reference axis, and c) the off-diagonal basis, which uses a reference axis chosen so that the contribution from like-spin $t - \bar{t}$ pairs vanishes at leading order in perturbation theory (Parke and Shadmi, 1996). The measured coefficient depends on the fraction of $t\bar{t}$ pairs produced at threshold, the fraction produced by gluon-fusion, and changes as a function of $m_{t\bar{t}}$. In the absence of selection or acceptance requirements C can be computed in terms of expectation values (Bernreuther *et al.*, 2004) $C = -9 < \cos\theta_1\cos\theta_2 >$, which vary with the choice of basis employed as shown in Table II.

The observation of $t - \bar{t}$ spin correlations would confirm that the top quark is a spin 1/2 particle and that it decays before strong interaction processes affect the t and $\bar{t}$ spins. Several BSM models could effect the measured coefficient. The presence of a techni-η in two scale technicolor (Eichten and Lane, 1994) would enhance the unlike spin contributions. A new vector particle associated with topcolor (Hill and Parke, 1994) would affect the spin correlations by changing the fraction of gluon-fusion produced $t\bar{t}$ pairs. On the decay side, BSM contributions from $t \to H^+ b$ decays, for example, would affect the correlations between the top-quark spin and its decay products and therefore modify the observed angular correlations (Mahlon and Parke, 1996).

Both CDF and DØ have performed preliminary measurements of the spin correlation in the *dil* channel using 2.8 fb^{-1} and 4.2 fb^{-1} of data, respectively. To fully reconstruct the $t\bar{t}$ kinematics CDF uses a likelihood method to determine the best solution for the unknown neutrino momenta using the observed lepton, jet, and $\not{E}_T$ energies and taking into account their relevant resolutions, while DØ uses the neutrino weighting technique described above in Sec. IX.C.1. After reconstructing the $t\bar{t}$ final state, two dimensional ($\cos\theta_{\ell-}$, $\cos\theta_{\ell+}$) templates are constructed. The signal templates are built by reweighing PYTHIA $t\bar{t}$ samples using Eq. 19. A maximum likelihood fit to the data, including systematic uncertainties via nuisance parameters, gives $C = 0.32^{+0.55}_{-0.78}$ for CDF in the off-diagonal basis and $C = -0.17^{+0.64}_{-0.53}$ for DØ in the beam basis.

CDF has also performed a preliminary measurement of the $t\bar{t}$ spin correlation in both the helicity and beam bases using the *ljt* channel in 5.3 fb^{-1} of data. A template fit to the two dimension distribution ($\cos\theta_\ell$, $\cos\theta_d$) is used to determine C. The difficulty here lies in determining which jet comes from the hadronization of the down-type quark. It is assumed to be the jet closest to the b-jet in the W-boson rest frame. This prescription gives the right assignment about 60 % of the time (Mahlon and Parke, 1996). CDF measures $C = 0.48 \pm 0.48$ (stat) ± 0.22 (syst) in the helicity basis and $C = 0.72 \pm 0.64$ (stat) ± 0.26 (syst) in the beam basis. Distributions from the DØ and CDF analyses are shown in Fig. 16.

All these results are completely dominated by the statistical uncertainty and will benefit from including the full Tevatron statistics in the future. This measurement will remain interesting at the Tevatron since a different spin correlation will be produced at the LHC where $t\bar{t}$ production is dominated by gluon-gluon fusion rather than $q\bar{q}$ annihilation.

X. DIRECT SEARCHES FOR NEW PHYSICS IN THE TOP-QUARK SECTOR

A. Search for $t\bar{t}$ Resonances

Many SM extensions predict massive new particles that can decay to a $t\bar{t}$ pair. For example, the scalar color-singlets predicted in two-Higgs doublets models (Dicus $et~al.$, 1994), the vector color-singlet Z' particles postulated in extended gauge theories (Leike, 1999), the KK_{gluon} and KK_Z states of extra dimension models (Lillie $et~al.$, 2007), and the axigluons, colorons, and vector color-octet particles that appear in top-color models (Hill and Parke, 1994; Sehgal and Wanninger, 1988), all couple to $t\bar{t}$ pairs and would affect the $m_{t\bar{t}}$ distribution. In particular, resonances whose natural width is small relative to the experimental resolution would appear as an anomalous peak. Both CDF and DØ have searched for such peaks using the ljt channel. In all such searches so far performed at the Tevatron, the natural width of the resonance, generically denoted Z' since Z' models are often used as benchmark models, is taken to be $\Gamma_{Z'} = 0.012 m_{Z'}$, well below the typical experimental resolution achieved of $0.05 - 0.10 \times m_{t\bar{t}}$. The resulting upper limits derived from these analyses are, in general, valid for all widths up to $\Gamma_{Z'} \approx 0.05 m_{Z'}$ unless otherwise specified.

Different approaches were used to reconstruct $m_{t\bar{t}}$ for each event. CDF uses (Aaltonen $et~al.$, 2008) a matrix element technique similar to the one developed for the top-quark mass measurement as described in Sec. IX.C.1. The mean of the event probability density distribution is used to determine the reconstructed $m_{t\bar{t}}$ value for that particular event. Templates are then formed for a variety of postulated Z' resonances and including background contributions from $t\bar{t}$, W+jets, and QCD processes. A binned likelihood fit to the data is performed letting the Z' production cross section float in the fit. Using 0.68 fb^{-1}, the data, shown in Fig. 17, is found to be consistent with SM expectations and CDF excludes a leptophobic top-color resonance candidate with a mass less than 725 GeV/c^2 (Aaltonen $et~al.$, 2008) at the 95% confidence level. A complementary analysis uses a slightly different event selection and a kinematic fit to obtain the reconstructed $m_{t\bar{t}}$ value for each event. With a 0.96 fb^{-1} data set this CDF analysis excludes a leptophobic Z' with a mass less than 720 GeV/c^2 (Aaltonen $et~al.$, 2008) at the 95% confidence level. The production cross section for any narrow Z'-like new particle decaying to $t\bar{t}$ is determined to be less that 0.64 pb at the 95% confidence level for all $m_{Z'} > 600$ GeV/c^2. All the above limits include the affects of systematic uncertainties on the background normalizations, the signal efficiencies, and the shapes of the signal and background $m_{t\bar{t}}$ distributions.

DØ has performed a similar search in the ljt channel requiring at least one identified b-jet in each event. A kinematic fit is employed to determine the reconstructed $m_{t\bar{t}}$ value for each event and a binned likelihood based on the template method is employed to fit the data. As no significant deviation from the SM expectation is observed, as shown in Fig. 17, a Bayesian approach is employed to set 95 % confidence level limits on $\sigma_X.\mathcal{B}(X \to t\bar{t})$ for different values of m_X. Systematic uncertainties that affect both the normalization and the shape of the signal and background $m_{t\bar{t}}$ distributions are taken into account. Using 0.9 fb^{-1} DØ excludes a lepto-phobic Z' with a mass less than 700 GeV/c^2 at 95 % confidence level (Abazov $et~al.$, 2008).

CDF has also searched for a massive vector color-octet particle, G, such as a massive gluon that preferentially couples to top quarks (Aaltonen $et~al.$, 2010). Neglecting the gluon-G coupling, the strength of the massive gluon coupling to any quark is $\lambda_q \alpha_s$, where α_s is the SM strong coupling constant. In this analysis the mass and width of the particle G are denoted M and Γ. If only SM top-quark decays are assumed, the $t\bar{t}$ production through an intermediate G interferes with the SM $t\bar{t}$ production. After selecting ljt events the $m_{t\bar{t}}$ spectrum is reconstructed using a dynamical likelihood method similar to the matrix element methods described in Sec. IX.C.1. A standard unbinned likelihood technique is then applied to fit the data. If the mass M and Γ/M are fixed, the signal $m_{t\bar{t}}$ distribution depends only on the assumed coupling strength λ_t. Taking into account systematic effects, limits on λ_t as a function of M for $\Gamma/M = 0.1$ and $\Gamma/M = 0.5$ are determined. Using 1.9 fb^{-1} the data are consistent with SM expectations and CDF excludes the presence of massive gluons with couplings to the top quark larger than 0.5 for $400 < M < 800$ GeV/c^2 and $0.05 < \Gamma/M < 0.5$ at the 95% confidence level.

B. Search for Top-quark like t' Quarks

A number of BSM models predict a fourth generation of massive fermions. The precise measurement of the Z-boson invisible width excludes the existence of a fourth neutrino family with mass less than half the Z-boson mass but a new neutral lepton with a mass larger than that is still compatible with electroweak data. An extra chiral fermion family appears in grand-unified theories (GUTs) (Ross, 1984) or $N = 2$ SUSY models (He *et al.*, 2001). Often a small mass splitting between the fourth generation t' and its down-type partner b' is preferred so that for $m_{t'} > m_{b'} + m_W$ and moderate mixing between t' and the SM light down-type quarks q, the decay mode $t' \rightarrow Wq$ dominates (Frampton *et al.*, 2000).

In case the fourth generation fermions are vector-like, experimental constraints are even weaker. Such heavy exotic vector-like quarks are predicted by little Higgs models (Dobrescu and Hill, 1998; Han *et al.*, 2003) or models with large extra-dimensions. If not too heavy, such particles can be pair produced at the Tevatron and can decay to Wq with a substantial branching fraction. Some models predict the production of a single vector-like heavy t' in association with a SM top quark (Dobrescu *et al.*, 2009).

Using 0.76 fb^{-1}, CDF has searched for the pair production of massive up-type t' quark/anti-quark pairs that each decay to Wq using the ljt channel (Aaltonen *et al.*, 2008). The analysis employs a kinematic fit to determine $m_{t'}^{\mathrm{reco}}$ for each event and uses the H_T distribution to further discriminate a possible signal from SM processes. A two dimensional binned likelihood fit of the background and signal to the observed $(H_T, m_{t'}^{\mathrm{reco}})$ distribution in data is performed to set limits on the t' mass. Systematic uncertainties are treated as nuisance parameters and include variations in signal and background normalizations and shape. While still statistically limited systematic uncertainties are dominated by the uncertainty on the jet energy calibration. In the fit the $t\bar{t}$ production cross section is constrained to its SM value. Assuming $\mathcal{B}(t' \rightarrow Wq) = 1$, CDF excludes a t' mass below 256 GeV/c^2 at 95 % confidence level.

CDF and DØ have provided preliminary updates for this t' search with more luminosity under the same assumptions. Using 4.6 fb^{-1}, CDF excludes t' with masses below 335 GeV/c^2, while DØ using 4.3 fb^{-1} excludes t' masses below 296 GeV/c^2 both at 95 % confidence level.

C. Search for Scalar Top Quarks

In supersymmetric models (Haber and Kane, 1985; Martin, 1997; Nilles, 1984) each of the SM fermions has a scalar partner. In particular the left- and right-handed top quarks each have a scalar super-partner: $\tilde{t}_R$ and $\tilde{t}_L$. The mass eigenstates $\tilde{t}_1$ and $\tilde{t}_2$ of these two scalar top quarks are rotated with respect to $\tilde{t}_R$ and $\tilde{t}_L$. Due to the large top-quark mass, this mixing can be substantial and $\tilde{t}_1$ and $\tilde{t}_2$ can have a large mass difference. Hence, the lightest scalar top quark can be the lightest scalar quark and even lighter than the top quark itself. In the MSSM the scalar top quarks are mainly produced in $\tilde{t}_1\tilde{t}_1$ pairs via the strong interaction. In general the production cross section is relatively small. For example, when $m_{\tilde{t}} = m_t$ the $\tilde{t}_1\tilde{t}_1$ pair production cross section is about 10 times smaller than the $t\bar{t}$ production cross section. The $\tilde{t}$ decay differs according to the parameters of the model and is particularly dependent on the masses of the super-particles involved. If kinematically possible, it can decay though the two body processes $\tilde{t} \rightarrow t\tilde{\chi}_1^0$, $\tilde{t} \rightarrow b\tilde{\chi}_1^+$, or $\tilde{t} \rightarrow c\tilde{\chi}_1^0$, where $\tilde{\chi}_1^0$ is the lightest neutralino and $\tilde{\chi}_1^+$ the lightest chargino. Three-body decays are also possible, $\tilde{t} \rightarrow W^+b\tilde{\chi}_1^0$, $\tilde{t} \rightarrow b\tilde{l}^+\nu_l$, or $\tilde{t} \rightarrow bl^+\tilde{\nu}_l$, where $\tilde{l}$ and $\tilde{\nu}_l$ are the super-partners of a given lepton l and neutrino ν_l. For scalar top quarks lighter than the top quark the decay channel $\tilde{t} \rightarrow \tilde{\chi}_1^+b \rightarrow (\tilde{\chi}_1^0W^+)b$ can dominate. In this decay channel the $\tilde{t}_1\tilde{t}_1$ pair signature is similar to the $t\bar{t}$ one apart from the presence of the neutralinos, whose experimental signature mimics that of a neutrino and are mostly produced back-to-back.

DØ searched for some admixture of $\tilde{t}_1\tilde{t}_1$ pairs in the $t\bar{t}$ final state using the ljt channel (Abazov *et al.*, 2009). In this analysis the neutralino mass has been fixed to a value close to the experimental LEP limit, $m_{\tilde{\chi}_1^0} = 50$ GeV/c^2, while the $\tilde{t}$ mass has been varied from 130 to 190 GeV/c^2 and the chargino mass from 90 to 150 GeV/c^2. Events with at least three jets and at least one identified b-jet have been used. For events with at least four jets, a kinematic reconstruction to the $t\bar{t}$ hypothesis is performed. As the $t\bar{t}$ signature is very similar to the $\tilde{t}$ signal, a multivariate likelihood discriminant is employed to separate the two processes. Separate discriminants have been trained for the three-jet and the four-jet events. Variables based on the two jet or three jet invariant masses, the reconstructed top-quark mass, the jet p_T, the scalar sum of the jet p_T, and the angular separation between the jets are used as inputs to the discriminants. As no excess over the SM expectation is observed, a binned likelihood over the discriminant distributions is constructed using Bayesian statistics to extract the upper limits on the $\tilde{t}_1\tilde{t}_1$ pair production cross section taking systematic uncertainties into account. Using 0.9 fb^{-1}, DØ obtains limits that are a factor of 2 to 13 times larger than the MSSM theory prediction and agree with the expected limits within uncertainties (Abazov *et al.*, 2009).

When both scalar top quarks decay as $\tilde{t} \to bl\tilde{\nu}_l$, the experimental signature is similar to the $t\bar{t}$ *dil* signature. Searches exploiting this decay channel have been performed by CDF (Aaltonen *et al.*, 2010) and DØ (Abazov *et al.*, 2008). In these analyses the selection criteria are optimized to suppress the $t\bar{t}$ contributions. The data are consistent with the SM expectation and the resulting limits significantly extend the LEP2 exclusions when $m_{\tilde{t}} >> m_{\tilde{\nu}}$.

XI. PROSPECTS AND CONCLUSIONS

Owing to its large mass, the top quark was discovered relatively recently and potentially offers a unique window into Beyond-the-Standard-Model physics. Using data samples with $\mathcal{O}(10^3)$ candidate $t\bar{t}$ events, the CDF and DØ experiments at the Fermilab Tevatron have pioneered numerous analyses to exploit these unique events. They have instituted a broad physics program that tests the Standard Model descriptions of the $t\bar{t}$ production mechanisms, the top-quark decay widths, and the intrinsic properties of the top quark such as its electric charge and mass. They have also probed the $t\bar{t}$ event samples for direct evidence of new particles that might mimic the experimental signature of the top-quark, such as the scalar top quarks of Supersymmetry or the fourth generation t' quark of Grand Unified Theories. A few of the measurements are systematics limited and have reached precisions comparable to those associated with the relevant theory predictions, such as the measured production cross section and the measured top-quark mass. The data provide strong evidence that the top quark carries electric charge $+2/3$ in units of the electron electric charge. Measurements of the polarization fractions of W bosons from top-quark decay and of $t\bar{t}$ spin correlations are consistent with the Standard Model expectation of a spin 1/2 particle with a $V - A$ coupling to the charged weak current. The decay widths of the top-quark are also consistent with the Standard Model expectations, being dominated by $t \to W^+ b$ and with no evidence of anomalous flavor-changing-neutral-current or charged higgs decays. The results of these many measurements when compared across the various $t\bar{t}$ final states yield consistent results - again as expected by the Standard Model. In general, the detailed exploration of the $t\bar{t}$ sample so far performed by the Tevatron experiments reveals no significant discrepancies with the Standard Model. Except for a few cases, most all the measurements are limited by their statistical uncertainty. So the precise study of the top quark will persevere as the Tevatron is continuing to deliver collision data focusing on the unique features offered by a $t\bar{t}$ production dominated by $q\bar{q}$ annihilation process. The LHC experiments expect to collect $t\bar{t}$ samples that are a few orders of magnitude larger in the coming several years. With these sorts of statistics most all the measurements should achieve levels of precision that more thoroughly probe the Standard Model expectations and more stringently restrict the parameter space of a wide variety of new physics models. Even for those measurements already systematics limited at the Tevatron, the LHC experiments may be able to exploit the larger statistics to identify a sub-set of events less affected by the systematics in question or to employ analysis techniques which trade statistical uncertainties for systematic uncertainties to achieve an improvement in the total uncertainty. The LHC is poised to build upon the foundation laid by the Tevatron experiments, and use the physics of the top quark to more fully elucidate the workings of nature at its most fundamental level.

XII. ACKNOWLEDGEMENTS

REFERENCES

Aaltonen T., *et al.* (CDF) (2007), Phys. Rev. Lett., **98**, 142001, arXiv:hep-ex/0612026
Aaltonen T., *et al.* (CDF) (2008a), Phys. Rev. Lett., **100**, 062005, arXiv:0710.4037 [hep-ex]
Aaltonen T., *et al.* (CDF) (2008b), Phys. Rev., **D78**, 111101, arXiv:0712.3273 [hep-ex]
Aaltonen T., *et al.* (CDF) (2008c), Phys.Rev., **D77**, 112001, arXiv:0708.3642 [hep-ex]
Aaltonen T., *et al.* (CDF) (2008d), Phys. Rev. Lett., **101**, 202001, arXiv:0806.2472 [hep-ex]
Aaltonen T., *et al.* (CDF) (2008e), Phys. Rev., **D77**, 051102, arXiv:0710.5335 [hep-ex]
Aaltonen T., *et al.* (CDF) (2008f), Phys. Rev., **D 78**, 052006, arXiv:0807.2204 [hep-ex]
Aaltonen T., *et al.* (CDF) (2008g), Phys. Rev. Lett., **100**, 161803, arXiv:0801.3877 [hep-ex]
Aaltonen T., *et al.* (CDF) (2008h), Phys. Rev. Lett., **100**, 231801, arXiv:0709.0705 [hep-ex]
Aaltonen T., *et al.* (CDF) (2008i), Phys. Rev. Lett., **101**, 192002, arXiv:0805.2109 [hep-ex]
Aaltonen T., *et al.* (CDF) (2009a), Phys. Rev., **D79**, 112007, arXiv:0903.5263 [hep-ex]
Aaltonen T., *et al.* (CDF) (2009b), Phys. Rev. Lett., **102**, 042001, arXiv:0808.2167 [hep-ex]
Aaltonen T., *et al.* (CDF) (2009c), Phys. Rev. Lett., **102**, 222003, arXiv:0903.2850 [hep-ex]

Aaltonen T., *et al.* (CDF) (2009d), Phys. Rev., **D79**, 092005, arXiv:0809.4808 [hep-ex]

Aaltonen T., *et al.* (CDF) (2009e), Phys. Rev., **D79**, 031101, arXiv:0807.4262 [hep-ex]

Aaltonen T., *et al.* (CDF) (2009f), Phys. Rev., **D79**, 072005, arXiv:0901.3773 [hep-ex]

Aaltonen T., *et al.* (CDF) (2009g), Phys. Rev., **D80**, 051104, arXiv:0906.5371 [hep-ex]

Aaltonen T., *et al.* (CDF) (2009h), Phys. Rev. Lett., **102**, 152001, arXiv:0807.4652 [hep-ex]

Aaltonen T., *et al.* (CDF) (2009i), Phys. Rev. Lett., **103**, 101803, arXiv:0907.1269 [hep-ex]

Aaltonen T., *et al.* (CDF) (2009j), Phys. Rev., **D79**, 072001, arXiv:0812.4469 [hep-ex]

Aaltonen T., *et al.* (Tevatron Electroweak Working Group) (2010a), arXiv:1007.3178 [hep-ex]

Aaltonen T., *et al.* (CDF) (2010b), Accepted by Phys.Rev. D, arXiv:1006.4597 [hep-ex]

Aaltonen T., *et al.* (CDF) (2010c), Phys. Rev. Lett., **105**, 012001, arXiv:1004.3224 [hep-ex]

Aaltonen T., *et al.* (CDF) (2010d), Phys. Rev., **D81**, 052011, arXiv:1002.0365 [hep-ex]

Aaltonen T., *et al.* (CDF) (2010e), Phys.Rev., **D81**, 092002, arXiv:1002.3783 [hep-ex]

Aaltonen T., *et al.* (CDF) (2010f), Phys.Rev.Lett., **105**, 042002, arXiv:1003.0224 [hep-ex]

Aaltonen T., *et al.* (CDF) (2010g), Phys. Rev., **D81**, 032002, arXiv:0910.0969 [hep-ex]

Aaltonen T., *et al.* (CDF) (2010h), Phys. Lett., **B691**, 183, arXiv:0911.3112 [hep-ex]

Aaltonen T., *et al.* (CDF) (2010i), Submitted to Phys.Rev. D, arXiv:1009.0266 [hep-ex]

Abachi S., *et al.* (D0) (1995), Phys.Rev.Lett., **74**, 2632, arXiv:9503003 [hep-ex]

Abazov V., *et al.* (D0) (2006a), Nucl.Instrum.Meth., **A565**, 463, arXiv:0507191 [physics]

Abazov V., *et al.* (D0) (2009a), Phys.Rev.Lett., **103**, 141801, arXiv:0908.0766 [hep-ex]

Abazov V., *et al.* (D0) (200n), Nucl.Instrum.Meth., **Annn**, nnn

Abazov V. M., *et al.* (D0) (2004), Nature, **429**, 638, arXiv:hep-ex/0406031

Abazov V. M., *et al.* (D0) (2006b), Phys. Rev., **D74**, 112004, arXiv:hep-ex/0611002

Abazov V. M., *et al.* (D0) (2007a), Phys. Rev. Lett., **98**, 181802, arXiv:hep-ex/0612052

Abazov V. M., *et al.* (D0) (2007b), Phys. Rev. Lett., **98**, 041801, arXiv:hep-ex/0608044

Abazov V. M., *et al.* (D0) (2007c), Phys. Rev., **D75**, 092001, arXiv:hep-ex/0702018

Abazov V. M., *et al.* (D0) (2008a), Phys. Rev., **D78**, 012005, arXiv:0803.0739 [hep-ex]

Abazov V. M., *et al.* (D0) (2008b), Phys. Rev. Lett., **100**, 142002, arXiv:0712.0851 [hep-ex]

Abazov V. M., *et al.* (D0) (2008c), Phys. Rev. Lett., **100**, 062004, arXiv:0711.0032 [hep-ex]

Abazov V. M., *et al.* (D0) (2008d), Phys. Rev. Lett., **101**, 182001, arXiv:0807.2141 [hep-ex]

Abazov V. M., *et al.* (D0) (2008e), Phys. Lett., **B668**, 98, arXiv:0804.3664 [hep-ex]

Abazov V. M., *et al.* (D0) (2008f), Phys. Lett., **B659**, 500, arXiv:0707.2864 [hep-ex]

Abazov V. M., *et al.* (D0) (2008g), Phys. Rev. Lett., **100**, 192003, arXiv:0801.1326 [hep-ex]

Abazov V. M., *et al.* (D0) (2009b), Phys. Rev., **D80**, 071102, arXiv:0903.5525 [hep-ex]

Abazov V. M., *et al.* (D0) (2009c), Phys. Rev. Lett., **103**, 132001, arXiv:0906.1172 [hep-ex]

Abazov V. M., *et al.* (D0) (2009d), Phys. Rev., **D80**, 092006, arXiv:0904.3195 [hep-ex]

Abazov V. M., *et al.* (D0) (2009e), Phys. Lett., **B679**, 177, arXiv:0901.2137 [hep-ex]

Abazov V. M., *et al.* (D0) (2009f), Phys. Lett., **B674**, 4, arXiv:0901.1063 [hep-ex]

Abazov V. M., *et al.* (D0) (2009g), Phys. Rev. Lett., **102**, 092002, arXiv:0901.0151 [hep-ex]

Abazov V. M., *et al.* (D0) (2009h), Phys. Rev. Lett., **102**, 191802, arXiv:0807.0859 [hep-ex]

Abazov V. M., *et al.* (D0) (2009i), Phys. Lett., **B682**, 278, arXiv:0908.1811 [hep-ex]

Abazov V. M., *et al.* (The D0) (2010a), Nucl. Instrum. Meth., **A620**, 490, arXiv:1002.4224 [hep-ex]

Abazov V. M., *et al.* (D0) (2010b), Phys. Lett., **B693**, 515, arXiv:1001.1900 [hep-ex]

Abazov V. M., *et al.* (D0) (2010c), arXiv:1009.5686 [hep-ex]

Abazov V. M., *et al.* (D0) (2010d), arXiv:1008.4284 [hep-ex]

Abazov V. M., *et al.* (D0) (2010e), Phys. Lett., **B682**, 363, arXiv:0907.4259 [hep-ex]

Abazov V. M., *et al.* (D0) (2010f), Phys. Rev., **D82**, 032002, arXiv:0911.4286 [hep-ex]

Abazov V. M., *et al.* (D0) (2010g), To be submitted

Abazov V. M., *et al.* (D0) (2010h), Phys. Lett., **B693**, 81, arXiv:1006.3575 [hep-ex]

Abbiendi G., *et al.* (2006), Eur.Phys.J, **C45**, 291, 0508062 [hep-ex]

Abe F., *et al.* (CDF) (1994), Phys.Rev.Lett., **73**, 225, arXiv:9405005 [hep-ex]

Abe F., *et al.* (CDF) (1995), Phys.Rev.Lett., **74**, 2626, arXiv:9503002 [hep-ex]

Abreu P., *et al.* (DELPHI) (1998), Eur. Phys. J., **C2**, 581

Abulencia A., *et al.* (CDF) (2006a), Phys. Rev., **D73**, 112006, arXiv:hep-ex/0602008 [hep-ex]

Abulencia A., *et al.* (CDF) (2006b), Phys. Rev. Lett., **96**, 042003, arXiv:hep-ex/0510065

Abulencia A., *et al.* (CDF) (2006c), Phys. Rev., **D73**, 032003, arXiv:hep-ex/0510048 [hep-ex]

Abulencia A., *et al.* (CDF) (2007), J.Phys., **G34**, 2457, arXiv:0508029 [hep-ex]

Acosta D., *et al.* (CDF) (2005a), Phys.Rev., **D72**, 032002, arXiv:0506001 [hep-ex]

Acosta D., *et al.* (CDF) (2005b), Phys.Rev., **D71**, 052003, arXiv:0410041 [hep-ex]

Agashe K., A. Delgado, M. J. May, and R. Sundrum (2003), JHEP, **08**, 050, arXiv:hep-ph/0308036

Aguilar-Saavedra J. A. (2004), Acta Phys. Polon., **B35**, 2695, arXiv:hep-ph/0409342

Aguilar-Saavedra J. A., *et al.* (2007), Eur.Phys.J, **C50**, 519, arXiv:hep-ph/0605190

Ahrens V., A. Ferroglia, M. Neubert, B. D. Pecjak, and L. L. Yang (2010), arXiv:1003.5827 [hep-ph]

Almeida L. G., G. Sterman, and W. Vogelsang (2008), Phys. Rev., **D78**, 014008, arXiv:0805.1885 [hep-ph]

Alwall J., *et al.* (2007), JHEP, **0709**, 028, arXiv:0706.2334 [hep-ph]

Alwall J., *et al.* (2008), Eur.Phys.J., **C53**, 473, arXiv:0706.2569 [hep-ph]

Antoniadis I., K. Benakli, and M. Quiros (1994), Phys. Lett., **B331**, 313, arXiv:hep-ph/9403290

Antoniadis I., K. Benakli, and M. Quiros (1999), Phys. Lett., **B460**, 176, arXiv:hep-ph/9905311

Antunano O., J. H. Kuhn, and G. Rodrigo (2008), Phys. Rev., **D77**, 014003, arXiv:0709.1652 [hep-ph]

Appelquist T., H.-C. Cheng, and B. A. Dobrescu (2001), Phys. Rev., **D64**, 035002, arXiv:hep-ph/0012100

Aubert J., *et al.* (1974), Phys.Rev.Lett., **33**, 1404

Augustin J., *et al.* (1974), Phys.Rev.Lett., **33**, 1406

Bardeen W. A., A. J. Buras, D. W. Duke, and T. Muta (1978), Phys. Rev., **D18**, 3998

Barger V. D., J. Ohnemus, and R. J. N. Phillips (1989), Int. J. Mod. Phys., **A4**, 617

Beenakker W., H. Kuijf, W. L. van Neerven, and J. Smith (1989), Phys. Rev., **D40**, 54

Beneke M., and V. M. Braun (1994), Nucl. Phys., **B426**, 301, arXiv:hep-ph/9402364

Berends F. A., C. G. Papadopoulos, and R. Pittau (1998), Phys. Lett., **B417**, 385, arXiv:hep-ph/9709257

Bernreuther W., A. Brandenburg, Z. G. Si, and P. Uwer (2004a), Nucl. Phys., **B690**, 81, arXiv:hep-ph/0403035

Bernreuther W., M. Fuecker, and Y. Umeda (2004b), Phys. Lett., **B582**, 32, arXiv:hep-ph/0308296

Bhatti A., *et al.* (CDF) (2006), Nucl.Instrum.Meth., **A566**, 375, arXiv:0510047 [hep-ex]

Bigi I. I. Y., M. A. Shifman, N. G. Uraltsev, and A. I. Vainshtein (1994), Phys. Rev., **D50**, 2234, arXiv:hep-ph/9402360

Blaire R., *et al.* (CDF) (1996), "The CDF II Detector: Technical Design Report," FERMILAB-Pub-96/390-E

Boos E. E., V. E. Bunichev, L. V. Dudko, V. I. Savrin, and A. V. Sherstnev (2006), Phys. Atom. Nucl., **69**, 1317

Bowen M. T., S. D. Ellis, and D. Rainwater (2006), Phys. Rev., **D73**, 014008, arXiv:hep-ph/0509267

Brandt S., and H. D. Dahmen (1979), Zeit. Phys., **C1**, 61

Cacciari M., S. Frixione, M. L. Mangano, P. Nason, and G. Ridolfi (2008), JHEP, **09**, 127, arXiv:0804.2800 [hep-ph]

Cao J., Z. Heng, L. Wu, and J. M. Yang (2010), Phys. Rev., **D81**, 014016, arXiv:0912.1447 [hep-ph]

Carena M. S., and H. E. Haber (2003), Prog. Part. Nucl. Phys., **50**, 63, arXiv:hep-ph/0208209

Carlson D. O., and C. P. Yuan (1995), arXiv:hep-ph/9509208

Cembranos J. A. R., A. Rajaraman, and F. Takayama (2008), Europhys. Lett., **82**, 21001, arXiv:hep-ph/0609244

Chang D., W.-F. Chang, and E. Ma (1999), Phys. Rev., **D59**, 091503, arXiv:hep-ph/9810531

Chang S., J. Hisano, H. Nakano, N. Okada, and M. Yamaguchi (2000), Phys. Rev., **D62**, 084025, arXiv:hep-ph/9912498

Cheng H.-C., K. T. Matchev, and M. Schmaltz (2002), Phys. Rev., **D66**, 056006, arXiv:hep-ph/0205314

Cheung K., W.-Y. Keung, and T.-C. Yuan (2009), Phys. Lett., **B682**, 287, arXiv:0908.2589 [hep-ph]

Cheung K.-M., and G. L. Landsberg (2002), Phys. Rev., **D65**, 076003, arXiv:hep-ph/0110346

Chivukula R. S., A. G. Cohen, and E. H. Simmons (1996), Phys. Lett., **B380**, 92, arXiv:hep-ph/9603311

Choudhury D., R. M. Godbole, R. K. Singh, and K. Wagh (2007), Phys. Lett., **B657**, 69, arXiv:0705.1499 [hep-ph]

Choudhury D., T. M. P. Tait, and C. E. M. Wagner (2002), Phys. Rev., **D65**, 053002, arXiv:hep-ph/0109097

Chung D., L. Everett, G. Kane, S. King, J. Lykken, and L. Wang (2005), Phys. Rep., **407**, 1

Colladay D., and V. A. Kostelecky (1997), Phys. Rev., **D55**, 6760, arXiv:hep-ph/9703464

Contino R., and G. Servant (2008), JHEP, **06**, 026, arXiv:0801.1679 [hep-ph]

Corcella G., *et al.* (2001), JHEP, **0101**, 010, see also http://hepwww.rl.ac.uk/theory/seymour/herwig/, arXiv:0011363 [hep-ph]

Csaki C., J. Erlich, and J. Terning (2002), Phys. Rev., **D66**, 064021, arXiv:hep-ph/0203034

Dalitz R. H., and G. R. Goldstein (1992), Phys. Rev., **D45**, 1531

Dalitz R. H., and G. R. Goldstein (1999), Proc. Roy. Soc. Lond., **A455**, 2803, arXiv:hep-ph/9802249

Davidson N. Nanava, G., T. Przedzinski, E. Richter-Was, and Z. Was (2010), "Universal Interface of TAUOLA Technical and Physics Documentation," IFJPAN-IV-2009-10; see also http://wasm.home.cern.ch/wasm/goodies.html, arXiv:1002.0543 [hep-ph]

Davoudiasl H., J. L. Hewett, and T. G. Rizzo (2000), Phys. Lett., **B473**, 43, arXiv:hep-ph/9911262

Davoudiasl H., J. L. Hewett, and T. G. Rizzo (2001), Phys. Rev., **D63**, 075004, arXiv:hep-ph/0006041

Dicus D., A. Stange, and S. Willenbrock (1994), Phys. Lett., **B333**, 126, arXiv:hep-ph/9404359

Dienes K. R., E. Dudas, and T. Gherghetta (1998), Phys. Lett., **B436**, 55, arXiv:hep-ph/9803466

Dienes K. R., E. Dudas, and T. Gherghetta (1999), Nucl. Phys., **B537**, 47, arXiv:hep-ph/9806292

Dittmaier S., P. Uwer, and S. Weinzierl (2007), Phys. Rev. Lett., **98**, 262002, arXiv:hep-ph/0703120

Djouadi A., G. Moreau, F. Richard, and R. K. Singh (2009), arXiv:0906.0604 [hep-ph]

Dobrescu B. A., and C. T. Hill (1998), Phys. Rev. Lett., **81**, 2634, arXiv:hep-ph/9712319

Dobrescu B. A., K. Kong, and R. Mahbubani (2009), JHEP, **06**, 001, arXiv:0902.0792 [hep-ph]

Eichten E., I. Hinchliffe, K. D. Lane, and C. Quigg (1986), Phys. Rev., **D34**, 1547

Eichten E., and K. D. Lane (1980), Phys. Lett., **B90**, 125

Eichten E., and K. D. Lane (1994), Phys. Lett., **B327**, 129, arXiv:hep-ph/9401236

Falk A. F., and M. E. Peskin (1994), Phys. Rev., **D49**, 3320, arXiv:hep-ph/9308241

Feldman G. J., and R. D. Cousins (1998), Phys. Rev., **D57**, 3873, arXiv:physics/9711021

Ferrario P., and G. Rodrigo (2008), Phys. Rev., **D78**, 094018, arXiv:0809.3354 [hep-ph]

Ferrario P., and G. Rodrigo (2009), J. Phys. Conf. Ser., **171**, 012091, arXiv:0907.0096 [hep-ph]

Fiedler F. (2010), Habilitation thesis at Munich University, arXiv:1003.0521 [hep-ex]

Fiedler F., A. Grohsjean, P. Haefner, and P. Schieferdecker (2010), arXiv:1003.1316 [hep-ex]

Flächer H., *et al.* (Gfitter) (2009), Eur.Phys.J., **C60**, 593, see also http://gfitter.desy.de/, arXiv:0811.0009 [hep-ph]

Frampton P. H., P. Q. Hung, and M. Sher (2000), Phys. Rept., **330**, 263, arXiv:hep-ph/9903387

Frederix R., and F. Maltoni (2009), JHEP, **01**, 047, arXiv:0712.2355 [hep-ph]

Frixione S., and B. Webber (2002), JHEP, **0206**, 029, see also http://www.hep.phy.cam.ac.uk/theory/webber/MCatNLO/, arXiv:0204244 [hep-ph]

Galea C. (D0) (2007), Acta Phys. Polon., **B38**, 769

Gribov V., and N. Lipatov (1972), Sov.J.Nucl.Phys., **15**, 438, also Altarelli G. and Parisi G. (1977), Nucl.Phys. **B126**, 298, and Dokshitzer Yu.L. (1977), Sov.Phys. JETP, **46**, 641

Grossman Y. (1994), Nucl. Phys., **B426**, 355, arXiv:hep-ph/9401311

Grossman Y., and M. Neubert (2000), Phys. Lett., **B474**, 361, arXiv:hep-ph/9912408

Gunion J. F., H. E. Haber, G. L. Kane, and S. Dawson (1989), *THE HIGGS HUNTER'S GUIDE*, sCIPP-89/13

Haber H. E., and G. L. Kane (1985), Phys. Rept., **117**, 75

Han T., H. E. Logan, B. McElrath, and L.-T. Wang (2003), Phys. Lett., **B563**, 191, arXiv:hep-ph/0302188

He H.-J., N. Polonsky, and S.-f. Su (2001), Phys. Rev., **D64**, 053004, arXiv:hep-ph/0102144

Herb S., *et al.* (1997), Phys.Rev.Lett., **39**, 252

Hewett J. L., F. J. Petriello, and T. G. Rizzo (2002), JHEP, **09**, 030, arXiv:hep-ph/0203091

Hill C. T. (1991), Phys. Lett., **B266**, 419

Hill C. T. (1995), Phys. Lett., **B345**, 483, arXiv:hep-ph/9411426

Hill C. T., and S. J. Parke (1994), Phys. Rev., **D49**, 4454, arXiv:hep-ph/9312324

Hoang A. H., and I. W. Stewart (2008), Nucl. Phys. Proc. Suppl., **185**, 220, arXiv:0808.0222 [hep-ph]

Hocker A., and V. Kartvelishvili (1996), Nucl. Instrum. Meth., **A372**, 469, arXiv:hep-ph/9509307

Huber S. J., and Q. Shafi (2001), Phys. Rev., **D63**, 045010, arXiv:hep-ph/0005286

Jezabek M., and J. Kühn (1993), Phys.Rev., **D48**, 1910, arXiv:9302295 [hep-ph]

Jezabek M., and J. Kühn (1994), Phys.Rev., **D48**, 4970

Jezabek M., and J. H. Kuhn (1989), Nucl. Phys., **B314**, 1

Juste A. (1999), "Measurement of the W mass in e+ e- annihilation," CERN-THESIS-99-012

Kane G. L., G. A. Ladinsky, and C. P. Yuan (1992), Phys. Rev., **D45**, 124

Kane G. L., and S. Mrenna (1996), Phys. Rev. Lett., **77**, 3502, arXiv:hep-ph/9605351

Kidonakis N., and R. Vogt (2008), Phys. Rev., **D78**, 074005, arXiv:0805.3844 [hep-ph]

Kobayashi M., and T. Maskawa (1973), Prog. Theor. Phys., **49**, 652

Kondo K., T. Chikamatsu, and S. H. Kim (1993), J. Phys. Soc. Jap., **62**, 1177

Kronfeld A. S., and C. Quigg (2010), arXiv:1002.5032 [hep-ph]

Kuhn J. H., and G. Rodrigo (1998), Phys. Rev. Lett., **81**, 49, arXiv:hep-ph/9802268

Kuhn J. H., and G. Rodrigo (1999), Phys. Rev., **D59**, 054017, arXiv:hep-ph/9807420

Langacker P. (1981), Phys. Rept., **72**, 185

Lange D., and A. Ryd (1998), "The EvtGen Event Generator Package," See http://hep.ucsb.edu/people/lange/EvtGen/

Langenfeld U., S. Moch, and P. Uwer (2009), Phys. Rev., **D80**, 054009, arXiv:0906.5273 [hep-ph]

Larios F., R. Martinez, and M. A. Perez (2006), Int. J. Mod. Phys., **A21**, 3473, arXiv:hep-ph/0605003

Leike A. (1999), Phys. Rept., **317**, 143, arXiv:hep-ph/9805494

Lillie B., L. Randall, and L.-T. Wang (2007), JHEP, **09**, 074, arXiv:hep-ph/0701166

Loader C. (1999), *Local regression and likelihood* (Springer)

Lyons L., D. Gibaut, and P. Clifford (1988), Nucl. Instrum. Meth., **A270**, 110

Mahlon G., and S. J. Parke (1996), Phys. Rev., **D53**, 4886, arXiv:hep-ph/9512264

Mahlon G., and S. J. Parke (1997), Phys. Lett., **B411**, 173, arXiv:hep-ph/9706304

Mahlon G., and S. J. Parke (2010), Phys. Rev., **D81**, 074024, arXiv:1001.3422 [hep-ph]

Malkawi E., T. M. P. Tait, and C. P. Yuan (1996), Phys. Lett., **B385**, 304, arXiv:hep-ph/9603349

Mangano M., M. Moretti, F. Piccinini, R. Pittau, and A. Polosa (2003), JHEP, **0307**, 001, see also http://mlm.web.cern.ch/mlm/alpgen/, arXiv:0206293 [hep-ph]

Martin A., R. Roberts, W. Stirling, and G. Watt (MRST/MRSW) (2007), Phys.Lett., **B652**, 292, see also http://durpdg.dur.ac.uk/hepdata/mrs.html, arXiv:0706.0459 [hep-ph]

Martin A. D., R. G. Roberts, W. J. Stirling, and R. S. Thorne (2004), Eur. Phys. J., **C35**, 325, arXiv:hep-ph/0308087

Martin S. P. (1997), arXiv:hep-ph/9709356

Moch S., and P. Uwer (2008), Phys. Rev., **D78**, 034003, arXiv:0804.1476 [hep-ph]

Nadolsky P. M., *et al.* (2008), Phys. Rev., **D78**, 013004, arXiv:0802.0007 [hep-ph]

Nakamura K., *et al.* (2010), J. Phys., **G 37**, 075021

Nam S.-h. (2002), Phys. Rev., **D66**, 055008, arXiv:hep-ph/0206037

Nilles H. P. (1984), Phys. Rept., **110**, 1

Parke S. J., and Y. Shadmi (1996), Phys. Lett., **B387**, 199, arXiv:hep-ph/9606419

Perl M., *et al.* (1975), Phys.Rev.Lett., **35**, 1489

Pomarol A. (2000), Phys. Lett., **B486**, 153, arXiv:hep-ph/9911294

Pumplin J., D. Stump, J. Huston, H. Lai, P. Nadolsky, and W. Tung (CTEQ) (2002), JHEP, **07**, 012, see also http://www.phys.psu.edu/ cteq, arXiv:0201195 [hep-ph]

Quigg C. (2009), Ann.Rev.Nucl.Part.Sci., **59**, 505, arXiv:0905.3187 [hep-ph]

Randall L., and M. D. Schwartz (2001), JHEP, **11**, 003, arXiv:hep-th/0108114

Randall L., and M. D. Schwartz (2002), Phys. Rev. Lett., **88**, 081801, arXiv:hep-th/0108115

Randall L., and R. Sundrum (1999), Phys. Rev. Lett., **83**, 3370, arXiv:hep-ph/9905221

Read A. L. (1999), Nucl. Instrum. Meth., **A425**, 357

Rizzo T. G. (2001), Phys. Rev., **D64**, 095010, arXiv:hep-ph/0106336

Rizzo T. G., and J. D. Wells (2000), Phys. Rev., **D61**, 016007, arXiv:hep-ph/9906234

Ross G. G. (1984), *Grand Unified Theories*, reading, USA: Benjamin/cummings (Frontiers In Physics, 60)

Schaile D., and P. Zerwas (1992), Phys.Rev., **D45**, 3262

Scott D. W. (1992), *Multivariate density estimation: theory, practice, and visualization* (Wiley-Interscience)

Sehgal L. M., and M. Wanninger (1988), Phys. Lett., **B200**, 211

Shu J., T. M. P. Tait, and K. Wang (2010), Phys. Rev., **D81**, 034012, arXiv:0911.3237 [hep-ph]

Silverman B. W. (1998), *Density estimation for statistics and data analysis* (Chapman and Hall)

Simmons E. H. (1997), Phys. Rev., **D55**, 1678, arXiv:hep-ph/9608269

Sinervo P. (2003), Prepared for PHYSTAT2003: Statistical Problems in Particle Physics, Astrophysics, and Cosmology, Menlo Park, California, 8-11 Sep 2003

Sjöstrand T., P. Eden, C. Friberg, L. Lönnblad, G. Miu, S. Mrenna, and E. Norrbin (2001), Comput.Phys.Commun., **135**, 238, see also http://home.thep.lu.se/ torbjorn/Pythia.html, arXiv:0010017 [hep-ph]

Smith M. C., and S. S. Willenbrock (1997), Phys. Rev. Lett., **79**, 3825, arXiv:hep-ph/9612329

Stanley K. O., and R. Miikkulainen (2002), Evol. Comput., **10**, 99

Valassi A. (2003), Nucl. Instrum. Meth., **A500**, 391

Yuan C. P. (1993), arXiv:hep-ph/9308240

Yuan C. P. (1995), arXiv:hep-ph/9509209

FIGURES
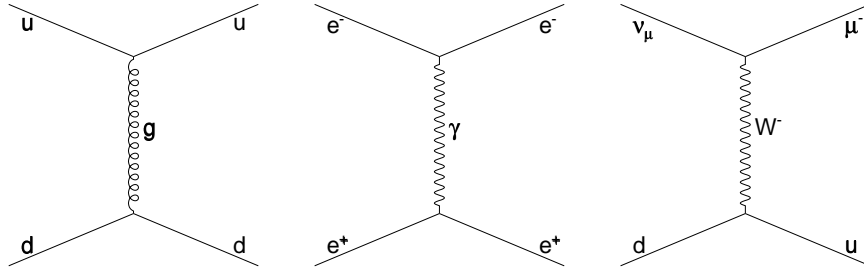
FIG. 1 Example of Feynman diagrams depicting SM interactions for the strong (left), electromagnetic (middle), and weak (right) forces.
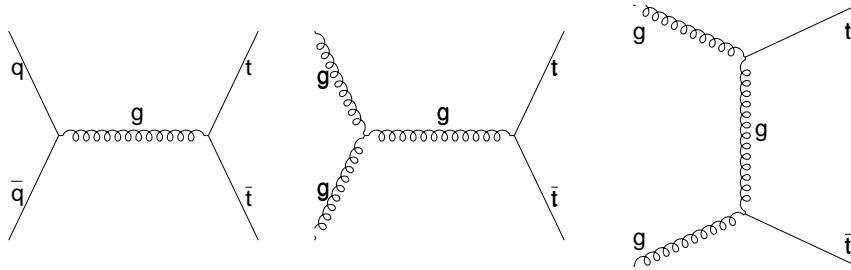
FIG. 2 Feynman diagrams of $p\overline{p} \to t\overline{t}$ for the $q\overline{q}$ annihilation process (left) and the gluon-gluon fusion process (middle and right).
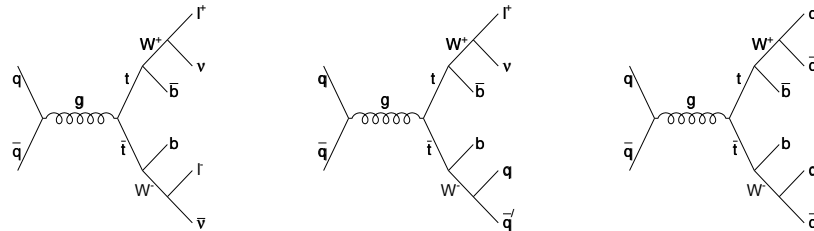
FIG. 3 Feynman diagrams of $p\overline{p} \to t\overline{t}$ production with the $t\overline{t}$ decaying to the dilepton (left), lepton-plus-jets (middle), and all hadronic (right) final states.

CENTRAL DRIFT CHAMBER

ELECTROMAGNETIC
CALORIMETER

EM SHOWER
MAXIMUM CHAMBER

HADRONIC CALORIMETER

MUON DRIFT CHAMBERS

STEEL SHIELDING

MUON SCINTILLATOR
COUNTER

ISL (3 LAYERS)

SVX II (3 BARRELS)

INTERACTION POINT (B0)
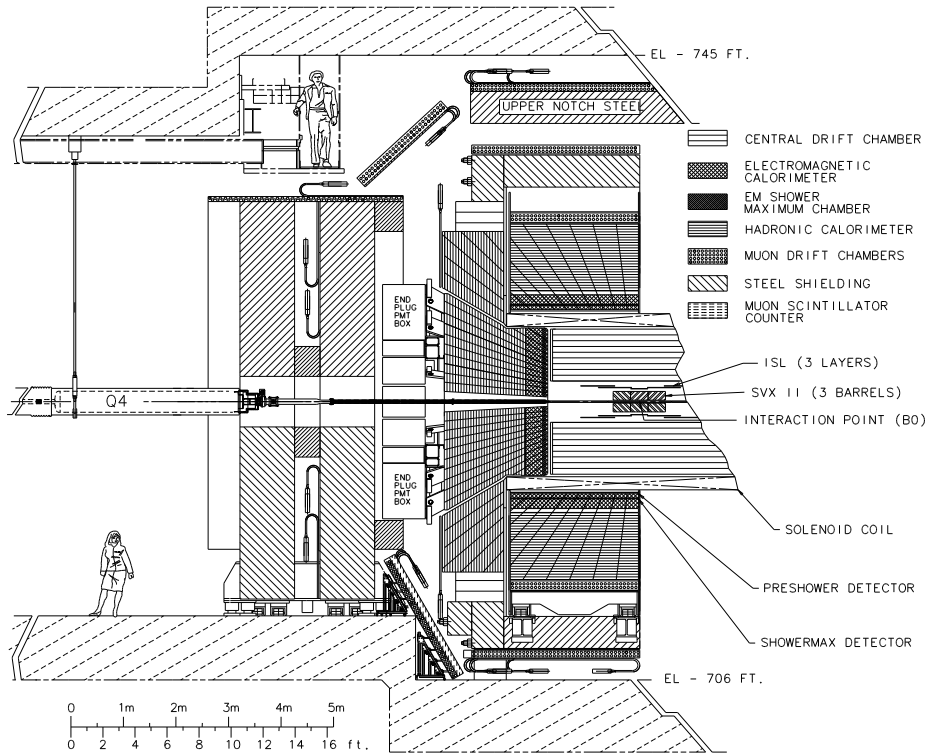
SOLENOID COIL

PRESHOWER DETECTOR
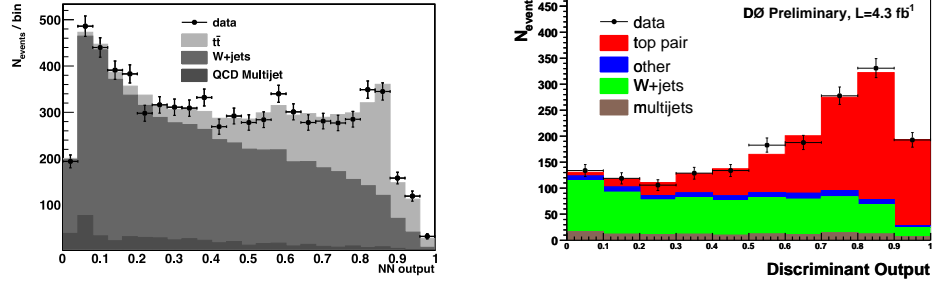
SHOWERMAX DETECTOR
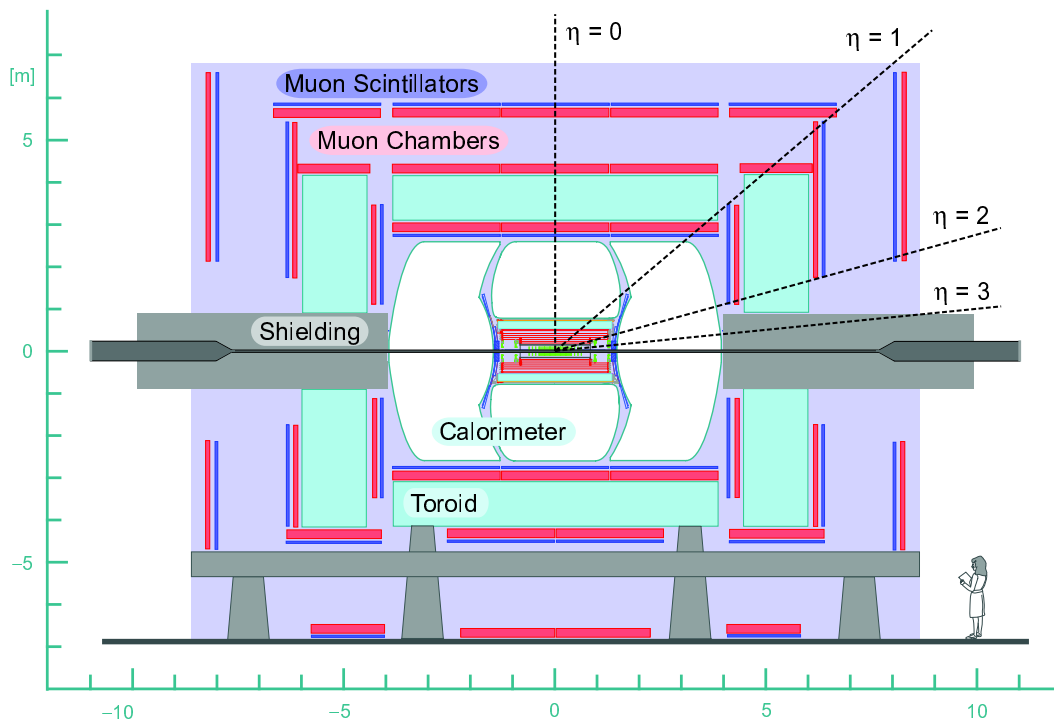
FIG. 4 A cut away view of the CDF (top) and DØ (bottom) detectors.

FIG. 5 Output of the NN used by CDF (left) and the BDT used by DØ (right) to determine the $t\bar{t}$ cross section in the ljt channel using topological information (Aaltonen *et al.*, 2010; Abazov *et al.*, 2010).
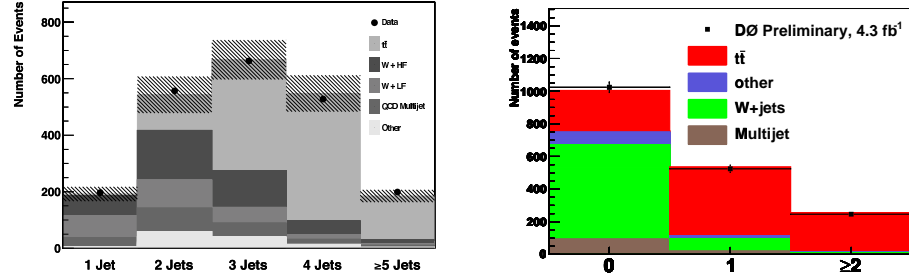
FIG. 6 The predicted and observed number of events as a function of jet multiplicity for CDF (left) and DØ (right) in their $t\bar{t}$ cross section analysis in the ljt channel using b-jet identification to suppress background (Aaltonen *et al.*, 2010; Abazov *et al.*, 2010).
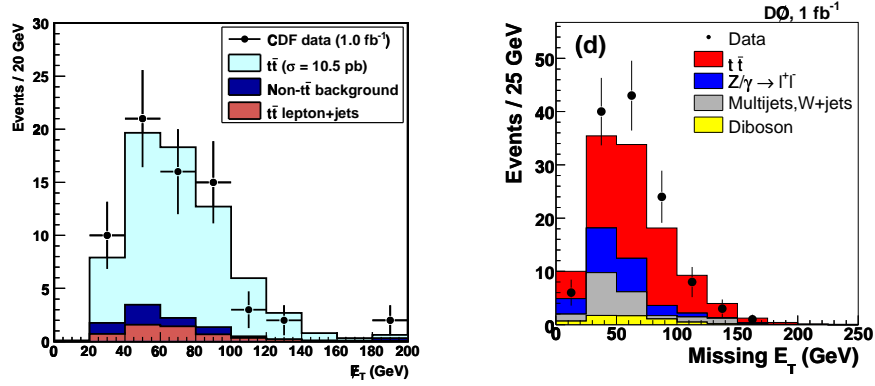
FIG. 7 The observed $\not{E}_T$ distribution compared to the SM expectations for the $t\bar{t}$ cross section measurement using CDF *dil* events (left) and using DØ $\ell\ell$ and $\ell\tau$ events combined (right) (Aaltonen *et al.*, 2009; Abazov *et al.*, 2009).
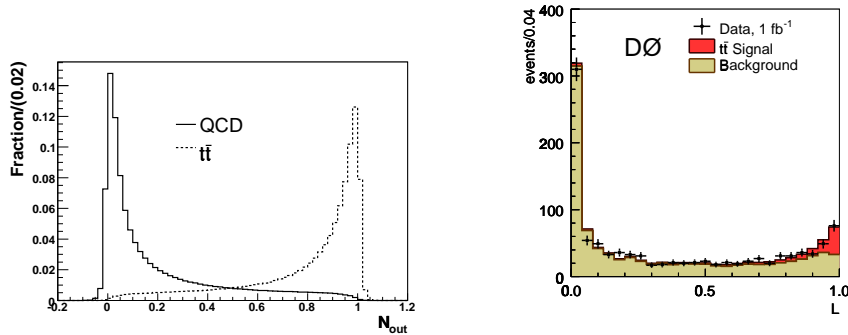
FIG. 8 The NN output distribution for QCD data (solid) and $t\bar{t}$ MC events (dashed) from CDF (left). A comparison of the likelihood distribution between data and MC using the signal purity fit from the data from DØ (right). Fits to these distributions are used to measure the $t\bar{t}$ cross section in the all hadronic channel (Aaltonen *et al.*, 2010; Abazov *et al.*, 2010).
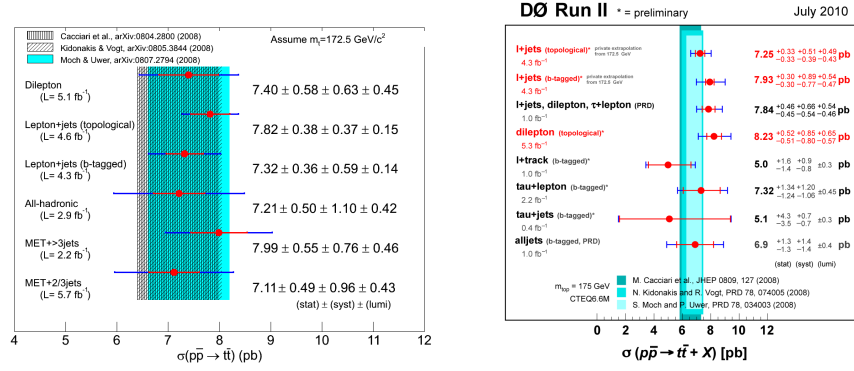
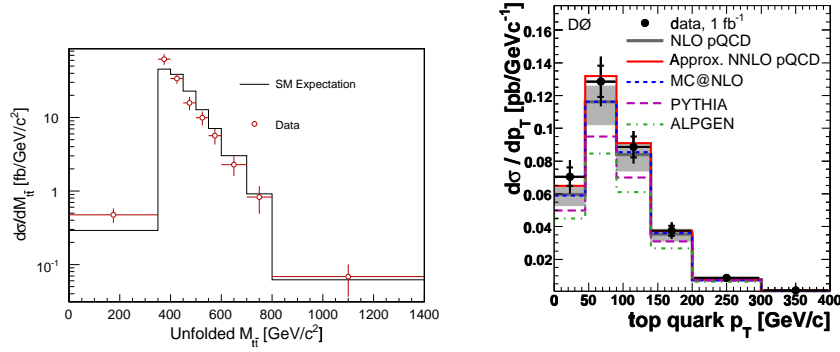FIG. 9 Summary of the latest $t\bar{t}$ cross section measurements performed by CDF (left) and DØ (right).

FIG. 10 The measured $d\sigma/dm_{t\bar{t}}$ from CDF (left) compared to the SM expectation. The measured $d\sigma/dp_T$ from DØ (right) compared to QCD calculations and various MC generators (Aaltonen *et al.*, 2009; Abazov *et al.*, 2010).
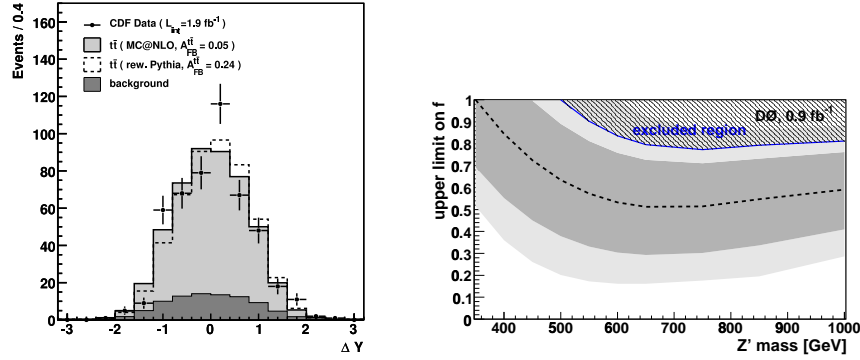
FIG. 11 The raw Δy distribution used by CDF (left) to measure $A_{fb}^{t\bar{t}}$ in the $t\bar{t}$ rest frame. The 95% confidence level limits on the fraction of $t\bar{t}$ produced via a Z' resonance as a function of the Z' mass (right) obtained from the DØ $A_{fb}^{t\bar{t}\,obs}$ measurement (Aaltonen *et al.*, 2008; Abazov *et al.*, 2008).
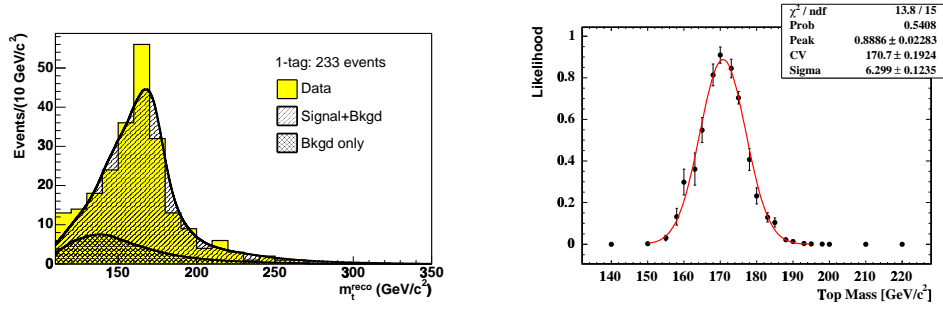
FIG. 12 The m_t^{reco} distribution (left) in the CDF ljt channel with the signal and background template estimates overlaid using $m_t = 172$ GeV/c^2 and the nominal jet energy corrections for events with 1 identified b-jet (Aaltonen *et al.*, 2009). The likelihood curve from the data fit (right) in the ljt channel using L_T and lepton p_T as top-quark mass estimators (Aaltonen *et al.*, 2010).
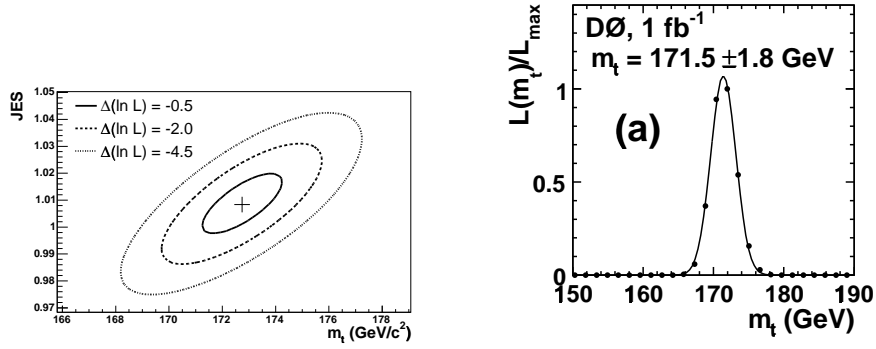

FIG. 13 Results from m_t measurements in the ljt channel using the matrix element method. The 2-D likelihood (left) from CDF data and the DØ data likelihood projected onto the m_t axis (Aaltonen *et al.*, 2009; Abazov *et al.*, 2008).
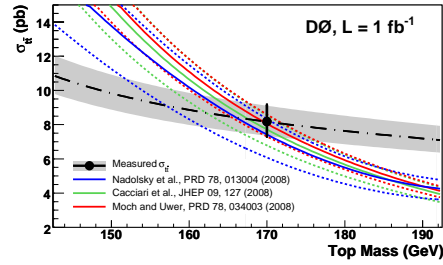

FIG. 14 A DØ measurement of the top-quark mass determined by comparing the measured and the SM predicted $t\bar{t}$ cross section as a function of m_t (Abazov *et al.*, 2009).
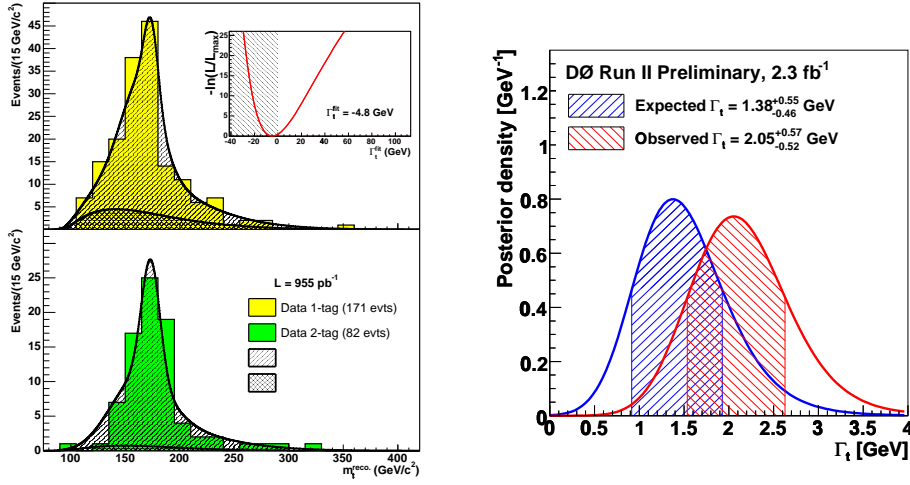
FIG. 15 The m_t^{reco} distribution (left) for CDF events with identified b-jets overlaid with signal and background distributions and the posterior probability density (right) for the expected and measured Γ_t determination from DØ (Aaltonen *et al.*, 2009; Abazov *et al.*, 2010).
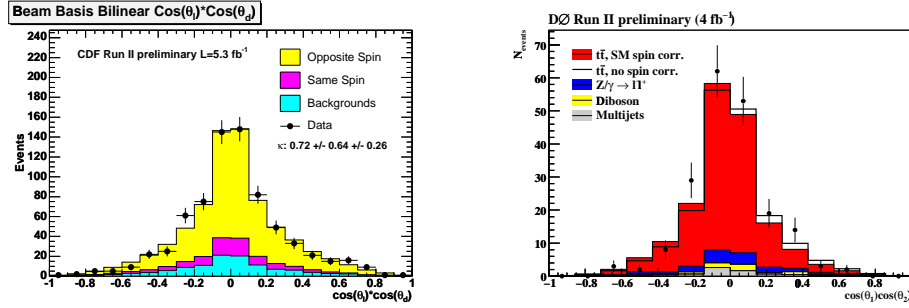

FIG. 16 The CDF ($\cos\theta_\ell$, $\cos\theta_d$) distribution (left) in ljt events using the beam basis. The DØ ($cos\theta_{\ell-}$, $\cos\theta_{\ell+}$) distribution in *dil* events using the beam basis.
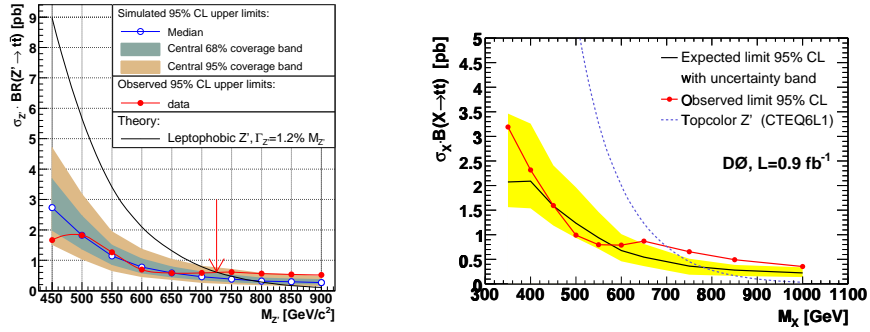

FIG. 17 Expected and observed experimental upper limits at 95 % confidence level on $\sigma_{Z'}\mathcal{B}(Z' \to t\bar{t})$ from CDF (left) and DØ (right); the bands define the $\pm 1\sigma$ range for the expected limits (Aaltonen *et al.*, 2008; Abazov *et al.*, 2008).

TABLES

TABLE I The measured masses of the elementary particles in the Standard Model. For the neutrino masses only limits exist. Those listed are at the 90% confidence level (Nakamura *et al.*, 2010).

quark masses			
$m_u \sim 0.002$	$m_c = 1.27$	$m_t = 171.2$	(GeV/c^2)
$m_d \sim 0.005$	$m_s = 0.104$	$m_b = 4.20$	(GeV/c^2)
lepton masses			
$m_\nu < 2 \times 10^{-6} \text{ eV}/c^2$, $\sum_i m_{\nu_i}^2 > 2 \times 10^{-17} (\text{eV}/c^2)^2$			
$m_e = 0.511$	$m_\mu = 105.6$	$m_\tau = 1776.8$	(MeV/c^2)

basis	dilepton channel	lepton+jets channel
helicity	-0.352	-0.168
beam	0.777	0.370
off-diagonal	0.782	0.372

TABLE II NLO computation for the spin-correlation coefficient, C, discussed in Sec. IX.C.5 (Bernreuther *et al.*, 2004)